Bathymetry of Reykjanes Ridge: A methodological approach

Karolina Banul

Faculty of Life and Envirnonmental Sciences
University of Iceland
June 2014

Bathymetry of Reykjanes Ridge: A methodological approach

Karolina Banul

30 ECTS thesis submitted in partial fulfilment of a
Magister Scientiarum degree in Geo-information Science and Earth Observation for Environmental Modelling and Management

Advisor(s)
Ármann Höskuldsson
Inga Jónsdóttir
Rannveig Ólafsdóttir

Examiner
Árni Vésteinsson

Faculty of Life and Environmental Sciences
School of Engineering and Natural Sciences
University of Iceland
Reykjavik, June 2014

Bathymetry of Reykjanes Ridge: A methodological approach
Bathymetry of Reykjanes Ridge
30 ECTS thesis submitted in partial fulfillment of a *Magister Scientiarum* degree in Geo-information Science and Earth Observation for Environmental Modelling and Management

Faculty of Life and Environmental Sciences
School of Engineering and Natural Sciences
University of Iceland
Askja, Sturlugata 7
101, Reykjavik
Iceland

Telephone: 525 4000

Bibliographic information:
Karolina Banul, 2014, *Bathymetry of Reykjanes Ridge: A methodological approach*, Master's thesis, Faculty of Life and Environmental Sciences, University of Iceland, 123p.

Printing: Háskólaprent
Reykjavik, Iceland, June 2014

Abstract

The sea floor is one of the Earths parts that still are mostly unexplored. Recent multibeam technology has now opened up new opportunities to increase our knowledge in this hitherto hidden part of the world. In this study part of the Reykjanes Ridge was analysed in order to create a high resolution and comprehensive topographic map of this northern part of the Mid-Atlantic Ocean Ridge. The general aims of the study were to i) develop seamless method from Caris, a raw analytical program for multibeam data, to ArcInfo, a spatial analytical program of geographical data; ii) to assess and modify multibeam datasets from different time periods (1994, 2006, 2007 and 2013); and iii) to conduct time-separated comparison analysis of morphological structures of the sea floor, and in that way assess potential submarine volcanic activity through time. High-resolution model of the spreading oceanic crust was created using data from precise multibeam echo-sounders. Based on the mapped topography volcanic structures were identified and analysed. Time-separated change detection analysis was further conducted using both quantitative raster based method and qualitative visual assessment. The results of the comparison analysis do reveal evidence about changes in topography of the Reykjanes Ridge. Thus, for the first time an area of the ridge has been identified as a potential eruption and/or volcano-tectonic site between 1994 and 2013.The resulting high resolution mapping furthermore add valuable knowledge as regard the Reykjanes Ridge morphology and subsequently the Mid-Atlantic Ocean Ridge, and moreover opens possibilities for further geographical and geological interpretations of submarine volcanic and tectonic processes along the Ocean Ridge.

Key words: Sea floor morphology, multibeam data, GIS, Reykjanes Ridge, Iceland

Útdráttur

Hafsbotninn er einn af fáum stöðum jarðar sem enn eru að miklu leyti órannsakaðir. Nýleg fjölgeislamælinga tækni hefur hins vegar opnað ný tækifæri til að auka þekkingu okkar á þessum óþekkta hluta jarðar. Í þessari rannsókn er sjónum beint að norðurhluta Reykjaneshryggjar, og fjölgeislamæligögn notuð til að búa til kort í hárri upplausn af landslagi hafsbotnsins á þessum hluta Atlantshafshryggjarins. Meginmarkmið rannsóknarinnar er i) að þróa aðferðafræði til að færa hrágögn úr Caris forritinu yfir ArcInfo landupplýsingakerfi; ii) að meta og samræma hrágögn frá mismunandi tímabilum (1994, 2006, 2007 og 2013); og iii) að gera samanburðargreiningu á mögulegum breytingum á landslagi hafsbotnsins frá 1994-2013, og á þann hátt meta virkni neðansjávar eldgosa á þessu 20 ára tímabili. Reiknilíkan í hárri upplausn af plötuskilunum var þróað út frá fjölgeisla endurkastsgögnum. Á grunni hafsbotnskortsins var unnt að greina mismunandi landform og gosmyndanir. Greining á breytingum yfir tíma var einnig gerð þar sem stuðst var hvort tveggja við rastagögn til að meta allt rannsóknarsvæði og sjónrænt mat til að meta nákvæmari breytingar á minna svæði. Niðurstöðurnar gefa til kynna að einhverjar breytingar hafa átt sér stað í landslagi hafsbotnsins á rannsóknartímabilinu. Þannig sýna niðurstöður rannsóknarinnar í fyrsta skipti breytingar á ástandi lands á hafsbotni vegna eldvirkni á Atlantshafshryggnum. Niðurstöður kortlagningar gefa enn fremur dýrmæta þekkingu á landmótun Reykjaneshryggjarins og opna á þann hátt möguleika fyrir frekari land- og jarðfræðilegar túlkanir á sjávargosum og jarðskorpubreytingum á Atlantshafshryggnum.

Lykilorð: Landmótun hafsbotnsins, fjölgeislagögn, LUK, Reykjaneshryggur, Ísland

Table of Contents

List of Figures

List of Tables

Abbreviations

m – Meter;

km – kilometer;

cu km– cubic kilometer;

sq km - square kilometer;

mb - body-wave magnitude;

Hz – Hertz; unit of frequency; one cycle per second;

Radar - RAdio Detection And Ranging;

LIDAR - LIght Detection And Ranging;

Sonar - SOund Navigation And Ranging;

R/V – Research Vessel;

RRS - Royal Research Ship;

IHO – International Hydrographic Organization;

SVP – Sound Velocity Profile;

TPU – Total Propagated Uncertainty;

HVF – HIPS Vessel File;

HIPS and SIPS - Hydrographic and Sonar Data Processing System;

ASCII - American Standard Code for Information Interchange;

MAR – Mid-Atlantic Ridge;

AVR – Axial Volcanic Ridges;

Glossary

Caldera – large depression caused by collapse of the summit area of a volcano following a violent eruption;

Crater – depression at the summit of a volcano;

Crust – very thin, outermost layer of Earth;

Mantle – thick layer of Earth located below the crust;

Lava – magma that reaches Earth surface;

Magma – a body of molten rock with dissolved gasses and crystals found at depth;

Normal fault – the rock above the fault plane has moved down relative to the rock below;

Graben – a valley formed by the downward displacement of a fault-bounded block;

Oceanic ridge – continuous mountainous ridge on the floor of the major ocean basins. It is characterized by the rift at the crests that represent divergent plate boundary;

Pillow lava – basaltic lava that solidifies in an underwater environment;

Seamount – isolated volcanic peak that rises above the deep sea floor;

Bathymetry – a measurement of ocean depths and the charting of the topography of the sea floor;

Sea floor- a bottom of the sea, or ocean. Known also as seabed;

Topography – surface configuration of Earth; variations in elevation;

Geomorphology – study of characteristics, origin and development of landforms;

Acknowledgements

I first want to express my gratitude to my supervisor Armann Höskuldsson for excellent guidance, fruitful discussions, advices and availability always I needed help. I also wanted to give special thanks to Ingibjörg Jónsdóttir for valuable instructions and support throughout the project as well as help in arranging study visit in Icelandic Coast Guard Office. My gratitude goes to Rannveig Ólafsdóttir for her patience and assistance with all arrangements related to GEM study programme, valuable comments, and encouragement to finalize this project on time. Many thanks to Árni Vésteinsson for interesting discussion about creating nautical maps from bathymetric data.

My gratitude goes also to all those that helped to finalize this thesis project: Dave Ostman for language corrections, and Willem Gerrit Tims for all discussions about the project, support in solving all GIS related problems, and especially keeping me updated about deadlines.

Many thanks to colleagues at Askja for their interesting discussions and support. Finally I want to express my gratitude to my family and friends who inspired me to start and motivate me to complete this study

.

1 Introduction

1.1 Sea floor mapping

The history of the world's exploration is followed by creating maps of previously unknown places. In the current world of satellites and GPS, mapping of the terrestrial environments and land cover have become much more efficient, and the main question is rather about the level of map detail than about the discovery of the unknown land. The only place in the world that is still mostly unexplored by humans is the ocean. Especially the sea floor hidden under kilometers of water column as it does not allow for exploration and uncovering the secrets of the underwater world.

According to the International Hydrographic Organization [IHO] (2013), only 10% of sea floor has been mapped with high resolution data, while many places have not been mapped at all. The new multibeam technology definitely improves the quality and amount of data possible to gather during the bathymetric survey. However, even with improved efficiency of echo sounders, it will take hundreds of years to map the whole sea floor (Tarbuck, Lutgens & Tasa, 2011).

Because of inhospitable conditions for humans and deep water factors such as high pressure and temperature, vast ocean areas are inaccessible for the "in situ" research or sampling. Thus, remote sensing utilizing both electromagnetic and acoustic energy is the main technique to obtain bathymetric data (Kearns & Breman, 2010). Techniques of remote sensing for sea floor mapping includes sonar systems, satellite images, and altimetry using space-born (GEOSAT, SEASAT) or aircrafts radars (LIDAR) (Sabins, 1996; Jensen, 2000). Recently LIDAR data has been applied to estimate both intensity and depth of the water bodies. Because electromagnetic waves are absorbed by the water, it is possible to penetrate only shallow coastal areas, approximately 10 meter depth depending on the water properties (Costa, Battista & Pittman, 2009). Therefore, the only way to explore deep sea floor is by using data from sonar systems, such as multibeam.

Bathymetry, as a part of hydrography, measures the water column depth and studies the formation of the bottom of sea. Mapping the sea floor and using hydrographic surveys creates a framework for studies within marine geophysics and geology. In turn such studies not only improve our understanding of geomorphology, structures, origin and processes behind the development of ocean basin, but also have application in many socially important issues such as exploration of mineral resources and prediction of natural hazards (IHO, 2011). In addition, the improvement in extent and accuracy of mapping is results of recent developments of instruments used for sampling, advances in navigation, availability of wide range of vessels, including even military submarines, for research purposes (Jones, 1999).

The primary application of bathymetric data and surveying oceans is to produce accurate hydrographic maps of the sea floor. Those are important for both navigation purposes – nautical charts - as well as research advances in Earth science, marine ecology, fishing and coastal

management (IHO, 2013). General application of hydrographic maps include habitat studies of fish and marine mammals; geophysical studies of earthquakes and faults, as well as prediction and modelling of storm surge and tsunami effects; research on sediment and pollutant flows; geological exploration of potential offshore oil and gas deposits; and delineation of bottom features for commercial fisheries and coastal zone management (National Oceanic and Atmospheric Administration [NOAA], 2013).

In the last century, development of sonar system and detailed bathymetric surveys of the world oceans revealed that continuous mountain ranges with valleys in between are located along the center of the oceans. This resembled similar structures on land caused by rifting and consequently was interpreted as evidence on the pulling apart of the ocean basin, and, in turn, yielded evidence for Wagner's theory on plate tectonics and continental drift. This theory revolutionized geological studies and allows explaining locations of volcanoes, earthquakes and other various land formations such as mountain ranges in particular places (Krom, 2005; Pumer, MacGeary, Carlson, 2005). In light of the fact that the majority of global volcanism occurs underwater and is located along mid-ocean ridges, it is of vital importance to collect long-term and high-resolution data to monitor the sea floor.

1.2 Mid-Atlantic Ocean Ridge and the Reykjanes Ridge

Iceland is a part of the Mid-Atlantic Ocean Ridge, located at the divergent boundaries of the North American and Eurasian tectonic oceanic plates. Iceland has therefore a unique geological history. Its landmass is believed to be a product of a hot spot located on the plate boundary resulting in a very active volcanic system with diversity of landform structures (e.g. Thordarson & Larsen, 2007). Because of the long history of volcanic eruptions resulting in dramatic consequences for the Icelandic population as well as significant disruption in mainland Europe - there is a need for its constant monitoring. This can be challenging as some of the volcanoes are subglacial or submarine, which demands application of special methods to observe or measure the deformation of volcanoes (e.g. Sturkell et al., 2006).

The Reykjanes Ridge is a part of the Mid-Atlantic Ocean Ridge that connects to Southwest Iceland. Due to the fact that Iceland was created in the place where oceanic spreading rises above the sea level, it is considered a perfect location to study Mid-Ocean Ridge processes (Höskuldsson, Hey, Kjartansson & Guðmundsson, 2007). Multiple studies recognize that the Reykjanes Ridge is especially important to study morphology structures, characteristics for both slow and fast spreading centers, and to understand plume-ridge interactions (e.g. Smith, Humphris & Bryan, 1995; Appelgate & Shor, 1994; Magde & Smith, 1995), such as increase of crust thickness with distance closer to the plume center and reduction of axial faulting northwards along the Reykjanes Ridge. Studies on the ridge segmentation pattern further identify that it is made up of basins and axial volcanic ridges, while it lacks transform faults (Höskuldsson et al., 2007). Those observations would not have been possible without echo sounder measurements. However, so far only few bathymetric surveys have been conducted over

the Reykjanes Ridge. In order to better understand this dynamic part of our planet, it is critical to increase a larger scale mapping of the oceanic ridges.

New high-resolution acoustic bathymetry data creates an increased potential to identify landforms occurring on the junction of the two sub-oceanic tectonic plates in large scale. This leads to an improved understanding of volcanic and sedimentary processes within geologically active areas (Bacon et al., 2002). Studies on structure and segmentation of the ridge also allow the ability to monitor and forecast potential volcanic eruptions that originate in the oceans. This in turn has a great importance for public security, as it can bring serious consequences for coastal communities and damage of settlements.

1.3 Aim of research and main questions to answer

To date, only coarse maps of the sea floor in the location of Reykjanes Ridge exist (Keeton, 1997). Only the northern part of the Reykjanes Ridge was mapped in detail (Höskuldsson et al., 2007). Detailed topographic maps over the entire Reykjanes Ridge can reveal characteristics of morphological structures and segmentation of the spreading oceanic crust. Therefore, the general aim of this research is to increase the knowledge and understanding of submarine volcanic and tectonic processes by creating a high-resolution model of the Reykjanes Ocean Ridge using multibeam sonar data. Specific aims of the research are as follows:
i) to develop seamless method from Caris, a raw analytical program for multibeam data, to ArcInfo, a spatial analytical program of geographical data;
ii) to assess and modify multibeam datasets from different time periods (1994, 2006, 2007 and 2013);
iii) to conduct time-separated comparison analysis of morphological structures of the sea floor, and in that way assess potential submarine volcanic activity through time.

The following research question is put forward: Are there any significant changes in morphological structures of the Reykjanes Ridge between 1994 and 2013?

The spreading continental plates cause the Reykjanes Ridge to be under constant change originating from the endogenous forces of the Earth. Consequently the constant formation of new oceanic crust occurs in this area and yields the following hypothesis: The change in morphological structures and bathymetry of the Reykjanes Ridge occurred between years 1994 and 2013.

1.4 Structure of the thesis

The thesis follows the principals of an academic research. It starts with theoretical background and a literature review. This chapter presents the methods and techniques of bathymetric measurements using sonar and principles of multibeam system. It also discusses the state of knowledge and past research conducted in relation to Reykjanes Ridge – especially bathymetry and morphology. This is followed by the methodology chapter, which presents a detailed

description of all data used and data analysis steps that were conducted within this study – from data conversion, through its processing and modelling and to final analyzing. The results chapter presents the main product – comprehensive maps over the Reykjanes Ridge sea floor created by combining the various datasets of sonar data conducted over the area within the last 20 years. It also presents the results of the comparison analysis to verify the hypothesis of the thesis. The final chapter presents the research conclusion drawn from the study results and critically discusses the results.

2 Theoretical Background

2.1. Bathymetry using sonar system

High-resolution mapping of sea floor is essential not only for navigation purposes, but also for scientific investigation within marine geology and geophysics. It allows the tracing of specific elements of the topography and to return to the position of previous measurements or observations. Bathymetry measures the depth of the sea utilizing both electromagnetic (Radar and LIDAR) and acoustic (Sonar) methods. While the radar system is successfully utilized to measure the sea surface[1] and sea bottom in the shallow areas, sonar systems - single beam echo soundings, side-scan sonar, multibeam swath soundings, and hybrid systems - are principal means to explore deep ocean basin (Jones, 1999; Kearns & Breman, 2010; Sabins, 1996; Jensen, 2000).

2.1 Principals of sound in water

Hydrographic survey is conducted to get information on both the depth of water and the nature of seabed. All acoustic methods for obtaining bathymetric data are based on the same physical principals of sound's ability to travel in water. Sound waves are series of pressure fronts that propagate in a water column at a specific local speed. In general the speed of sound, also called velocity, is a product of frequency and wavelength (Equation 1). The former is the number of pressure fronts that pass a point in water per unit time, and the latter is the distance between pressure fronts (Figure 1) (L-3 Communications SeaBeam Instruments, 2000). While the frequency of sound wave is constant, wavelength varies with local conditions of the water, such as salinity, pressure and temperature, which in turn influence how fast the acoustic wave propagates in water (Figure 2). Local speed of sound in oceanic conditions is approximately 1500 meters per second (m/s) (L-3 Communications SeaBeam Instruments, 2000). Acoustic energy carried by the wave is measured in terms of the amplitude of the wave – the size of the oscillations in pressure when the sound wave passes the receiving device – hydrophone. The higher the amplitude of the wave, the higher acoustic energy being transmitted. However, some of the energy is lost when the sound wave is transferred between the water molecules. This process, called attenuation, reduces the amplitude of a sound wave, and depends on its frequency. High frequency sound waves attenuate quickly, while low frequency sounds may travel very long distances through the ocean without significant energy lost (L-3 Communications SeaBeam Instruments, 2000). Therefore, transducer utilized in a hydrographic

[1] Satellite altimetry uses the radar pulses to measure distance between satellite and a target surface. Also electromagnetic waves are used for bathymetric measurements, but because of strong attenuation their ability to propagate through water is limited to short path. Therefore, only shallow waters can be effectively mapped using radar or Lidar systems.

survey of shallow waters of the continental shelf operates on the much higher frequencies (30-219 kHz) than those being used for deep ocean soundings (10-15 kHz) (Jones, 1999).

Equation 1

$$Speed\ of\ sound\ \left(\frac{m}{s}\right) = frequency(Hz)x\ wavelength(m)$$

The acoustic energy is lost not only because of the attenuation in water, but also when the sound wave encounters a change in medium. When the sound meets some matter on its travel path, three kinds of interaction occurs (Figure 3). Some amount of energy is transmitted into new material at the level depending on the following factors:

- Density of material (impedance)
- Angle of sound pulse strike (incidence)
- Roughness of the medium surface

The remaining energy is reflected from the surface and scattered in all directions. This energy returned to the water is called an echo and the amount of it depends on the material properties and the angle of incidence (L-3 Communications SeaBeam Instruments, 2000).

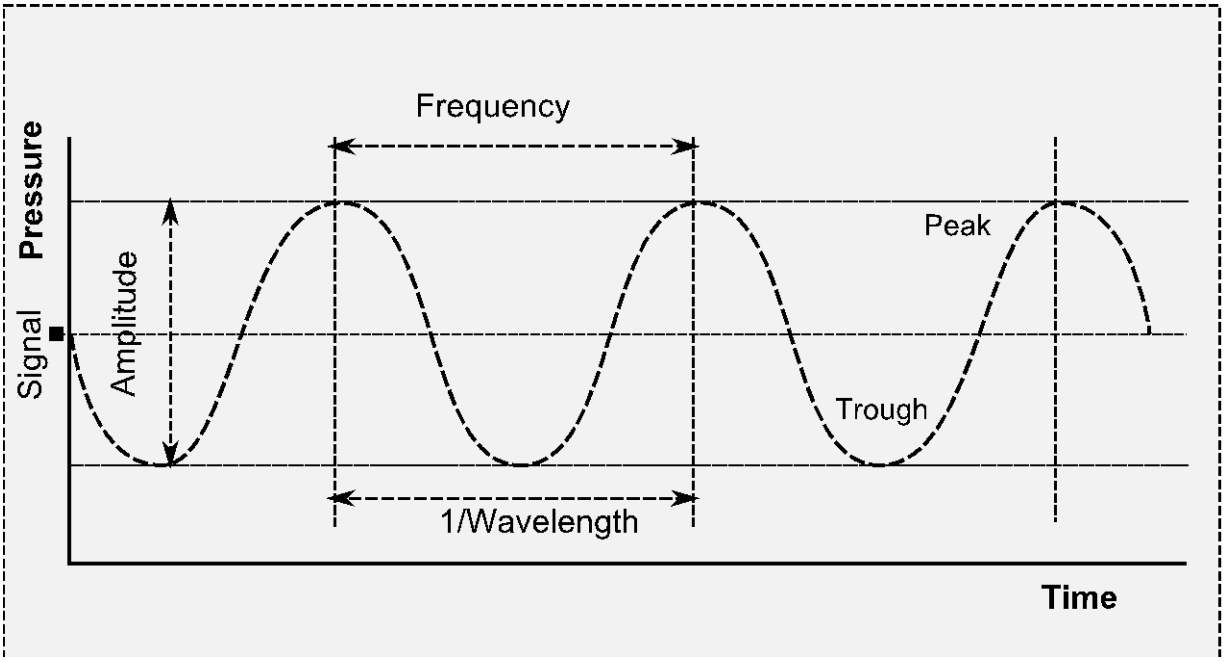

Figure 1 Sound wave components. Frequency is a number of peaks occurring in the time unit, measured as a number of complete sinusoidal cycles in one second (Hz). Wavelength is a distance between two adjacent peaks or troughs in a wave. Amplitude is a size of oscillation, defined as the maximum displacement of a point from the equilibrium. Modified from: L-3 Communications SeaBeam Instruments, 2000; Young & Freedman, 2012; http://www.fao.org/docrep/x5818e/x5818e03.htm#2.7 frequency and wavelength

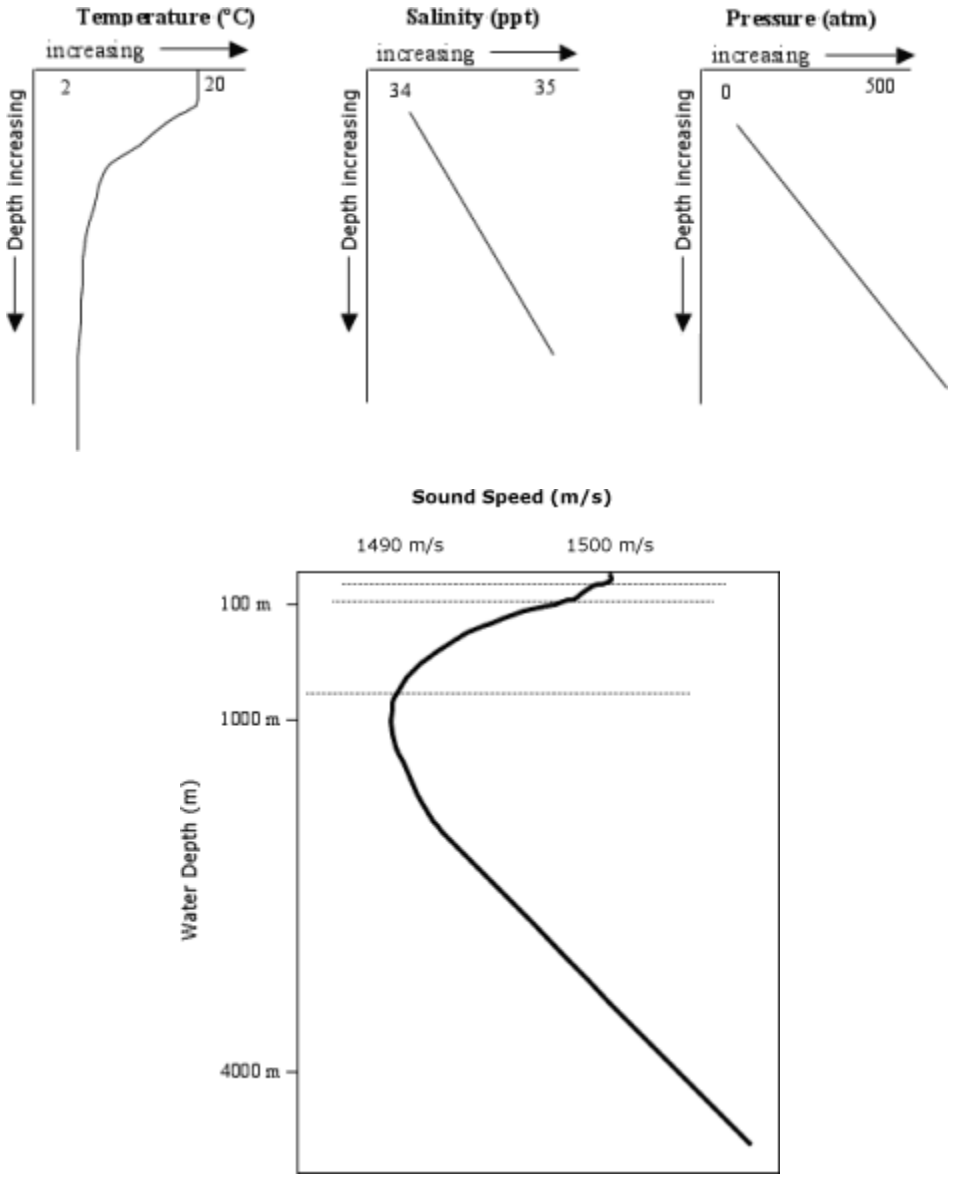

Figure 2 Speed of sound in water. The speed of sound waves propagating through a water column depends on the temperature, salinity and pressure that changes (decrease or increase) with depth. Source: University of Rhode Island, 2013.

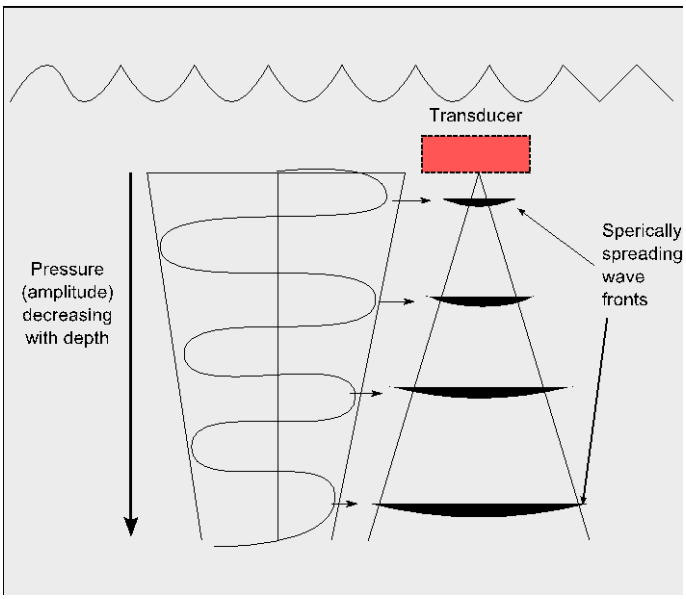

Figure 3 Illustration of how a sound wave spread spherically as a small section of wave fronts from a point source. Because of the attenuation, pressure is transmitted into the water and amplitude decreases. It means that acoustic energy becomes weaker with increasing depth of wave propagation through the water column. Modified from: Benson, 1996; http://www.fao.org/docrep/x5818e/x5818e03.htm#2.4 acoustic pressure and intensity.

2.1.1 Principles of sonar system

Sonar stands for SOund Navigation and Ranging, and it refers to systems that remotely detect objects in water using properties of sound waves. Sonar systems can be divided into devices for just "listening" sounds emitted by objects in water (passive sonars), those that produce sound signals (pings) and then those that listen to their returning echoes (active sonars). Since this research project is conducted using data gathered by a multibeam eco sounder, when refereeing to sonar in the following sections of the thesis, the author means active sonar, specifically echo sounder.

Eco sounders measure the depth of the ocean on the basis of the sound traveling to the bottom and back. The principle of its operation includes two functions: A projector generates a ping, a short pulse of sound, and a hydrophone listens for its returning echo. The projector and hydrophone work analogously to a loudspeaker and microphone, respectively. First the projector converts electrical signals into oscillations, transmitting a pressure wave at a specific frequency into the water. After the sound pulse illuminates the seabed, it returns to the hydrophone, which in contrast to the projector, converts oscillations of the sound wave into voltages. Accuracy of measurement requires that the transducer - both projector and hydrophone - is characterized by precise, controllable and repeatable work. Having registered the "round trip" travel time and accurate value of sound velocity in water, it is possible to find out the distance to the bottom of the sea using following equation:

Equation 2

$$The\ range = \left(\frac{1}{2}\right)\ x\ velocity\ x\ echo\ time\ travel$$

The basic principal for depth calculation presented by the above equation (Equation 2) seems very simple; however the reality brings some obstacles that need to be addressed in order to obtain accurate measurements. (L-3 Communications SeaBeam Instruments, 2000)

There is a variety of effects determined by medium, target and equipment that influence the acoustic energy in water. The Sonar equation (Equation 3) takes those parameters into account and expresses logically their relationship in order to calculate the maximum range of sonar equipment. The basic sonar function is detection of underwater objects, which is achieved by receiving acoustic energy in natural acoustic background conditions. Therefore, the receiver of acoustic energy consists of the desired signal as well as undesired noise. There are many sources of unwanted sounds – ocean waves, marine creatures or research vessels - that affect each stage of the ping cycle process that make up the final signature of the signal. The aim of the sonar is to increase response to the signal and simultaneously decrease response to the noise level. When comparing the signal strength to the noise level, the ratio between them (signal-to-noise ratio) indicates detectability of the real signal. (Urick, 1979).

The signal propagation is influenced by equipment, medium and target, which are expressed as various sonar parameters in the sonar equation. The ping cycle is illustrated in Figure 4. The transducer (projector) produces a signal - source level (decibels per unit time) – which loses some part of energy when propagating through water – transmission loss[2]. When the sound wave strikes the ocean bottom, some part of incident energy is transmitted to the sea floor. The rest of the energy, known as backscattering strength, is scattered or reflected back into the water. The relation between reflected energy and the incident energy is called target strength. Finally, this backscattered signal, which on the way back is influenced again by the transmission loss, together with added noise level represents strength of returning echo at the transducer (hydrophone). The whole process of ping cycle is expressed by following Equation 3:

Equation 3

$$SE = SL - 2TL + TS - (NL - DI + DT)$$

Where: SL – Source Level (amount of acoustic energy generated by projector with initial signal), TL – Transmission Loss, NL – Noise Level, TS – Target Strength, DI – Directivity Index, and DT - Detection Threshold (signal to noise ratio), SE – Signal excess (strength of returning echo).

[2] The amount of transmission loss depend on the distance traveled and it includes spreading loss – effect of energy loss per unit area[2], and absorption loss resulting from attenuation.

More about sonar equation parameters, their definitions, reference locations and terminology combinations in book "*Principles of Underwater sound*" (Urick, 1979)

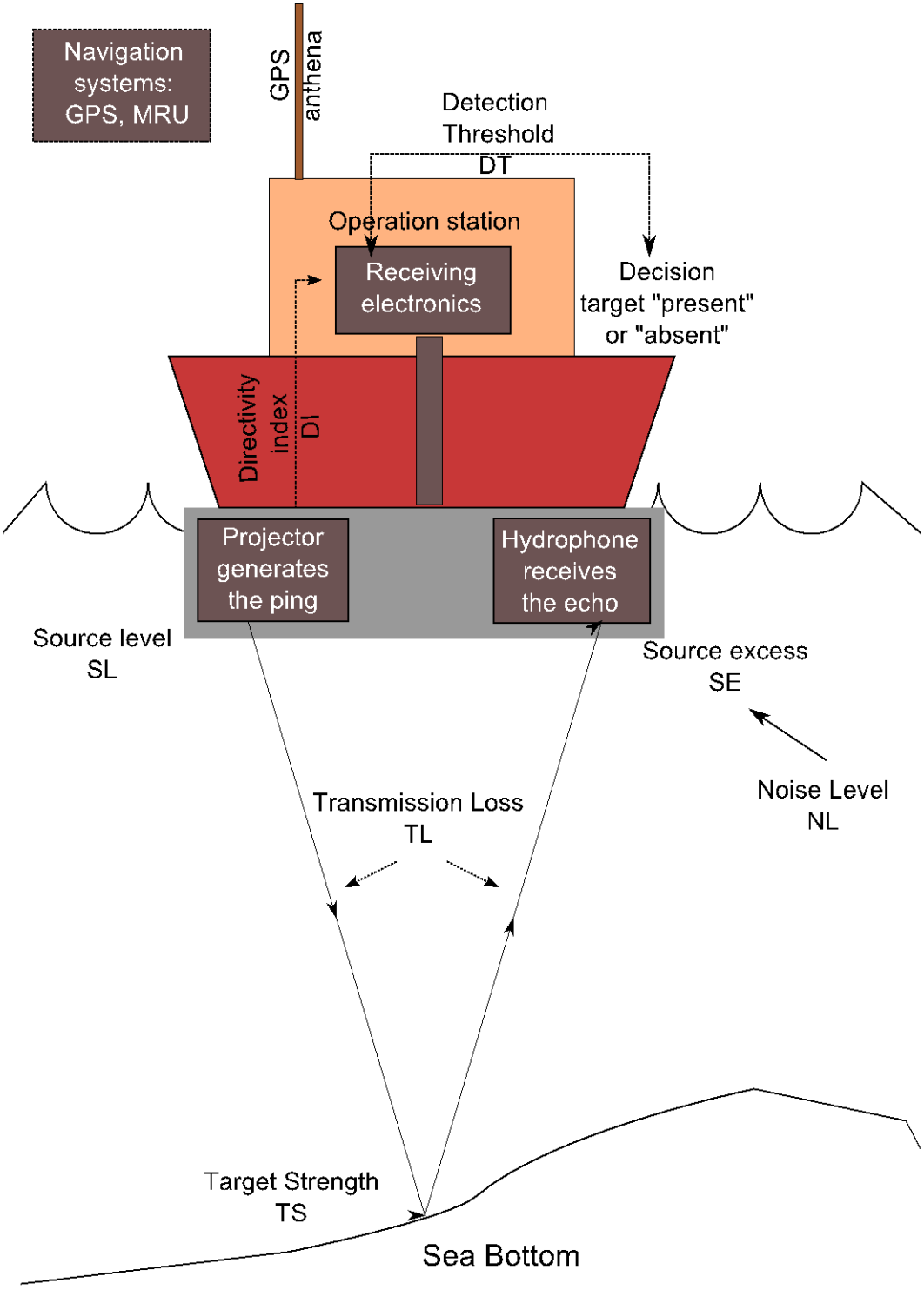

Figure 4 Illustration of ping cycle and sonar equation parameters. Author Karolina Banul. Modified from: Urick, 1979; L3-Communications SeaBeam Instruments, 2000.

The most traditional and conventional sonar system is a single beam echo sounder. Which was originally used by military vessels to detect various objects in the water, particularly submarines. Later this echo sounding system was utilized by hydrographic offices to generate seafloor profiles and to measure the depth of the water directly under the vessel. This instrument operates in a continuous ping cycle (Figure 4) and collects series of single measurements of water depth at many locations. It can be used in both shallow and deep water with different sound frequencies. The spatial resolution of bathymetric data from single beam echo sounder is determined by the sensor, water depth and survey route design, while its accuracy depends on complementary technologies that measure vertical and horizontal position as well as correct soundings for systematic offsets. (Kearns & Breman, 2012)

Measurements made with the single beam eco sounder are based on the assumption that the first echo from a ping determines the range to the bottom below the survey vessel. This creates many limitations in addressing problems such as an irregular sea floor, ship motion effects, and the size of the solid angle. Those in turn influence accuracy of the measurements, and consequently data quality. Those challenges require tradeoffs between the resolution and time-efficiency of surveying, consequently making this instrument unsuitable for large-scale, full coverage sea bottom mapping. Therefore, this situation led to the construction of a more complex system – multibeam echo-sounder - that overcomes accuracy, extent, and time-efficiency limitations of the single beam echo sounder. (L3-Communications SeaBeam Instruments, 2000)

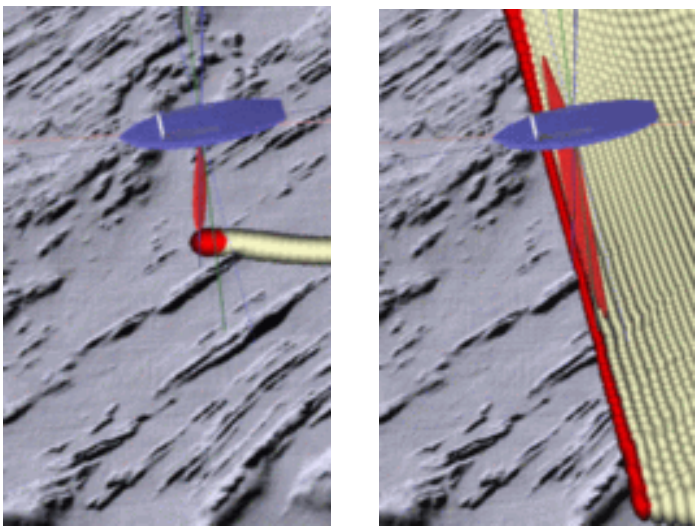

Figure 5 Narrow singe beam (left) and multibeam (right) sonar systems. Source: J.E.Hughes Clarke, OMG/UNG 2012. http://www.omg.unb.ca/omg/SwathSites.html.

2.1.2 Principles of Multibeam

A Multibeam echo sounder works similarly to a narrow single beam instrument, however its revolutionary improvement is the ability to gather echoes not only directly beneath the vessel, but also from off-track areas (Figure 5). It was originally developed for US Navy as a sonar array sounding system (SASS), but nowadays there are many commercially available systems[3] for shallow and deep-sea surveying. The principles of multibeam are illustrated by

Figure 6. The array of acoustic projectors transmit pings generated at equal interval set by the inboard recorder. The series of narrow pulses, usually with angle from 0.5° to 2° (Kearns & Breman, 2012), is arranged as a strip of points, or swath, that illuminates the area of the sea floor. This plane area is subtended by two angles – one in a direction perpendicularly *across-track* to the vessel path (*swath width*) and a second one aligned with the ship's track. Incoming echoes are received by the system of multiple line hydrophone arrays with axis in a fore-and-aft direction. Each returning beam comes from the zone of the sea floor limited by the angles – aligned with the ship's track and in the fore-and-aft direction. However, the recorded signal of acoustic energy come from the square zones delineated by the overlap of transmitting and receiving beams. (Jones, 1999)

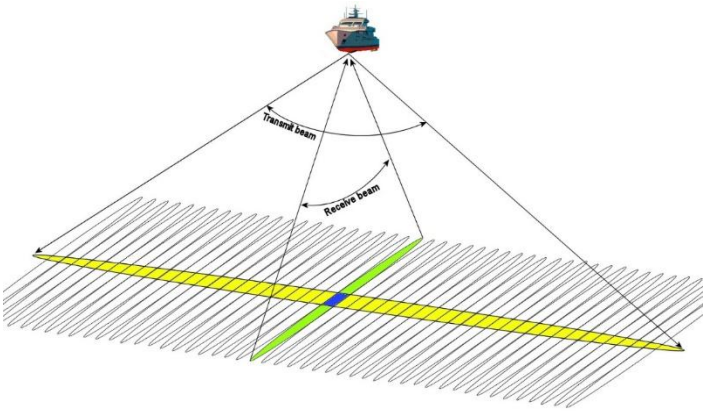

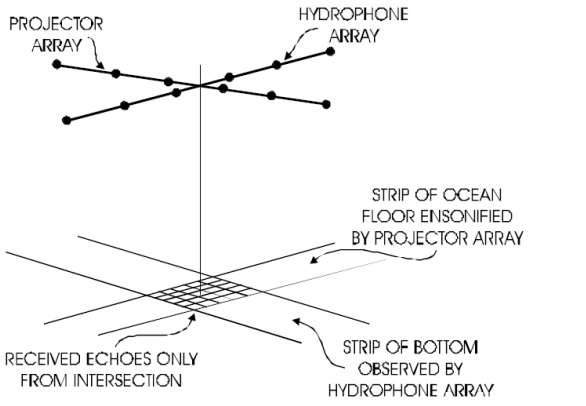

igure Chapter 3 - -20: Projector and Hydrophone Arrays Arranged in a "Mills Cross"

Figure 6 Multibeam swath mapping system. Both images present mills Cross technique applied by Seabeam sensor. Sources: AML Oceanographic, 2014. L-3 Communications SeaBeam Instruments, 2000.

[3] Seabeam, Hydrosweep, Echoes XD, EM Simrad.

In contrast to a single beam sensor, this solution offers the ability to cover wider areas with higher resolution within one survey line. For example Seabeam 2100 system using 151 beams with 1° angle for each ping covers areas up to tens of kilometers wide and a few kilometers deep. The sensor is able to perform this by applying two processes – beam forming and beam steering[4]. Finally,

Figure 6 presents Mille Cross technique to arrange and combine projector and hydrophone arrays in a way that the area illuminated by the projectors will intersect with perpendicular strip of the sea floor observed by the hydrophones. This method is applied by all modern multibeam systems. (L-3 Communications SeaBeam Instruments, 2000)

Distance between the centers of the footprints in each beam accounting for the spatial resolution of collected data depends on swath width and water depth. Also space between survey lines is designed in a way that lines overlap, ensuring complete and continuous coverage of the sea floor. Usually, a 20% overlap is applied to avoid degradation from outer beams and to provide 100% coverage from 60% of center beams. Therefore, this system address both main limitations of the single beam instrument, providing full coverage, high-resolution data in a much more timely and cost-efficient. (Kearns & Breman, 2012)

2.1.3 Data obtained from the Multibeam

Similarly to a single beam sensor, the final product of multibeam is point data, but with much greater volume. Incoming echoes are first registered by the hydrophone in a form continuous voltages representing amplitudes and phases of the signal. This analog data have to convert into discrete digital signals by applying time intervals and separating continuous signals into time slices (Figure 7). Those time slices that contain echoes of single ping creates a ping of data. Further processing reveals the following output: depth measurements with their positions (ranges and angles), and sidescan (intensity) – amplitude of returning echoes. (L-3 Communications SeaBeam Instruments, 2000)

Received signals with various attributes – beam identification, track identification, time and date of survey, vessel type, system model, ship attitude correction and GPS positions. All of this information is applied for cleaning and further processing of the acquired data. (Kearns & Breman, 2012)

---

[4] First process relates to the problem of sound waves that spherically and equally expand in all directions. Having two projectors emitting the identical signal, their wave patterns will interfere in a destructive or constructive way. To avoid this situation. Knowing the wavelength and spacing between projectors, energy pulses can be directed in a way that causes stronger echoes from the ensonified locations. Typically sonar spacing between projectors is equal to half a wavelength, what results in strongest acoustic energy being directed perpendicular to the axis of projector. Second process introduces time delay for the returning beam. It causes that the angle of the axis of the beam pattern can be changed in a way that maximizes its sensitivity to any angle. For more details: L-3 Communications SeaBeam Instruments, 2000.

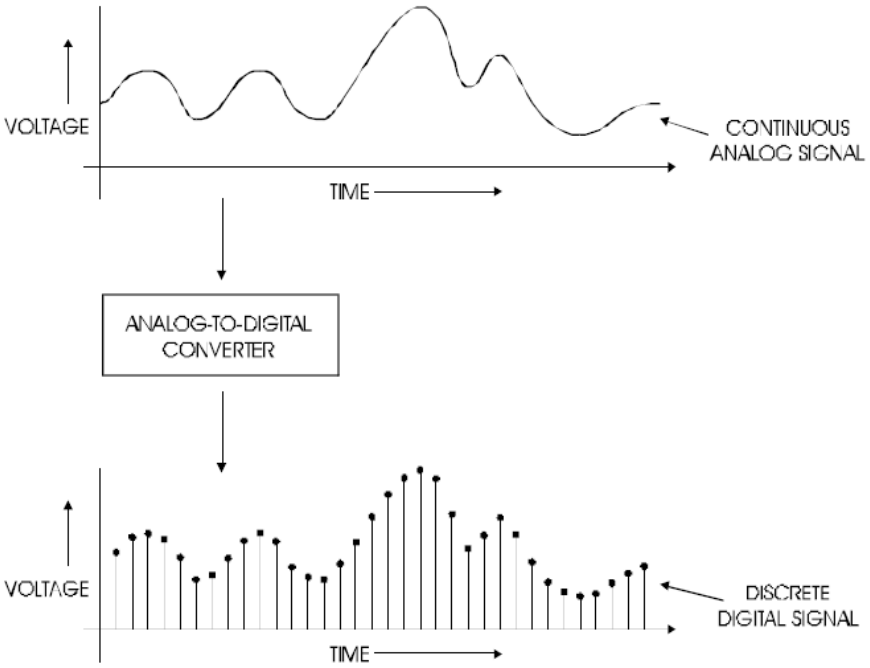

Figure Chapter 4 - -1: Analog-to-Digital Conversion of Hydrophone Data

Figure 7 Analog-to-Digital data conversion. L-3 Communications SeaBeam Instruments, 2000.

2.1.4 Seabeam on the R/V Knorr

In order to acquire bathymetric data, eco sounders are mounted on the vessels that survey the targeted sea floor area from the surface. Data for this research was acquired during two cruises – one in 2007 on the R/V Knorr using SeaBeam 3012-P1 system, and second one in 2013 on the R/V Marcus G. Langseth's ship with Konsberg EN122 sonar type.

R/V Knorr is a US Navy vessel operated for scientific purposes. It was designed and fully equipped with various scientific instruments in order to perform a wide range of oceanographic research such as bathymetry measurements or deep sediments sampling in all world's oceans and in Polar Regions. Installed propulsion systems together with navigation and satellite systems allows the vessel to maintain a fixed position even in rough seas and difficult weather conditions. (Woods Hole Oceanographic Institution [WHOI]a, n.d.). More vessel specifications can be found on the operator website.

SeaBeam 3012-P1 multibeam echo sounder is mounted under the vessel's hull (See Locations of the Knorr Sensors in Appendix 1), and it includes projectors and hydrophones. Beside the transducer, the complete system onboard includes the processing unit and operation station, as well as a navigation system consisting of GPS and Motion Reference Unit, which accounts for a position and altitude of the ship. An Additional Unix workstation with MB-System was installed onboard to allow processing and display of bathymetry and side-scanning data (WHOIb, n.d.).

Detailed specification of the transducers used to acquire the data for the project is presented in Table 1. Navigation instruments include the following: Satellite navigation (GPS antennas), Gyro compass, Speed log and Radar, as well as dynamic positioning system (WHOIc, n.d.).

2.1.5 Kongsberg on the R/V Marcus G. Langseth.

R/V Marcus Langseth is operated by Lamont-Doherty Earth Observatory's Office of Marine Operations. It is equipped with various scientific instrumentation that provides extensive geophysical and seismic capabilities to conduct seismic surveys, collect samples of sediments, or to use the remote operated vehicles (ROV). Scientific instrumentation mounted on the vessel includes: Multibeam echo-sounders - Kongsberg EM-122 and Simrad deep ocean bottom swath mapping systems, and a Syntrak 960-24 seismic recording system. Position and navigation for all surveys are controlled by two independent GPS systems – primary C-Nav and secondary Seapath (Lamont -Doherty Earth Observatory, 2013). More vessel specifications and positioning systems can be found on the operator website – Office of Marine Operations.

2.1.6 Kongsberg on R/V Árni Friðriksson RE 200

R/V Árni Friðriksson RE 200 was designed for fisheries and oceanographic research. It is prepared to work in arctic waters and is equipped with various scientific instrumentation for tasks such as stock assessment, bottom research and communications. The electronics include echo sounders - Simrad EK60 and Kaijo Denk Sonar - for fisheries applications, as well as multibeam sonar Kongsberg EM300 for sea floor mapping. In addition, the vessel has Teledyne acoustic Doppler current profiler (ADCP) that records water current velocities at different depths and measures vessel movement, speed and direction. The communication is provided by satellite phone and internet connection, as well as Global Maritime Distress and Safety System (GMDSS)[5]. Other instrumentation include drop keel (lowered 3.2 m below the ship) for the echo sounder transducer, which eliminates flow noise and influence of wave action, and various towing and scientific winches, including CTD winch[6]. (Marine Research Institute [MRI], n.d.)

[5] Developed by International Maritime Organization (IMO) GMDSS is an integrated communications system using satellite and terrestrial radio communications to ensure that aid can be sent wherever ship is located. Under the GMDSS requirements, vessel has to be equipped with Inmarsat and/or NAVTEX receivers, to automatically provide Maritime Safety Information (MSI) – both meteorological and navigational information. For more information see Joint WMO-IOC Technical Commission for Oceanography and Marine Meteorology website: http://weather.gmdss.org/gmdss.html.

[6] It provides conductivity, temperature, and depth profiles while vessel is moving. See: http://www.oceanscience.com/.

Table 1 Technical specifications for multibeam systems.

Manufacturer	Kongsberg Maritime	L-3 Elac Nautik	Kongsberg Maritime
Product name	EM302	Seabeam 3012-P1	EN122
System Parameters:			
Frequency (kHz)	30 kHz	12 kHz band	12 kHz band
Depth Range, depth resolution	10 to 7000 m	50 – 11000 m	20 to 11000 m
Max. Swath coverage	8 000 m 5.5 x waterdepth	Approx. 31 000 m, > 140^0	Approx. 30 000 m 6 x Depth,
No beams per swath	144 or 288 per swath	250 individual beams (301 beams - maximum at equiangular mode)	144 or 288 per swath
Number of soundings per swath/ ping cycle	2 swaths per ping cycle, with up to 864 soundings.	/918 (multi-ping)	Up to 432/Up to 864 (multi-ping)
Beam width (degrees)	Across: 0.5, 1, 2, or 4^0 Along: 1, 2, or 4^0	Across: 1 or 2° Along: 1 or 2°	Across: 0.5, 1, 2, or 4^0 Along: 1, 2, or 4^0
Beam spacing	Equidistance or equiangular	Equidistance or equiangular	Equidistant on bottom/equiangular
Other specifications:			
Side-scan data possibility	Yes,	Yes	Yes, sidescan pixels for every ping cycle
Accuracy:	In accordance with IHO standards for depths greater than 100 meters		
Motion compensation (MRU)	Yaw. ± 10 degrees; Pitch. ± 10 degrees; Roll ± 15 degrees	Yaw. ± 5 degrees; Pitch. ± 7 degrees; Roll ± 10 degrees	Yaw. ± 10 degrees; Pitch. ± 10 degrees; Roll ± 15 degrees
Source:	http://www.km.kongsberg.com/ks/web/nokbg0240.nsf/AllWeb/871B055B3DE0DAC3C125715E002B5C68?OpenDocument	http://www.elac-nautik.de/_uploads/images/pdf/L3_ELAC_Nautik_SeaBeam3012.pdf	http://www.km.kongsberg.com/ks/web/nokbg0240.nsf/AllWeb/01FB0F22974EA50FC125715E002B2143?OpenDocument)

2.2 Reykjanes Ridge

Reykjanes Ridge – part of the Mid-Atlantic Ridge (MAR) that connects to the Reykjanes Peninsula - is recognized as especially important to study mid-ocean ridge processes (Höskuldsson, Hey, Kjartansson & Guðmundsson, 2007) and morphological structures - characteristic for both slow and fast spreading centers – as well as to understand plume-ridge interactions (e.g. Smith, Humphris & Bryan, 1995; Appelgate & Shor, 1994; Magde & Smith, 1995). Therefore, multiple studies have been conducted in this area, such as seismic, magnetic and gravity surveys, extracting sediments and core samples from the seafloor, and bathymetric measurements[7] (Atkins, 2013).

2.2.1 Mid-Atlantic Ridge and Reykjanes Ridge

MAR is one of the main oceanic structures in the Atlantic. It spreads along 60,000 km and its central rift is characterized by a steep walled valley, approximately 1 km deep and 30-50 km wide. While crest morphology is rather rugged, the flanks are characterized by smooth slopes resulting from sedimentation processes. The origin of MAR is proven to be a result of sea-floor spreading, which in turn is a sign for divergent movement of tectonic plates of Earth crust. Shallow earthquakes and volcanic activity often occur in this area. The entire MAR is divided into segments – fracture zones – that vary with morphological structures and length from 300-500 km long. Spreading rate is between 1-10 cm per year, and depth is rather uniform between 2500-3000 meters, except much shallower in the northern part, which is related to the "hot spot" located in Iceland (Seibold & Berger, 1993).

The Reykjanes Ridge is a small part of the MAR that connects Bright Fracture Zone at 57°N with the Reykjanes Peninsula at 64°N (Figure 8). It extends 900 km northeast towards Iceland, which itself is an exceptional example of uplift above the sea level extension of MAR. The southern part of the Reykjanes Ridge is a transition zone, where rifted structure of MAR changes to non-rifted landforms. (Voght, 1986; Keeton et al., 1995)

7 Detailed description of various research studies conducted in the area can be found in the master thesis: Exploration Techniques for Locating Offshore Geothermal Resources by Atkins, 2013.

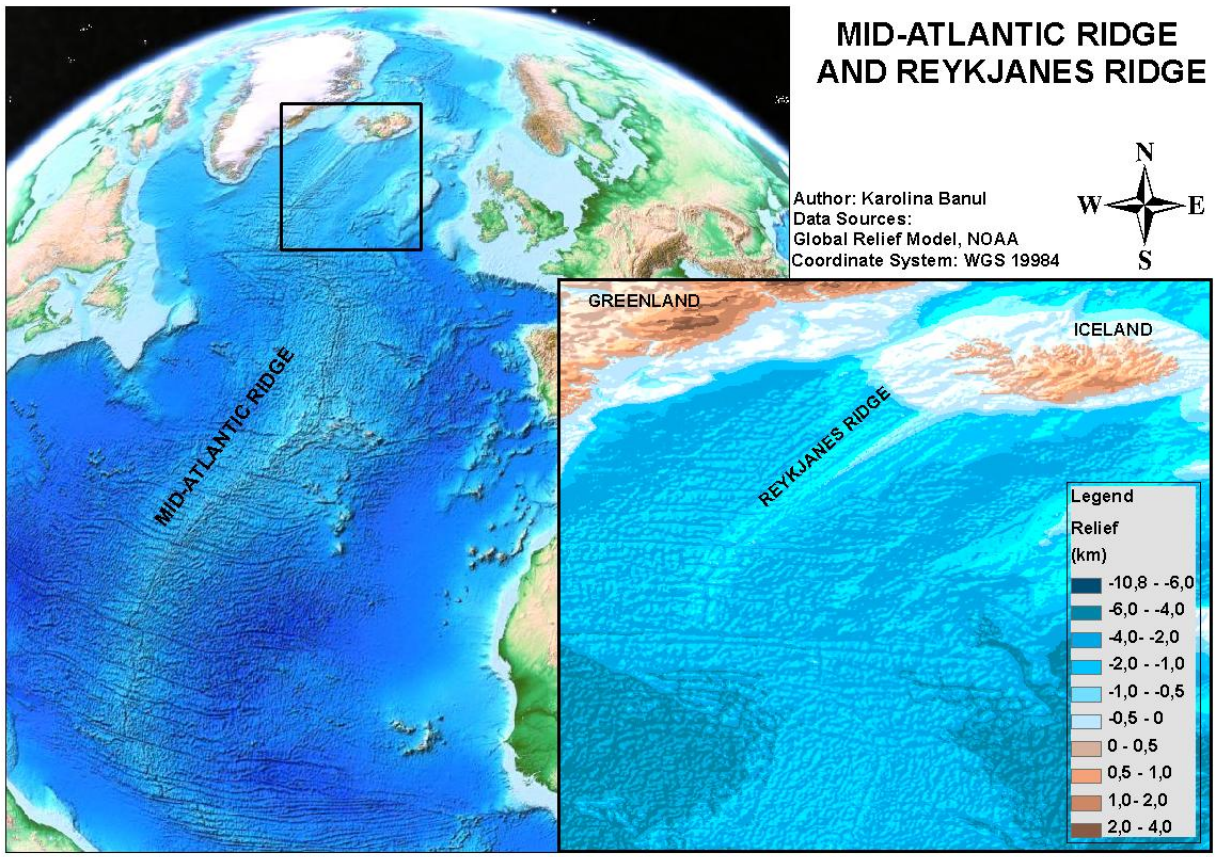

Figure 8 Location of the Reykjanes Ridge in a perspective of the Mid-Atlantic Ridge.

2.2.2 Topography and Morphology

Bathymetric surveys (Table 2), which has been conducted since the 1980's with gradually improving surveying and mapping technology, reveals the topography of the Reykjanes Ridge (Figure 9) (Voght, 1986; Keeton et al., 1997; Höskuldsson et al, 2007). The main characteristics of the ridge's structure include gradual shallowing of water depth from south to north, oblique pattern of spreading center, and transition from crest with medium valley to axial high (Voght, 1986). Bathymetric surveys show that axial depth increases from sea level at 63^0 50' (Reykjanes Peninsula), via 800 m at 62^0 N, up to 2600 m at 56^0 50'N (Bight transform fault). The orientation of the spreading center is oblique with average 27 degree to the normal orientation of MAR and spreading rate of 20 mm per year. This shapes an en-echelon pattern of axial volcanic ridges (AVR). While moving towards Iceland, there is a transition from an axial valley - typical for slow spreading MAR - to an axial high occurring at around 59^0 N. This form of the crest, usually characteristic for fast spreading ridges, is associated with the proximity to the mantle plume located under Iceland (Keeton et al., 1997; Searle et al., 1998; Höskuldsson et al, 2007).

Table 2 Bathymetric surveys conducted over the Reykjanes Ridge between years 1990–2005.

Year of survey	Geographic extent	Type of multibeam sensor	Author
1990	55°50'N and 63°00'N, single track line short survey at 59°50'N extended coverage to 15 km on either side of the neovolcanic zone	SeaMARC II - shallow-towed 11-12 kHz swath seafloor imaging Hydrosweep seafloor imaging system -15.5 kHz hull-mounted multinarrow beam bathymetry system that samples a swath width twice water depth ,	Appelgate & Shor, 1994
1990	3 areas, centered at 58°N, 60°N, 62°N.	Hydrosweep multibeam sonar system – returns 59 cross-track depths for every sounding ping. The swath width is about twice the water depth. British towed ocean bottom instrument (TOBI) deep-towed side scan sonar system.	Magde & Smith, 1999 Smith, Humphris, & Bryan, 1995 Searle, Field & Owens, 1994
1990, 1993, 1994	57°30'-62°00N, extending 30-100 km off-axis	Simrad EM12S-120 multibeam echo sounder, at 13 kHz with 81 beams. Swath width of 3.5 times the water depth.	Keeton et al. 1997
2005	63°44'N and Reykjanes Peninsula	Kongsberg-Simrad EM300 high-resolution multibeam, 30 kHz with an angular coverage sector of Up to 150◦, resulting in swath widths that can be more than four times the water depth. For each ping, 135 beams are recorded.	Höskuldsson et al., 2007

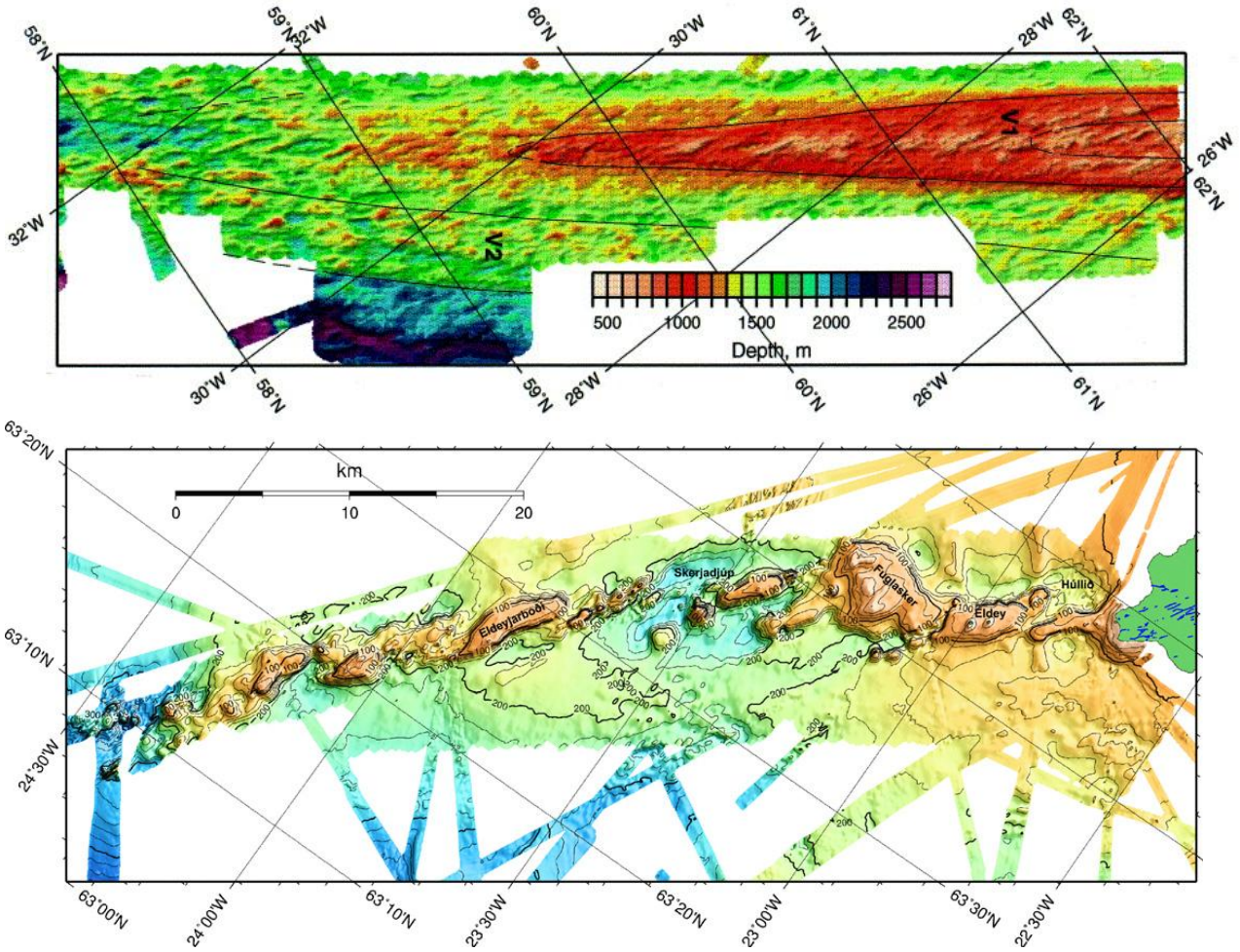

Figure 9 Topography of the Reykjanes Ridge. Upper image shows southern region, while lower image presents northern, connecting to Reykjanes Peninsula (Searle, 1998; Höskuldsson, 2007).

Morphology

Identified landforms (Table 3) such as V-shaped ridges (chevrons) converging southwards, an en-echelon pattern of axial volcanic ridges, and a higher density of seamounts than elsewhere in MAR are believed to be related to plume-ridge interactions, especially the elevated temperature causing enhanced melting and lower density of crust (Höskuldsson et al, 2007). Additionally, gravity and seismic data revealed that crustal thickness decreases with distance away from mantle plume located under Iceland. The Reykjanes Ridge crust is around 10 km thick, while an average oceanic crust is approximately 6 km (Smith et al., 1995). En-echelon arrangement of AVR is present along the whole length of the ridge, but there is much variation in height of AVR – from max 500 m in the south to 60 m in the North. Tectonic features include normal fault scarps that are directed towards the ridge axis. Their amplitude decreases northwards, and spacing between major faults decreases from BTF in the north direction (from 13 km near 58°N to 8 km near 59°N), but they increase again to 14 km at 62°N. There were no transform faults identified (Searle et al., 1998). Bathymetric data identified that chevron ridges are actually comprised of multiple, closely-spaced small ridges that, in turn, are composed of independent

fault blocks on the surrounding seafloor. In addition, seismic and gravity data revealed that chevrons have a 2 km thicker crust then neighboring areas (Searle et al., 1998).

Table 3 Landforms characteristics over the Reykjanes Ridge acquired from bathymetric maps.

	Keeton et al., 1997; Magde & Smith, 1995	Höskuldsson, 2007
Area:	58°-62°N	63°N – up to Reykjanes Peninsula
Axial Volcanic Ridges	No: 42 Length: 40-10 km Width: 4.5-1.5 km Height: 400-200 m above sea floor	No: 10 Length: 24.9-8.8 km Width: 7.1-1.6 km Height: max 190 above sea floor
Seamounts	399 with height from 50 to above 250 m	3 seamounts with height from 60-200 m
Faulting	Inward-facing normal fault scarps, with amplitude of faulting decreasing with proximity to Iceland. From max nearly 1 km at 58°N, to less than 100 m in the north.	

Segmentation

In four scales of segmentation for MAR, the Reykjanes Ridge displays similarity to 3rd order segmentation, such as small gaps between en-echelon AVR, but evidence for 2nd order axial offsets was found at transition zone around 58°N (Searle, 1994). In general, only four spreading segments were found between 58°- 62°N with a length of 60 - 170 km, which is much longer than the average, slow-spreading MAR (Searle et al., 1998).

2.2.3 Volcanic activity

The extensive record of volcanism from the last millennium reported submarine eruptions (Figure 10) occurring almost every century southwest from the Reykjanes Peninsula (Höskuldsson, 2007). Volcanic events were accompanied by ash falls, earthquakes and even cases of island formation. An Eruption in 1211 resulted in creation of new island – *Eldey* and rocks, currently called *Eldeyar* and located 7-16 km away from Reykjanes Peninsula. Another island – *Nyo* - was formed in an explosive eruption in 1783. Currently it is hidden 9-55 meters

under the sea surface as a submerged reef (Voght, 1986b). The last submarine volcanic eruption was reported in 1926, but recently discovered young lava flows[8] in the area at 59°87'N suggest possible volcanic activity on the Reykjanes Ridge. However, to confirm this hypothesis, further investigations in this area are necessary (Global Volcanic Program [GVP], 1992).

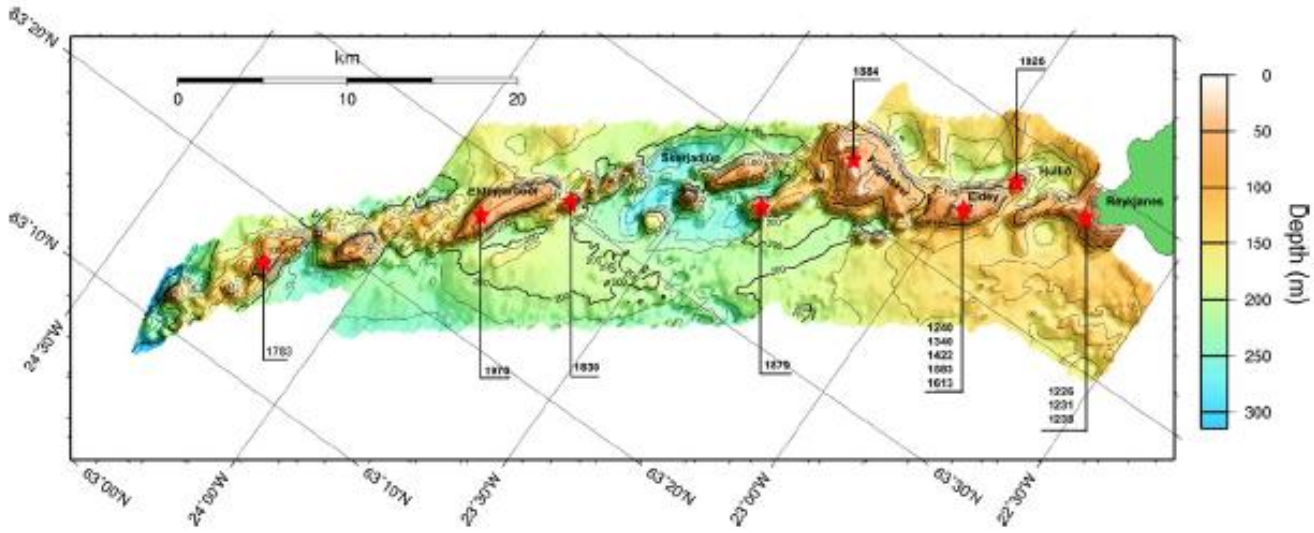

Figure 10 Historic volcanic activity along the Reykjanes Ridge. Source: Höskuldsson et al., 2007.

2.2.4 Earthquake activity

Although volcanic activity along the Reykjanes Ridge rarely occur, earthquake events are much more frequent. Daily information about the seismic activity in the area can be obtained from the Icelandic Meteorological Institute[9]. Many earthquakes with magnitude larger than 3.5 were registered by global, land-based seismic stations in the last 20 years (Figure 11). Also research using Ocean Bottom Seismometer revealed information on intense micro-earthquakes[10] (less than 2.0 magnitude and rarely felt further than 10 km away from epicenter) in the area. Finally, more than 800 events grouped into 5 sequences were registered by the SIRENA system between May 2002 and September 2003. Events with moderate to large magnitude (4.0-5.6) occurred at locations between 57-61^{0} N. Because they could not be described in terms of "mainshock-

[8] The deep-diving submersible observations identified lava flows without sediment cover and biological colonization, what suggest its young age from 10-20 years. See more: *Additional Report for Northern Reykjanes Ridge*, http://volcano.si.edu/world/vol_extra.cfm?name=Northern_Reykjanes_Ridge.

[9] *Reykjanes ridge - earthquakes during the last 48 hours*, http://en.vedur.is/earthquakes-and-volcanism/earthquakes/reykjanesridge/#view=map, Iceland Geology news, http://www.jonfr.com/volcano/. Recently the system register stronger seismic activity (magnitude 3.5) in the area at the beginning of April 2014. See news: http://www.visir.is/kroftug-skjalftahrina-vid-geirfugladrang/article/2014140409602.

[10] More about results from research on micro-earthquakes in article: *Detailed distribution of micro-earthquakes along the northern Reykjanes Ridge, off SW-Iceland* by *Mohizuki et al. 2000*. http://onlinelibrary.wiley.com/doi/10.1029/1999GL011264/abstract

aftershock" sequence, earthquake swarms were interpreted as driven by magmatic processes, rather than tectonic (Goslin et al., 2005).

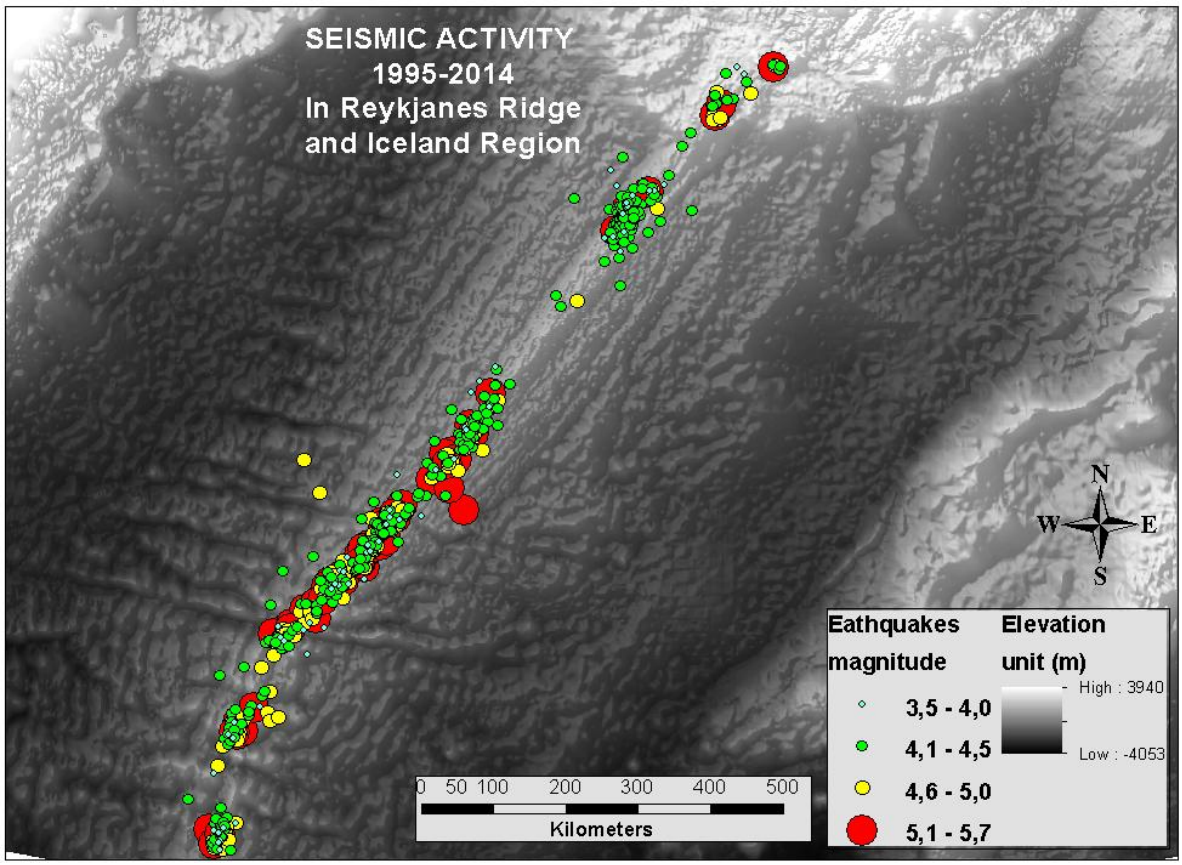

Figure 11 Seismic activity along the Reykjanes Ridge between years 1995-2014. Information recorded by USGS. Only events with magnitude larger than 3.5 mb are presented on the figure. ("Earthquake Hazard Programme", 2013 http://earthquake.usgs.gov/earthquakes/?source=sitenav)

2.2.5 Petrology

Deep drilling projects and dredging over the Reykjanes Ridge brought new information on composition and structure of the rock from the oceanic crust in this area (Atkins, 2013). The dominating rock type is pillow basalts formed by rapid cooling of extruded lava from the oceanic crust and tuff, which originates from the consolidation of volcanic ash. The age of the rock samples taken from the ridge is very young in geological terms - less than 10.000 years. This can also be recognized from the small amount of sediments, which gradually increase with distance from the ridge (Voght, 1986c). The mineral components of samples extracted from the seafloor are olivine, plagioclase and clinopyroxene. Moving northwards, crystal fractionation, which is linked to change in crustal thickness and melts supply, removes part of those elements from the rock. (Murton, Taylor & Thirlwall, 2002)

Even though bathymetry is a part of hydrography, maps of the sea floor are basic data to detect and identify various landforms. Landforms, on the other hand, are important evidence for various earth forces that create them. For example seamounts and ridges are of volcanic origin, while faults are tectonic formations. Detailed bathymetric maps therefore help to trace the observable signs of the endogenous Earth processes.

3 Methodology

In order to create a high-resolution model of the Reykjanes Ridge using multibeam sonar data and analyze potential morphological changes over time, a sequence of four research phases were performed, from data gathering, through its processing, and final analysis (Figure 12). The first phase includes preprocessing of raw data into usable format – both bathymetry soundings and backscatter images were corrected and exported into the format that may be harmonized with other datasets. The second phase includes harmonization of datasets formats, data gridding and modeling of digital elevation models for all datasets, as well as combining all maps to create comprehensive surface model over the ridge. The third phase comprises analysis of the ridge surface based on the created topographic maps. The first part of the analysis includes identification of volcanic features and their description. The second part of the analysis is a comparison of the time separated bathymetric maps, both a visual, 3D comparison as well as a raster-based analysis. The fourth and final phase includes the results, interpretation, and conclusions critically-drawn from the presented results.

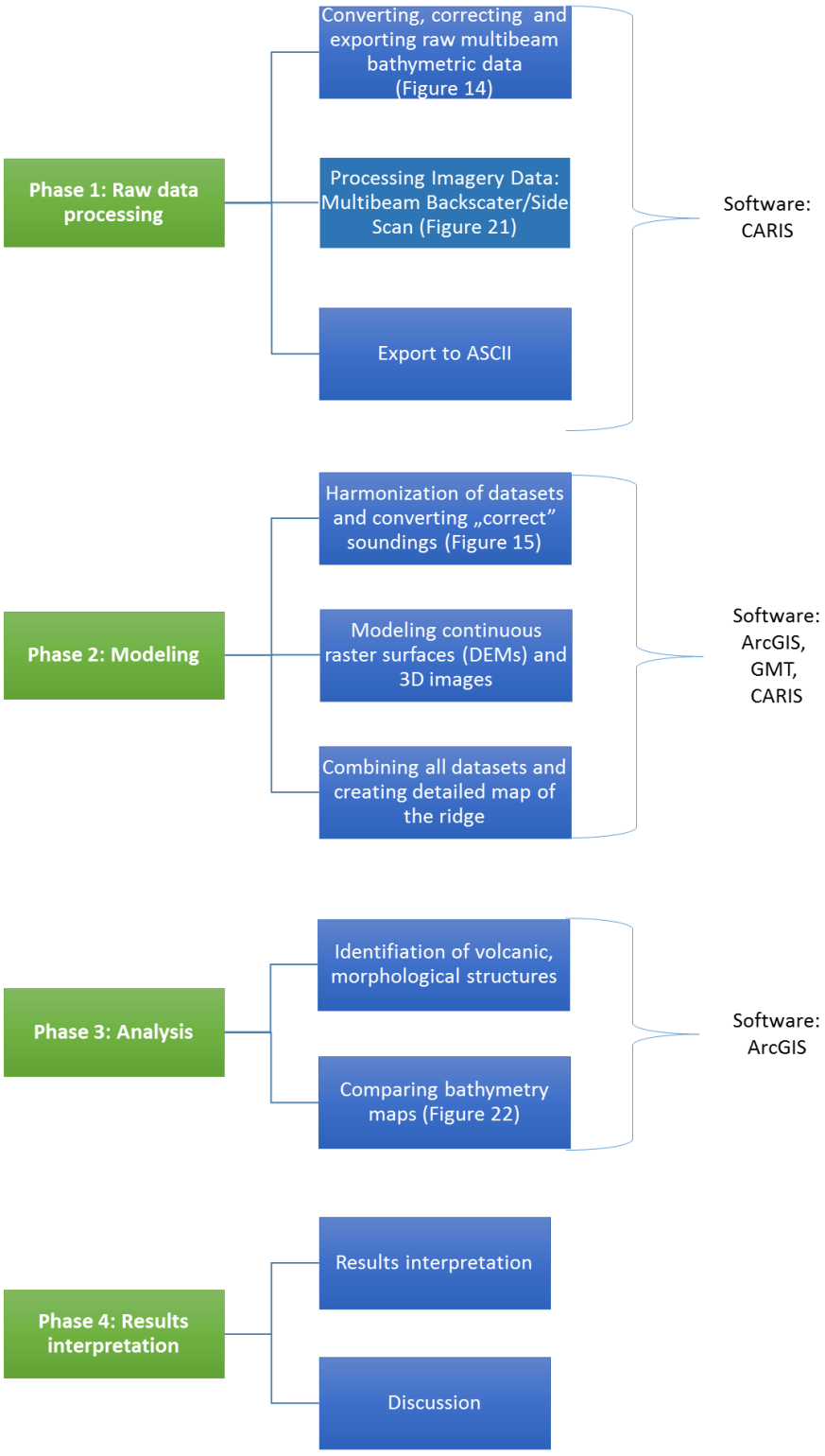

Figure 12 Flowchart of the research working procedure and major components.

3.1 Data acquisition

The raw multibeam data used in this research was acquired by three bathymetric surveys conducted over the Reykjanes Ridge from 2006-2013 (Figure 13). Information collected in all three cruises are presented in the table below (Table 4), while specific information about sonar systems used for data gathering is described in previous chapter.

Table 4 Details of bathymetric surveys over the Reykjanes Ridge that gathered multibeam data used in this research.

Date	Extent	Ship	Multibeam system	Overlap between track lines
2013	55º51' - 64º13'N 22º45' - 36º11'W	R/V Marcus G. Langseth	Kongsberg/Simrad EN122	20 %
2007	61º25' - 65º32'N 16º24' - 31º06'W	R/V Knorr	SeaBeam 3012-P1	20%
2006	62º30' - 63º00'N 24º39' - 25º29'W	R/V Árni Friðriksson RE 200 /2350	Kongsberg/Simrad EM 302	20%
1994	58º00' - 62º05'N	RRS Charles Darwin	Kongsberg/Simrad EM12S-120	50%

The first survey was conducted in 2006, aboard the Icelandic research vessel R/V Árni Friðriksson RE-200. It covered relatively small area between 62º30'N and 63ºN latitude and 24º39'W – 25º29'W longitude. The survey track lines were acquired with the Simrad EM302 instrument that operates at 30 kHz frequency and receives 288 beams per ping. The second survey, aboard the American research vessel R/V Knorr, covered a much wider area, with track lines extending between 61º25'N- 65º32'N and 16º24'W-31º06'W. It was gathered with SeaBeam 3012-P1 echo sounder operating at 12 kHz frequency with 121 beams per each ping. The last survey was conducted on board of R/V Marcus G. Langseth in summer 2013. The vessel gathered data with the Simrad EM122 instrument (12 kHz, 288 beams per ping). The two most recent surveys gathered not only information about depth, but also intensity reflection. Different sonar instruments were however applied during each of the surveys, resulting in data acquisition of various resolutions[11] as well as different levels of detail.

An auxiliary source of information used in this study is bathymetric data from a British survey conducted over the study area in 1994, as a part of the BRIDGE programme. This data was also gathered with a multibeam system (Simrad EM12S-120 operating at 13 kHz with 81 beams per each ping) over more than 500km of the Reykjanes Ridge's length (from 58º00'N to 62º05'N) with an extent minimum of 30 km on each side and up to 100 km off the main track. Line spacing from 3.5 to 5 km provided up to 50% overlap in deeper parts of the surveys area (Keeton

[11] http://www.ldeo.columbia.edu/~dale/projects/multibeam-support/2010-11-17/US-Research-multibeams-full.html

et al, 1997). Because the instrument collects smaller amounts of data points in every swath, the resolution of the data (120 m) is coarser than those from the latest surveys. However, it covers the wide area and provides good background information.

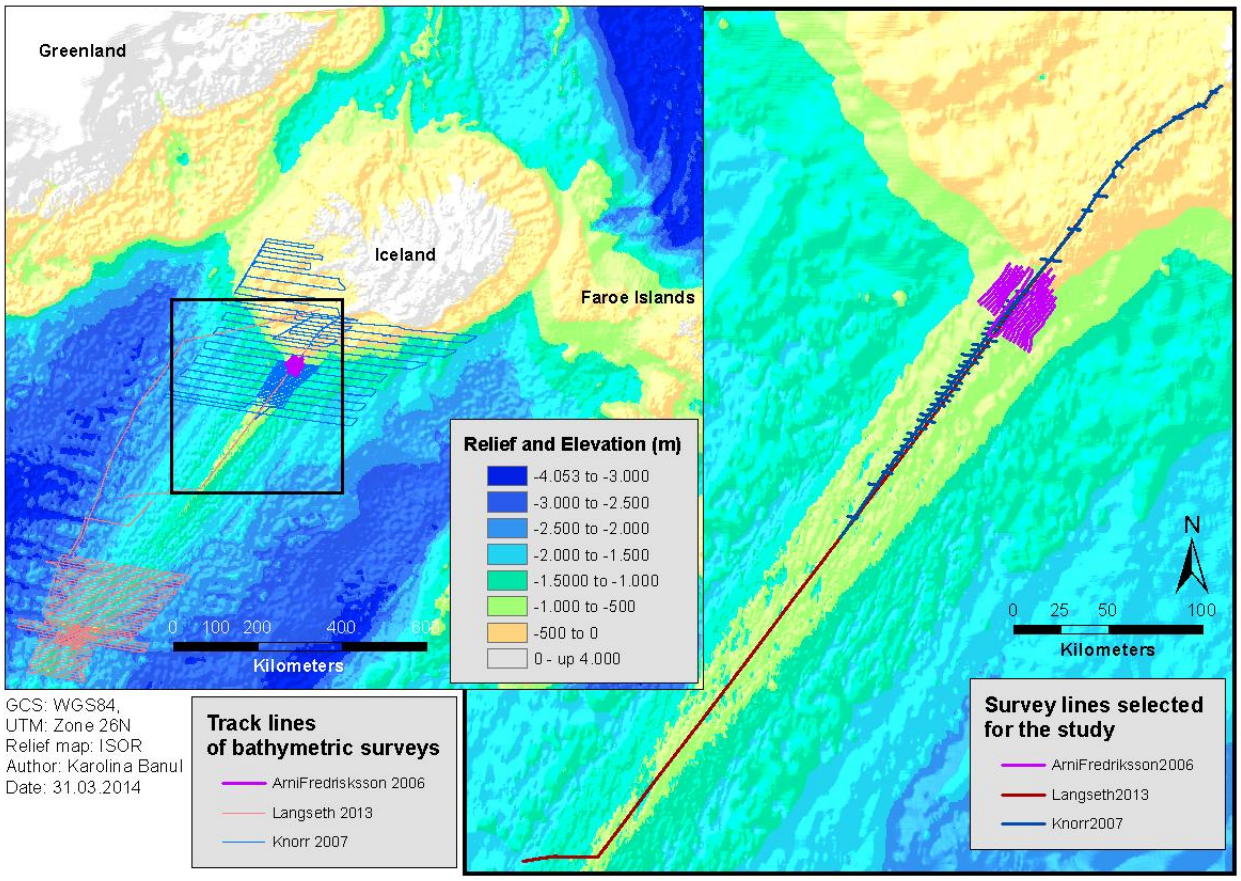

Figure 13 Ship track lines of bathymetric surveys conducted across Reykjanes Ridge in 2006, 2007, and 2013 respectively. Thicker lines on the map in the right are track lines used for this project.

3.2 Multibeam data processing

Obtaining correct depth measurements from a multibeam system is certainly more efficient and accurate than from a single beam system. But the processing stage - identification of correct soundings and their value calculation – appears to be much more of a complex procedure (Figure 14). According to Artilheiro (1998), oblique shapes of transmitted beams as well as involvement of other auxiliary sensors are the potential sources for increased uncertainty of results. Therefore, precise and careful processing of the raw data is a crucial step for further analysis of soundings and the quality of final products, such as bathymetric or nautical maps.

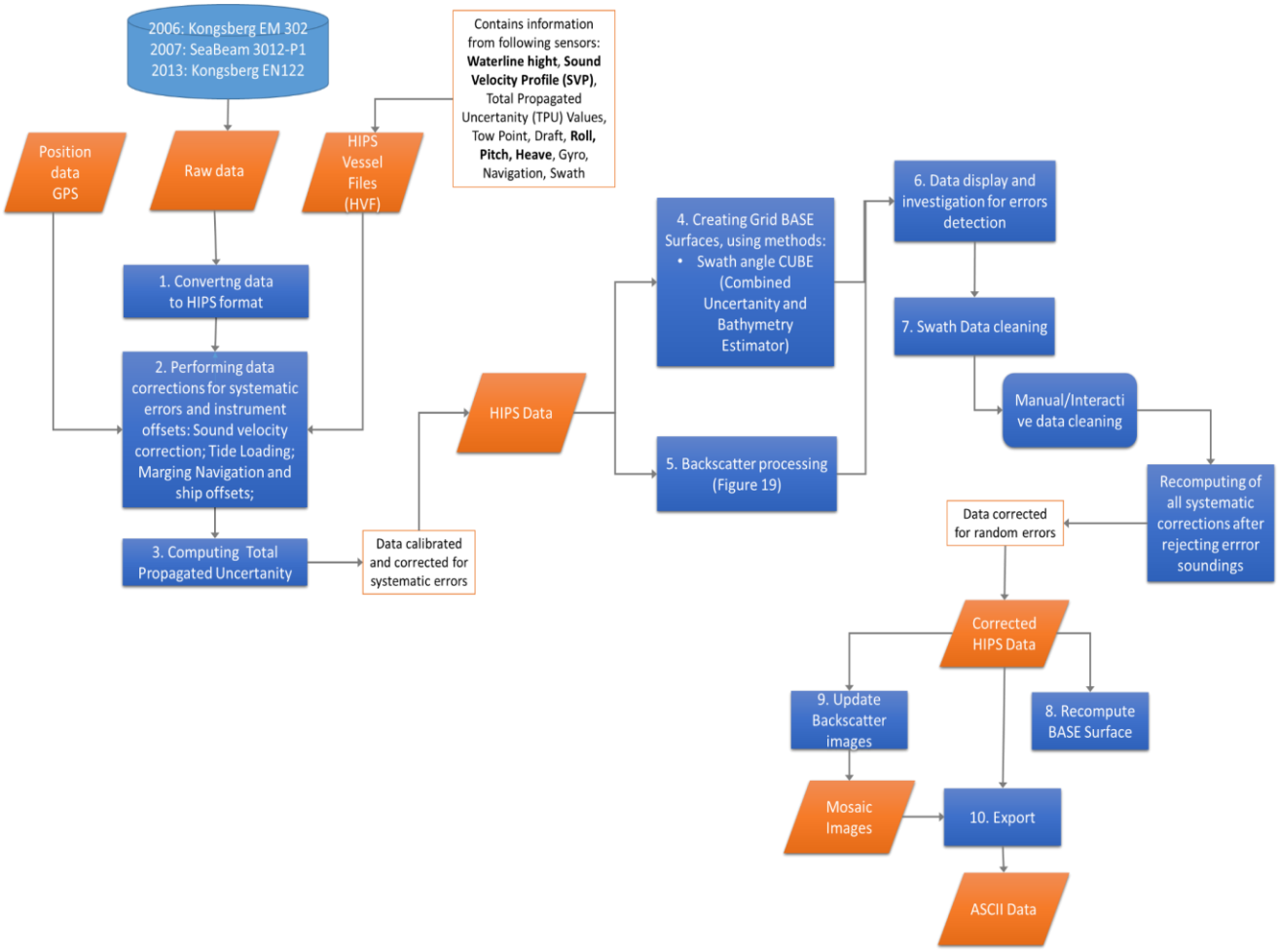

Figure 14 Multibeam data processing in Caris. Orange boxes show the data type and information applied. Blue boxes indicate processing stage. The boxes with orange outline describe what information data file contain.

3.2.1 Data converting and exporting

Because of various manufacturers of multibeam instruments[12], using diverse acquisition software for data conversion is an essential step for further data processing and mapping (Figure 15). Data conversion is the process of translating from one data format, which was used by the instrument to acquire data, to another preferred format that will allow unification of sonar data from various periods of time and sources into one project (GEBCO, 2013). Because data used for this study was gathered with two different multibeam systems, it had to be encoded. This was done with Caris software that converts from swath data formats - Elac/SeaBeam (.XSE) and Simrad/Kongsberg (.ALL and .WDC) - into the same HIPS format in order to conduct corrections and data cleaning (Caris, 2011).

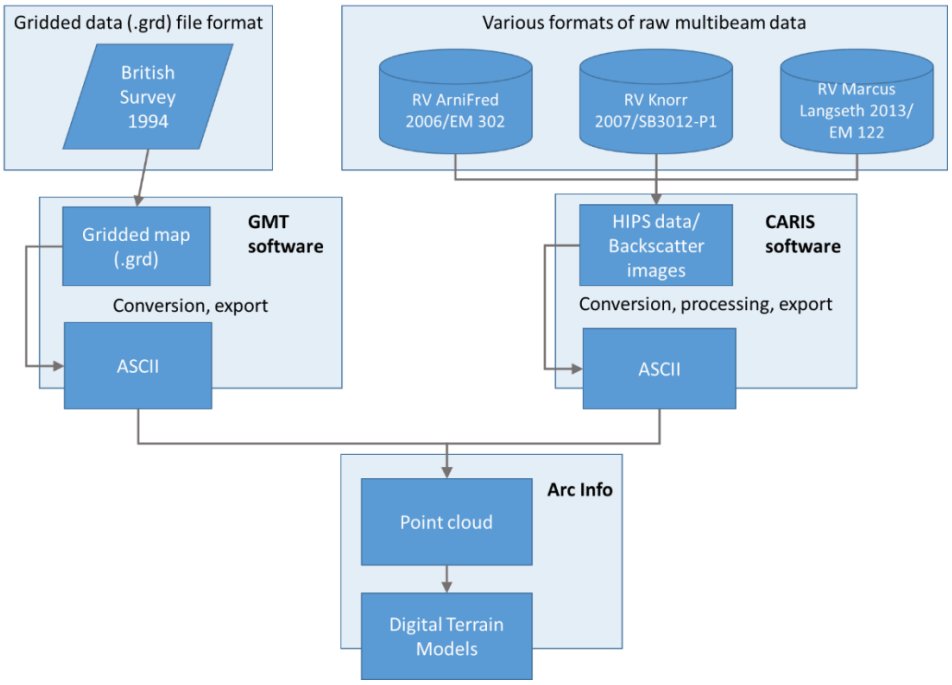

Figure 15 The data harmonization steps.

After the processing phase, all datasets are exported to the ASCII files (TXT) – including geographic position and depth or intensity information. The ASCII format allows for interoperability between Caris - a raw analytical program for multibeam data, and ArcInfo - a spatial analytical program of geographical data. Bathymetry and intensity data are further examined in ArcInfo, because it has multiple tools dedicated to surface analysis.

[12] Main manufacturers of the multibeam instruments are: Kongsberg, L-3 Elac Nautic, Reson, R2Sonic, or Atlas Hydrographic. See more: AML Oceanographic (2014) *Who Manufactures Multibeam Systems?* http://www.amloceanographic.com/CTD-Sound-Velocity-Environmental-Instrumentation-Home/Who-Manufactures-Multibeam-Systems.

3.2.2 Data correction/calibration

The second step is elimination of measurement errors from raw data. Several internal and external factors contribute to depth measurement errors – both systematic and random. Systematic errors result from instrument type and its settings, ship movements, tide and wave movements, and wrong sound and speed profiles. The following equation expresses the contribution of all above-mentioned factors to the inaccuracy of the depth measurements (Equation 4). To adjust data for those offsets, all information about the vessel and sensors are gathered. Calibration[13] of the instruments is performed before the survey. (Artilheiro, 1998)

Equation 4

$$\Delta z = \varepsilon_{sys} + \varepsilon_c z + \varepsilon_p x - \varepsilon_r y + \varepsilon_h$$

When soundings are represented as a vector of coordinates (XYZ) relative to the transducer, the error in depth measurements (Δz) is presented as a function of the following: multibeam measurement (sys); vessel motion – roll (r), pitch (p), heave (h); and sound velocity profile measurement (c). Multibeam measurement error depends on the instrument used during the survey, as each is characterized by a specific system and algorithm for bottom range detection. For more details about the uncertainty in range and angle that influence the error measurement, see Artilheiro, 1998.

Because sound recordings during surveys are influenced by vessel motion and conditions on the sea, loading raw data into Caris software is accompanied by the HIPS vessel file (HVF). Each vessel demands the creation of its own separate vessel file, which is prepared together with its crew, as it consists specific information like where an instrument is mounted and what the sensor offsets are to the water. Information about all sensors from HVF are combined with raw measurements to produce the final position and depth for soundings. Instrument offsets from HVF are applied during Sound Velocity Correction, Tide Loading, merging horizontal and vertical offsets to produce "correct" soundings, and finally Total Propagated Uncertainty (TPU) estimation (Caris, 2012).

3.2.3 Data cleaning

While systematic errors can be automatically eliminated thanks to instrument calibration and vessel information, random errors such as outliers require manual cleaning. Outliers are values that exceed the given tolerance from the true ocean bottom. But as the "true depth" to the bottom is not known from the beginning, beams that are significantly different from their neighbors are considered to be outliers (Lirakis & Bongiovanni, 2000). To be more specific, outliers are beams that lay outside expected limits of minimum and maximum values. They are identified by visual assessment of soundings as 'sharp' peaks in the data (Artilheiro, 1998).

[13] Gathering information about the redundancy of data collected in various conditions (different speed and directions).

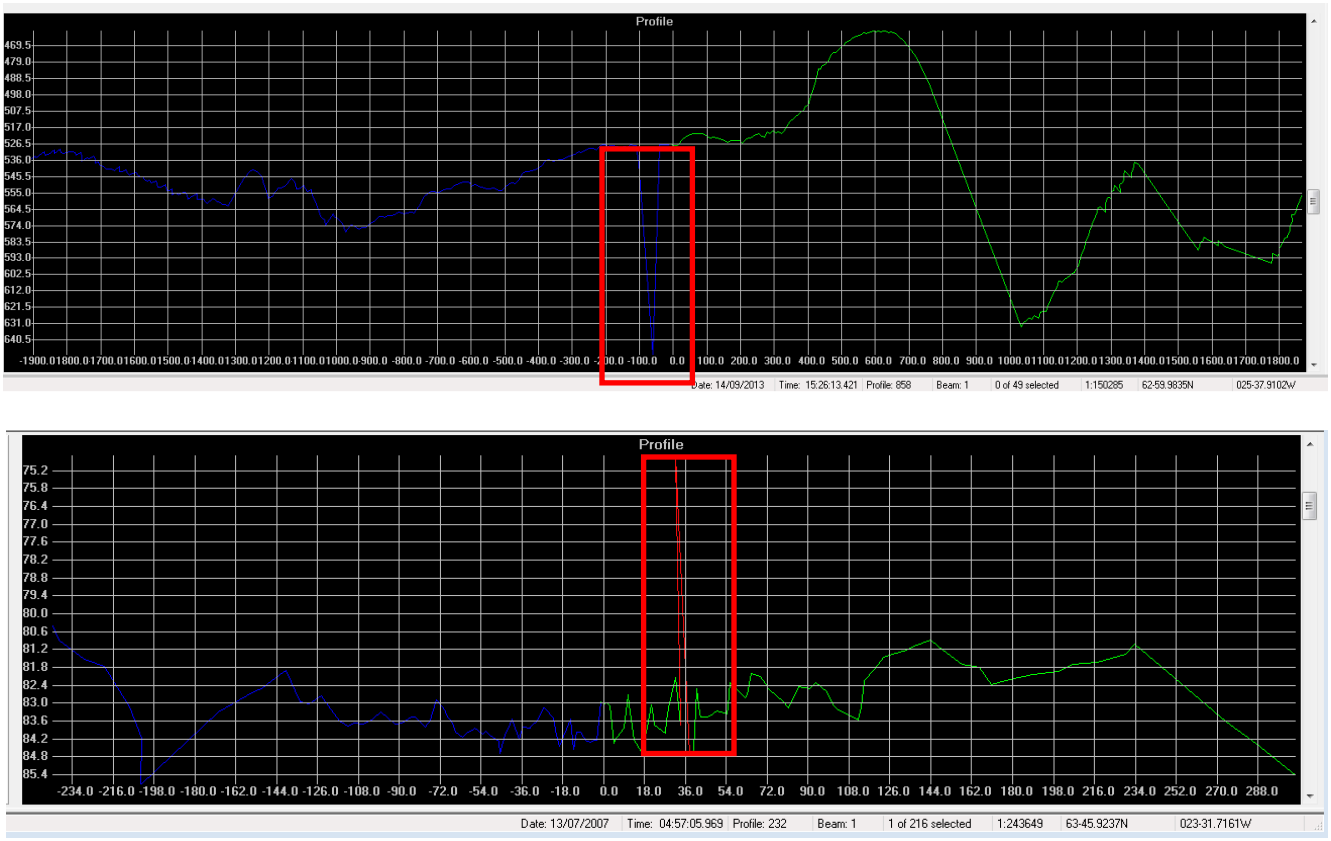

Figure 16 Screen shots from the Swath Editor in Caris. The lines represent connected data points from one ping. Relative depth and across track distance scales are in meters. Red boxes highlight outliers.

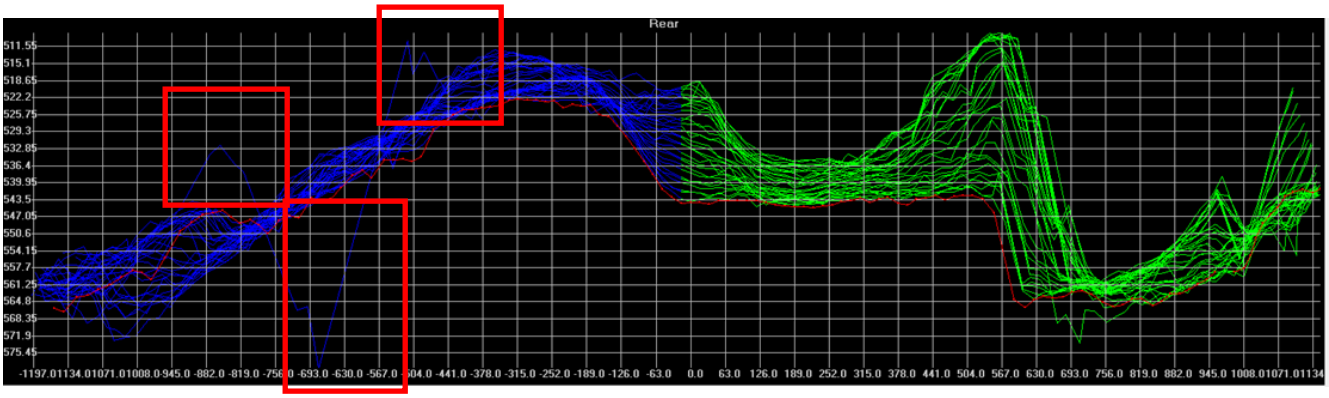

Figure 17 Example of bad data. Significant parts of data from this ping is out of the value range comparing to the adjacent soundings.

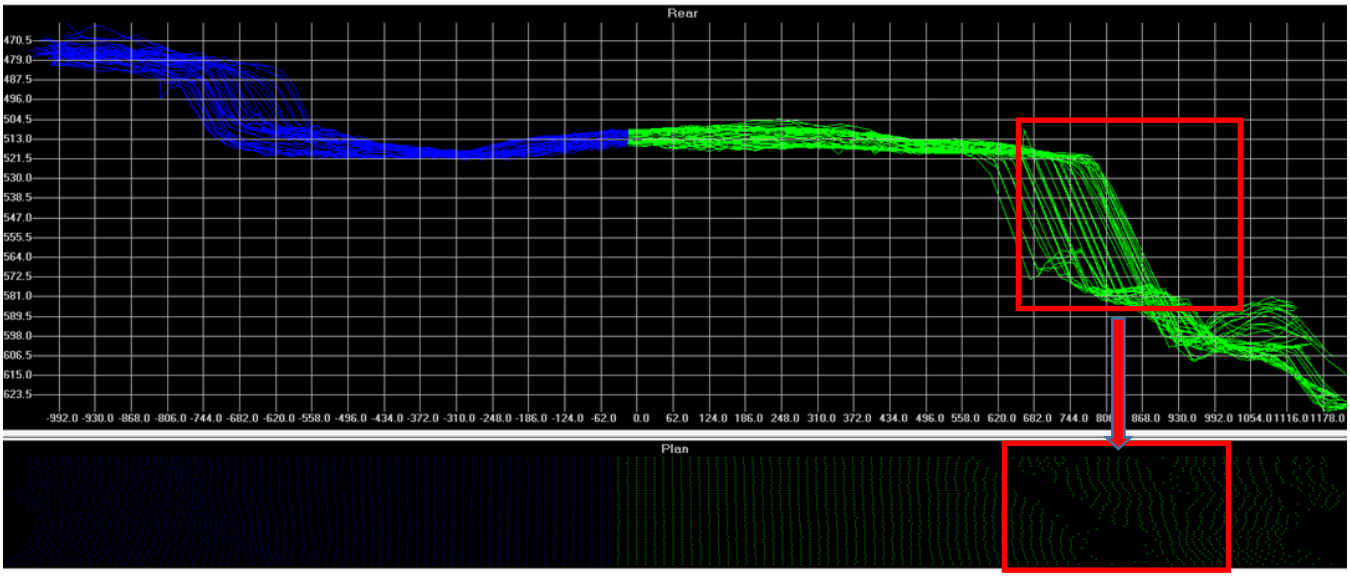

Figure 18 Example of the shadow effect. The steep fault results in space without data points in the plan view and consequently "empty" pixels when generating grid surface.

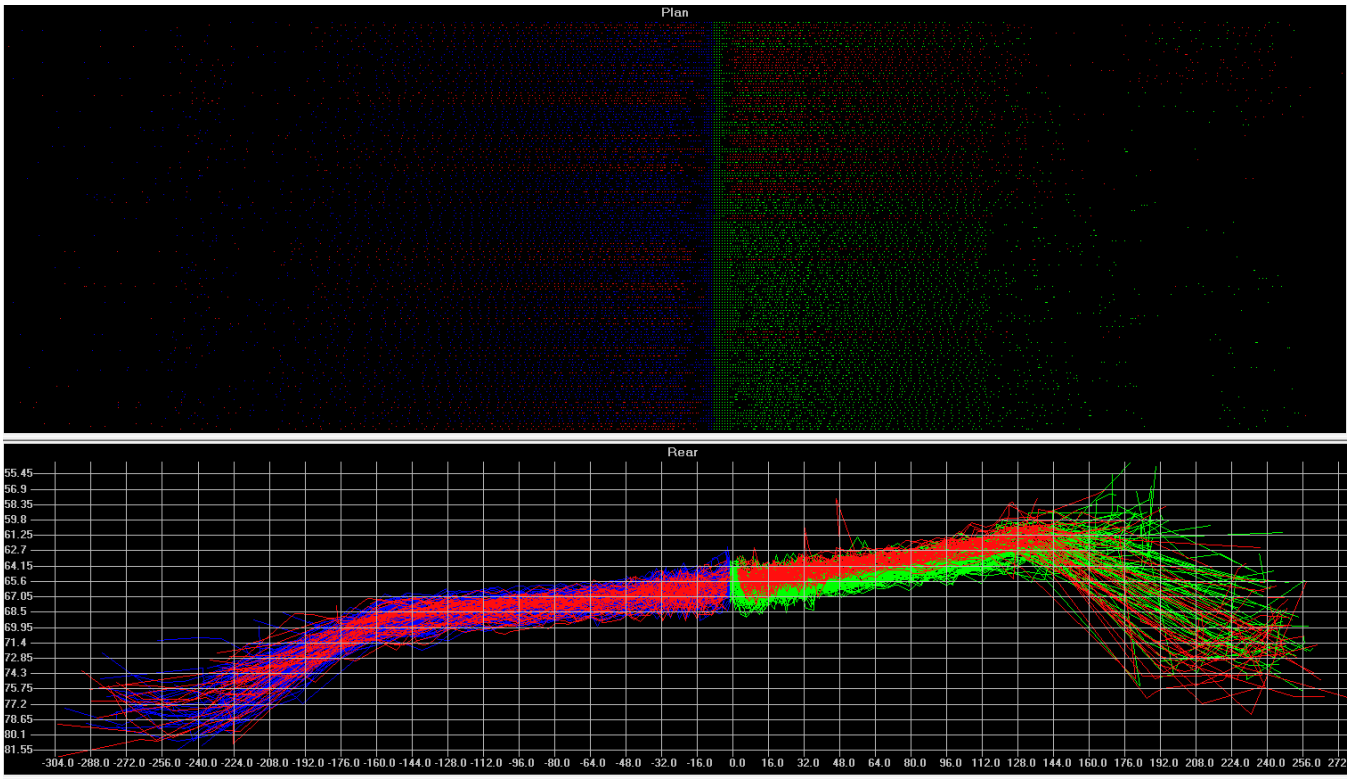

Figure 19 The plan and profile view of soundings from Elac/Seabeam instrument that were automatically flagged as bad (marked as red).

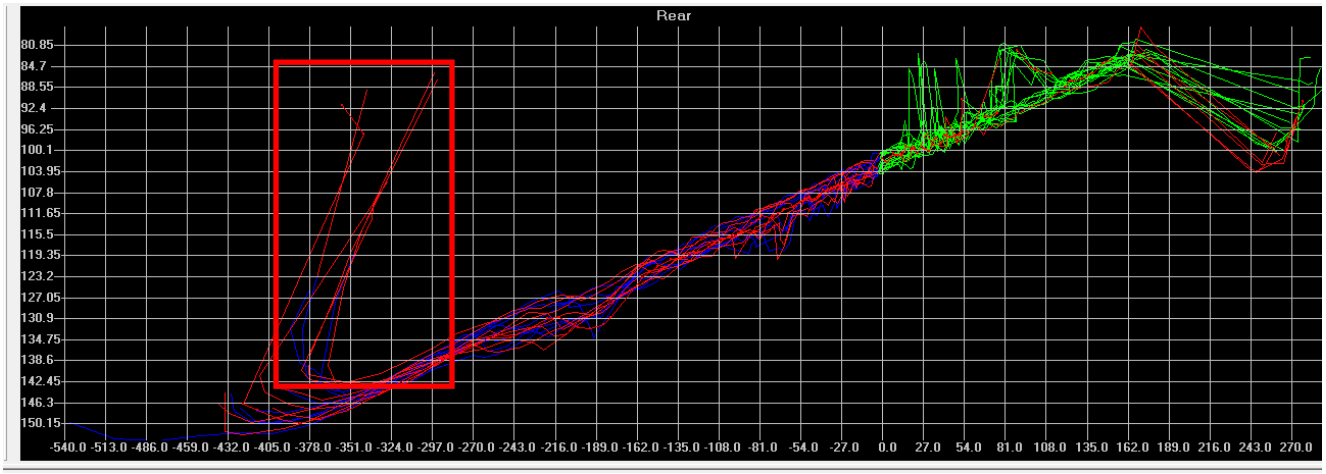

Figure 20 Example of automatically rejected soundings. All were re-assessed and many were acceptable to use in further analysis. However, soundings similar to those marked in the red box stay with status "rejected" as they overlap remaining data points.

Both external and internal factors determine outlier occurrences in the data. Existence of shoals of fish in the water column, abnormal temperature or salinity in sound velocity profiles, and multiple reflections or paths are classified as the external environmental factors while bottom detection algorithms, outer beam geometry, and equipment failure are internal system problems that may cause random errors. Unrecognized outliers result in reduced accuracy of bathymetric data, and consequently low quality of final products such as nautical maps. Thus data cleaning is an important processing step in creating a bathymetric map. (Artilheiro, 1998)

After performing the correction of soundings for systematic offsets, the field sheet[14] and first BASE surface[15] map are created. This is done in order to identify the outliers and errors in data as well as to check if there are any "empty" pixels in the grid, which would indicate that the applied resolution was not sufficient and needs to be decreased for the BASE surface generation.

There are multiple techniques to deal with outliers that fall into two main approaches. The first approach is manual-interactive cleaning, which is based on data visualization of depth contours and comparison of adjacent beams in each ping and profiles of soundings. The second approach, automatic filtering, uses statistical methods over the dataset of soundings. (GEBCO, 2013)

Interactive manual cleaning

In Caris interactive data cleaning is performed using Swath Editor, where each sounding can be displayed and examined separately from various perspectives. If the sounding is abnormally different from its surrounding neighbors, it is rejected. Figure 16 and Figure 17 present some examples of bad

[14] Field sheet is a basis for grid map. And one have to decide on its resolution and extent.
[15] BASE surface is created using various methods. Swath Angle for the sounding that are located in a deep water (on the depth more than 1km), while Cube for the sounding within shallower places. It does not have to have the same resolution as field sheet. BASE surface include multiple layers of maps, such as depth, but also uncertainty, density of soundings, mean or standard deviation.

data. Figure 18 presents the shadow effect, which affects the quality of the data but is not an error. After rejecting erroneous points in beams, all systematic corrections and merging have to be repeated. (Caris, 2012)

When data acquired from the Elac/Seabeam instrument (RV Knorr, 2007) was loaded to the post-processing software, the significant amount of soundings in some of the track lines appears to be already rejected (Figure 19 and Figure 20). Beams flagged as bad were mostly located on the edges and seem to be affected by shadow effect. The reason for that is the fact that the software has pre-determined criteria to identify good and bad soundings. Therefore, some of the pings or their parts are recognized as bad and excluded from the dataset. In this case, the big advantage of Caris software is its ability for data processing to be completely controlled by the user. Consequently, each of the beams flagged as questionable by the acquiring software will be visually assessed once more in order to make a final decision- either it should be brought back and accepted or it should remain excluded from the further analysis.

The criteria for the detection of outliers was discussed together with Prof. Armann Höskuldsson who has experience working with multibeam data, mapping sea bottoms, and expertise in studies on volcanic formations in the Reykjanes Ridge. According to Professor Höskuldsson, only data points that are totally inconsistent with data values of their neighbors should be rejected. Based on the analysis below, this is due to when the continuous surface is created, each pixel carries value that is estimated resulting from multiple soundings. However, those outstanding values may significantly affect the shape of the gridded surface. Following his advice, decisions about accepting or rejecting data already flagged as bad as well as eliminating soundings recognized as spikes were made after cautious visual assessment and removed manually (Höskuldsson, 2014).

Data filtering

In contrast to interactive manual cleaning, the automatic cleaning is conducted in a more objective manner. Instead of subjective decisions of the analyst during visual inspection of soundings, this method relies on statistics and mathematical algorithms. It allows the ability to set up criteria based on what data is automatically evaluated and deselect incorrect soundings.

The filtering possibilities for multibeam data can vary from simple methods for spike detection operating in the swath mode for single ping to more complicated algorithms applied to subset of pings representing a matrix of beams (Lirakis & Bongiovanni, 2000). Spike detection methods rely on prior knowledge of the study area. It uses depth limits and slope angle between neighboring beams that are specified by the analyst. In case there is no prior knowledge about the terrain, filtering options are based on statistical properties of the data. Consequently it is possible to perform various local (nearest neighbor, fitting polynomial function to measurements in the neighborhood of the point) and global operations (CUBE surface, average interpolating subdivision) on the subset of pings that serves as a matrix of beams. Some examples include: 1) incorporating local multi-pass algorithms into probability density function in order to conduct classification of bad and good soundings (Lirakis & Bongiovanni, 2000); 2) performing a multistep procedure that first searches for the real point based on density of points, then applies algorithms of erosion and dilation[16], and finally performs local window filter (Yang et al., 2007); or 3) using spatial correlation between data points to generate "global" trend surface that

[16] Both algorithms are based on math morphologic theory. Erosion eliminates edge points and makes edge shrink, while dilation combines all edge points to make edge wider and fill existing empty holes. See more: Yang at al. 2007.

is consequently subtracted from the data to easily identify errors within residuals (Bjorke & Nilsen, 2009).

Setting up Filters in Caris

Caris software offers two procedures for automatic cleaning of swath data – setting up filters or/and using CUBE algorithm when creating BASE surface (Caris, 2012). Filtering spikes from swath data is based on two methods. Firstly, a minimum-maximum depth filter rejects any sounding that is shallower or deeper than specified limits. Secondly, beam-to-beam mode calculates slopes for neighboring beams. If both slopes - towards the prior and post beams - exceed the defined value, then the beam is rejected. (Caris, 2012).

CUBE algorithm

CUBE approach allows the removal of up to 90% of the errors from the raw data. This technique is commonly accepted and utilized in most commercial software packages for hydrographic data processing (GEBCO, 2013). CUBE method uses the propagation of soundings to grid cell in order to create the hypothesis of depth value at every grid estimation node. It selects soundings that contribute to the estimation node or one of the hypotheses based on the algorithm that it takes into account: vertical and horizontal uncertainty as well as distance of the sounding to the node. Each estimation node may carry more than one hypothesis. A final decision about the "correct" depth value results from one of the disambiguation options, such as density, locale, density and locale[17]. Respectively, those methods give priority to a hypothesis that either has the greatest number of sounding samples, is the most consistent with surrounding nodes with only one hypothesis, or fulfills both previous conditions. The main outcome of the CUBE algorithm is a grid surface with depth values. In addition, the three other output surfaces are generated: uncertainty, density with number of hypotheses at each node, and strength of hypothesis (Caris, 2011).

Why filters are not applied

A disadvantage of the min-max depth filter is the requirement for prior knowledge about elevation of the study area. Additionally, different min-max values should be set for different parts of the Reykjanes Ridge, as the depth increases with distance from Iceland. The rough values for the depth limits can be found in the British survey conducted in this area in 1994 (Keeton et al., 1997). However, because of the lower level of detail in the 1994 survey compared to the data used for this study, the fact that values of some beams in data from current surveys exceed limits of the depth range obtained from British data does not mean that they are not true. Besides the spike detection, other filters may be also applied to the swath data. An example of this is a TPU filter that applies the IHO standards[18] to multibeam data. However, it is excluded from analysis because those standards are too strict for the purpose of exploring morphological structures in the Reykjanes Ridge area.

3.2.4 Backscatter data processing

After handling bathymetry data and creating topographic surfaces, the next step is to process multibeam backscatter imagery. The aim of the procedure is to improve the quality of the image, so that it can analyze properties of the sea bottom. The backscatter imagery represents the intensity of

[17] There is also possibility to use the initialization option that utilizes previously created surface.

[18] International Hydrographic Organization standards for hydrographic surveys (S-44) and for digital hydrographic data (S-57) can be found on the IHO website: http://www.iho.int/iho_pubs/IHO_Download.htm.

reflected acoustic energy. Each pixel of the image includes a value- a record of the signal strength- which in turn depends on various factors such as angle of incidence, surface roughness and properties of the seafloor (Gafeira, 2010). When the backscatter image is draped on the bathymetry map, it enhances recognition of the sea floor texture, structures and morphology (Chadwick et al, 1998; Macdonald & Collins, 2008).

Before processing in Mosaic Editor, the raw data have to be converted into the HIPS format. The first step is to create a Geo-referenced Backscatter Raster (GeoBaRs) without applying any corrections and using general options. The results aid to identify the suitable area (flat, homogenous and featureless as possible, preferably covered with sand) for the *Beam Pattern* file that is used in subsequent image corrections. The second step is to test various options available in the Mosaic Editor and different resolutions to create multiple GeoBaRs over a single line. Having different images for the same line provides the ability to visually compare results and decide on settings that bring the best imagery. The analyst has to set various options: processing engine, source of data type, and specified parameters for image corrections[19], which unfortunately differ depending on the processing engine. Next, radiometrically and geometrically corrected GeoBaRs (Fonseca & Calder, 2005) replace those created with general settings and new multiple backscatter imagery are turned into a Mosaic image. Because more than one GeoBaRs can be related to one track line, the analyst has to resolve the conflict[20] and make a choice which GeoBaRs will be included into Mosaic. By selecting one of the composing algorithms[21], he determines also which pixels have higher significance when data overlaps. Finally, the created mosaic may be edited by changing its brightness and contrast. (Caris, 2012)

[19] The corrections applied to improve quality of GeoBaRs include: Auto Gain, Time varying gain (TVG) Antialiasing, Slant range correction, Beam Pattern Correction, Angle Varying Gain (AVG), Despecle. More about the image processing in Geocoder in article by Fonseca & Calder, 2005.

[20] Selection options include: most recently created, finest resolution, or manual. See more: Caris (2012) Training Manual: HIPS and SIPS, p.81.

[21] Composing methods address the question which pixel should be used in case of overlapping. Caris includes following solutions: Auto seam - pixels closer to the center are given higher significance; Full blend – computing average of all pixel values; the latest pixel value overwrite the previous ones; the pixel with highest intensity value or the first pixel will be used. See more: Caris (2012) Training Manual: HIPS and SIPS, p.95.

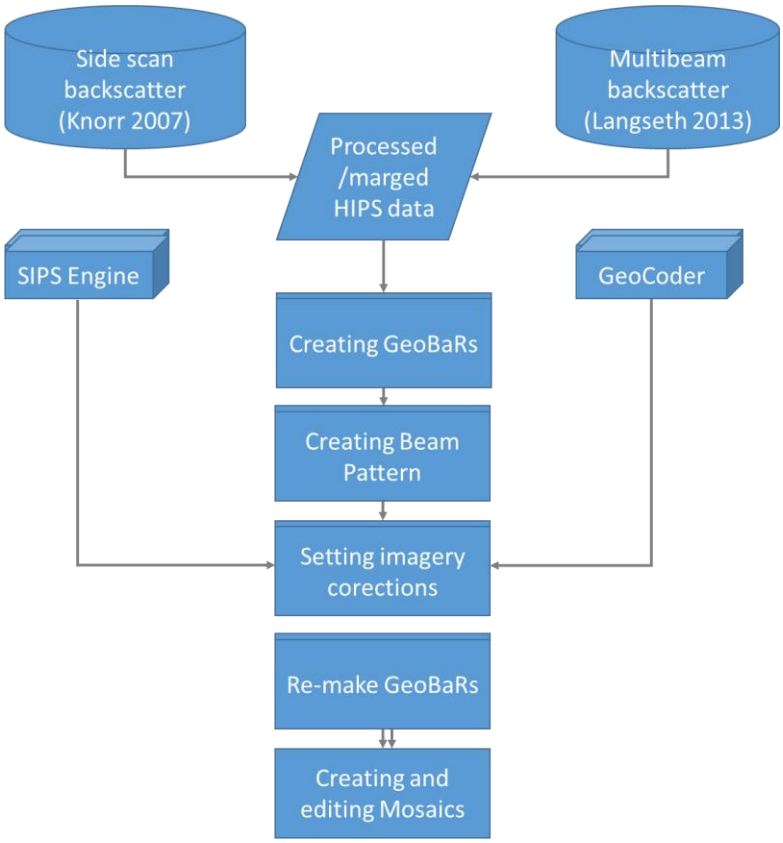

Figure 21 The workflow of imagery data processing in Mosaic Editor.

In this project, data from Simrad is handled with Geocoder engine, while a side scan backscatter from Elac/Seabeam is examined with a SIPS engine. This results in small differences in the processing, but the main steps remain the same and are presented above (Figure 21). Because of the fact that intensity is attached to the beams, after rejecting data points during bathymetry processing, the backscatter images have to be updated. (Caris, 2012)

3.3 Maps modeling

Processed and corrected high-density bathymetric data from each survey are transformed into regularly spaced grid surfaces that are used in further analysis. A Raster based surface model is a grid of height values, and in the case of bathymetry, depth values. Each cell of this grid contains only one value that is a representation of the surface elevation on the area covered by the cell.
Irregular spaced points are first grouped into bins (Artilheiro, 1998) and then, based on the chosen algorithm, interpolated into rectangular grid cells with a single value (Figure 22). This transformation is conducted on the basis of a seafloor model that uses a calculation method depending on the application of the bathymetric product (Kearns & Breman, 2010). This process shows the conversion between two basic data structures – from vector (point) to raster (pixel). The former symbolizes discrete objects with its position and attributes, but no area, while the latter better represents the surfaces that describe continuous variables, such as elevation, that have a value for every position within the map extent (Liu & Mason, 2009).

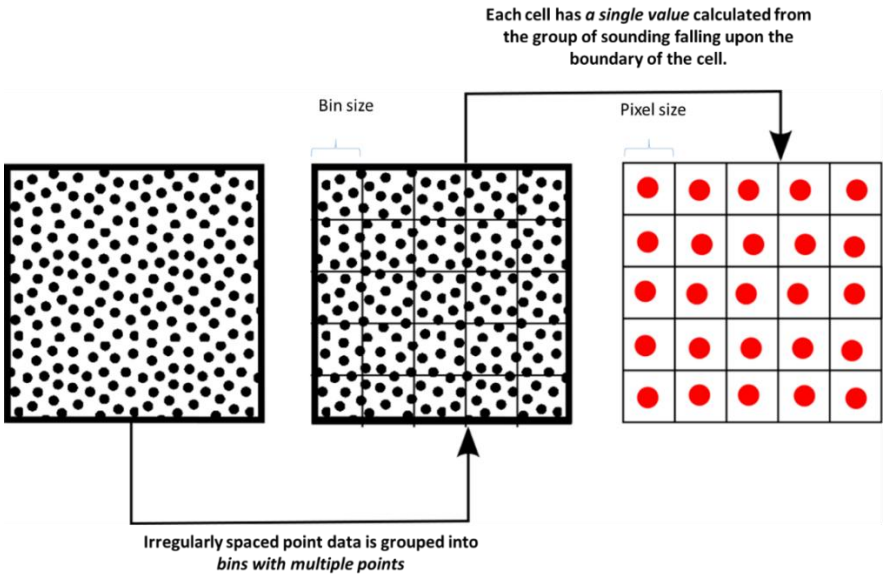

Figure 22 The conceptual model of transformation between vector point data and raster, regularly spaced grid map. Based on Kearns & Breman, 2010.

Gridded surfaces from raw data are generated in Arc Info. In order to find appropriate grid spacing, analysis of distances between points and their density within a raster cell is performed (Eysteinsson & Danielsen, 2003). Point data is transformed into digital terrain models (TIN and DEM). Maps modeling is performed with various resolutions - 15m, 25m, 30m, 50m - to test which pixel size keeps enough detail to recognize various morphological structures. At the same time, raster surfaces are generated with or without small amounts of empty ("Nodata") cell values.

3.3.1 Identification of main morphological structures

Based on the previous research on the Reykjanes Ridge as well as geological mapping in the other areas of spreading tectonic plates (Chadwick et al, 1998), morphological structures such as pillow lava, sheet flow, mounds, seamounts, hummocky ridges, axial valleys, and calderas are expected to be found in the study area.

Backscatter images support recognition of those structures as intensity reflection indicates some properties of the surface like age, roughness or material. Morphological features recognized from the bathymetric map will be compared with the intensity image.

Volcanic structures – axial ridges and seamounts – will be identified using the elevation contours and slope map layer. The description of the identified features include their measured dimensions and volume. The analysis will be performed for the area between 62°N and 63°N, as this is an area gap in mapping of volcanic edifices over the Reykjanes Ridge (Smith, Humphris & Bryan, 1995; Höskuldsson, 2007).

3.4 Comparison analysis

The comparison analysis between two time-separated bathymetric maps is conducted in order to detect significant changes in seafloor morphology. Time series bathymetric data was successfully used to verify water depth changes for navigation safety or to monitor sediment volumes. Various earth processes such as tectonic and volcanic activity can be uncovered and analyzed using multibeam sonar data (Schmitt et al., 2008). Multiple studies investigated submarine distribution and volume of lava flows (Fox et al, 1992; Chadwick et al., 1995; Chadwick et al., 1996; Embley et al., 1999; Caress et al., 2012) or changes in caldera's structures (Wright et al., 2008). Investigations of volcanic activity were also used as case studies in advancing methods for accurate and statistically significant change detection using time-separated bathymetric data (Dunn et al., 2001; Schmitt et al., 2008).

3.4.1 Change detection using bathymetric data

This project follows methodology presented by Fox et al. (1992). The quantitative technique was developed to detect significant changes in seafloor morphology. When comparing values in each pixel of raster maps (Digital Elevation Model), any change in elevation can be detected. "Significant" change in this context means change that exceeds the vertical and horizontal resolution of multibeam data. Vertical resolution refers to noise level below which the acoustic signal cannot be determined, while horizontal resolution means pixel size, what is turn implies the smallest size of the objects that may be recognized. Therefore, any differences between maps smaller than pixel size will not be detected.

The method is based on the simple rule of subtracting a one-year bathymetry map from another. However it includes a few processing steps before maps can be overlaid. Point data is gridded using one of the interpolation methods in order to create a smooth surface without data gaps. The navigation correction and co-registration are required to improve position accuracy. Also the bias related to sound velocity profile and instrument offsets has to be removed. After two maps are overlaid, a generated difference map has to be smoothed to reduce the influence of random noise. Finally a statistical threshold for significant change is applied (Fox et al., 1992; Chadwick et al., 1995). This so-called grid-differencing technique is applied to estimate the changes in bathymetry of the Reykjanes Ridge between 1994 and 2013. The steps of this analysis are outlines in Figure 23.

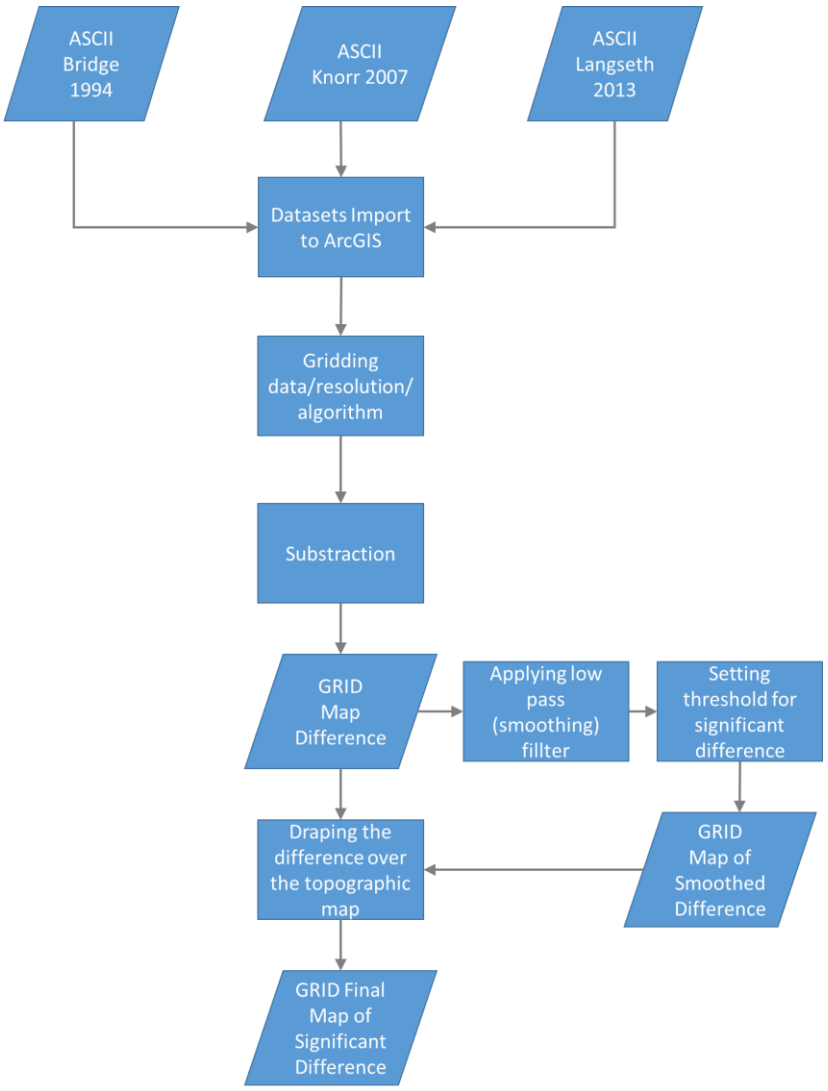

Figure 23 The comparison analysis steps. Workflow based on the grid-differencing methodology developed by Fox et al. (1992).

Ideally, there should not be any geometric distortion between images, as they are defined with the same geographic coordinate system and projection (WGS84 UTM 26N). Also gridding processes follow the same rules (point to raster, mean resampling method) in the same software, and all new rasters are aligned to each other to guarantee that cells overlap perfectly[22]. Therefore, co-registration[23] of two bathymetric maps is not applied. The comparison analysis starts from the gridding of maps, which is described in detail in the previous section (Maps modeling). Because the resolution that can be obtained from various datasets differs significantly, it is necessary to downscale maps from Langseth and Knorr surveys. Therefore, all datasets are gridded according to the cell size of the oldest map (120

[22] Snapping to the same layer during the raster creation.

[23] In general, co-registration means establishing a relation between the input image and the reference map projection or image in order to create the output image. It is usually performed on the selected subset area containing distinctive structures that are possible to identify on both images. The geometric transformation requires first to establish a deformation model based on ground control points (GCPs) and next to resample pixels positions and their values using one of the mathematical algorithms. The resampling methods include following functions: nearest neighbor, bilinear interpolation, third and higher order of polynomials. See more about the methods advantages, and disadvantages in: Liu & Mason, 2009.

meters). Using point to raster tool, two other maps are produced using a "mean" resampling method. Subtraction of one map from another is performed using a spatial analyst toolset (raster calculator). The calculations follow the time series, and the newer map is subtracted from the older map. In that way, three "difference" maps are generated for the following years: 1994-2007, 2007-2013, and 1994-2013. The following step is to apply the low pass filter (window size 3x3 kernel) to the "difference" maps in order to eliminate random noise (Liu & Mason, 2009)[24] and consequently to classify the results according to the threshold of two and three standard deviations. In that way, only values outside this threshold are displayed on the final "difference" maps. According to Fox et al. (1992) a threshold for the significant depth changes has to be developed on the basis of statistical confidence in case of comparing bathymetric data from different multibeam sonar systems. In addition a threshold may be based not only on the depth, but also on the horizontal extent on the differences[25] (Dunn et al., 2001). Final "difference" maps are draped over the topography to indicate locations of potential changes, which are further investigated by a visual analysis of topographic maps in 3D display.

All corrections related to instrument offsets, vessel motion, and navigation were performed in Caris, so data is assumed to be "clean" from systematic errors. Ideally the comparison analysis should be performed on the bathymetric data that fulfill the following conditions: collected with the same multibeam instrument, the navigation system and over the same track lines. In the case of this project, none of the conditions are fulfilled, but the method is optimized in a way that the comparison is still reasonable. Even after smoothing, the final map with significant differences may still contain anomalies that are not true, but fall within the statistical confidence threshold. Some of the following procedures may identify them: 1) changing the co-registration distance and repeating the whole process. The anomalies will change shape or place; 2) gradually increasing the threshold value in order to increase statistical confidence level of the difference grid. (Fox et al, 1992)

3.4.2 Evaluation of the results

Because there is no data to compare with and therefore evaluate our results, the verification of a final "difference" map will be conducted using backscatter images. The intensity change in those locations could additionally confirm the conclusion about volcanic activity during the last six years in the study area. As the backscatter imagery can reveal information about the age of the sediments covering the seafloor, the change in the time-separated multibeam backscatter indicates lava flows and creation of indigenous rocks (Chadwick et al, 1998). Another source of information about potential locations of changes is a map of seismic activity in the Reykjanes Ridge area. Therefore, comparing the results of grid-differencing technique with a map of earthquake locations supports drawing conclusions about the results of change detection analysis (Höskuldsson, 2014).

[24] The low pass filter available in ArcGIS is the average for pixel calculated from the kernel window. However, other options not available in this software might be a better choice for this project, such as the „k" nearest mean filter, median filter or conditional smoothing filter. More details about pros and cons of various smoothing filters in Liu & Mason, 2009, pp. 40-44.

[25] Detection of significant difference may also be performed using a topological algorithm that first group all soundings into region adjacency graph and then set a threshold based on depth difference and lateral area. See more in article by Dunn et al. (2001).

4 Results

All results – point data analysis for maps modelling, bathymetric maps of the study area, intensity images display and comparison analysis between time-separated bathymetric maps – were produced using ArcInfo software. Only 3D images were produced in Caris.

4.1 Maps modeling

The accuracy of the terrain representation depends on the grid map resolution (Heywood, Cornelius & Carver, 2006). Therefore, decision about the cell size is crucial to obtain the good quality map from the given point data. The reasonable resolution is defined after the analysis of data points. Ideally, it should reflect the distances between points and its density within the raster cell (Frye, 2007). Because the distances between beams from multibeam depend on the water depth, the resolution that can be obtained from the dataset will decrease together with distance from Iceland while the sea becomes deeper. Consequently, there are a few main questions to address in map modeling. What cell size should be determined for bathymetric datasets with diverse point's redistribution? If it is necessary, what interpolation (estimation of elevation values in between of measurement points) method should be applied? And finally what resampling technique (assignment of one value to the cell covering area with more than one observation) would be the best for the purpose of this study?

The proximity analysis of dataset – point distance - is executed to find out about the average spacing between points within a specified search radius (25 and 50 m). The amount of points that contribute to the cell values depending on the grid resolution (15, 25, 30 and 50 m) is analyzed with a point to raster tool. The results of this point data analysis are presented in Table 5 and Figure 24 below.

Table 5 The point data analysis results. The table presents the summary of statistics from point distance analysis. The subset data are the most outer (north - south) lines from two datasets.

Resolution	Knorr	Langseth
Point distance analysis		
Shallow (25 m search radius)	Mean distance: ≈16 m; Max: ≈24 m The most frequent mean values ≈14-18 m	Mean distance: ≈16,5 m; Max: ≈24 m The most frequent mean values ≈13-19 m
Deep (25 m search radius)	Mean distance: ≈15,5 m; Max: ≈24 m The most frequent mean values ≈16m	Mean distance: ≈18 m; Max: ≈24,5 m The most frequent mean values ≈16 -22 m
Deep (50 m search radius)	Mean distance: ≈33,5 m; Max: ≈49 m The most frequent mean values ≈34-35 m	Mean distance: ≈34,5 m; Max: ≈49 m The most frequent mean values ≈32-38 m

The subset of the data was used to speed up the analysis process and get an overview on the distances between points depending on the depth. The range of most frequent mean distance values between points in the shallow areas is 13-19 meters, while in the deeper parts is between 16-22 meters. The point density analysis (Figure 24) reveals that in the deeper areas, a majority of the cells have value nodes estimated on the basis of less than 10 data points[26]. Furthermore, the higher resolution, the bigger amount of cells with "Nodata" value appears. This is especially visible in the case of deeper areas where spaces between data points are greater.

Results from the previous studies on MAR bathymetry shows that gridding of multibeam data with resolution of 50 m is well enough to recognize volcanic edifices (Cochran, 2008). Also the repeated bathymetry method was successfully performed on both coarser (Dunn, 2001; Chadwick et al., 1996; Fox et al., 1992) and finer (Caress et al., 2012) resolution raster surfaces. Therefore, building up on those previous studies and theories of raster surface creation (DeMers, 2009), the decision about 30 m resolution is made to obtain grid map with the least amount of "Nodata". Simultaneously, 30 m cell size keeps enough detail to recognize morphological structures in the study area. Yet, gaps still exist between measurements in the deep locations and on the edges. In order to solve this problem, raster surfaces are created from previously generated Triangular Irregular Network model. This approach for interpolation follows the practice in hydrographic offices (Vésteinsson, 2014; Rogala, 1999), but other methods for bathymetry data gridding are also commonly used , but their application vary with software used for data processing (Amante & Eakins, 2009; Eysteinsson & Danielsen, 2003). Furthermore, quality of interpolation results depends on density of bathymetric measurements and the type of surface mapped (Sterling, 2003; Amante, Eakins & Taylor, 2010).

[26] 10 data points per grid cell was used in creating bathymetry map of Aegir Ridge. See: Eysteinsson & Danielsen, 2003.

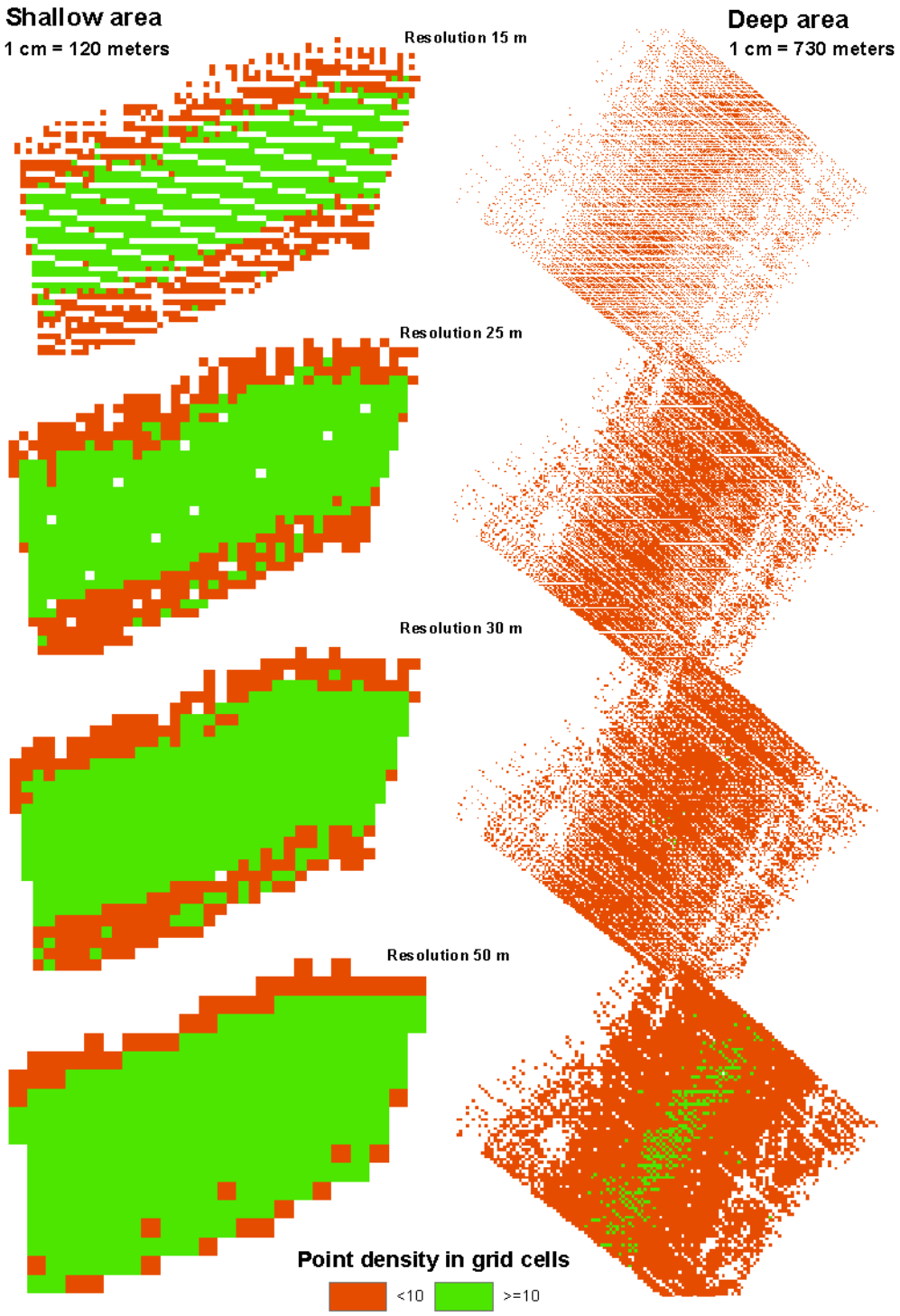

Figure 24 The results of point density analysis. The figure presents the comparison of grids created with various resolution (15, 25, 30, 50 meter) from point data (Knorr/Seabeam) located in the shallow and deep areas. The green color represents grid cells that have value estimated from at least 10 data points, while the red color represents those with smaller amounts of contributing points. The analysis shows that data gathered in the shallow areas is denser in comparison to data from deep locations. Therefore, the deeper water column shows a smaller amount of points falling under the cell when creating a grid map. This problem results from the data gathering technique and how echo-sounder works. The images also show the problem of empty cells ("Nodata") in the surface. The amount of empty pixels decreases with lower resolution.

4.2 Topographic maps

The result series from the topographic mapping along the Reykjanes ridge are presented in Figure 25, covering four detailed maps each at scale 1:500.000 (The maps are presented in larger scale (1:100.000) in appendix C). The maps are presented in Transverse Mercator projection and with contour lines at 100 and 50-meter intervals. The depth range is from -1812 to -37 m, represented by color scale from dark blue (deep areas) to red (shallow areas). Because three datasets with different depth ranges were combined, the color scale is stretched between -2000 m and sea level. All the topographical maps were created from first generated TIN terrain model and then gridded at a 30-meter cell size.

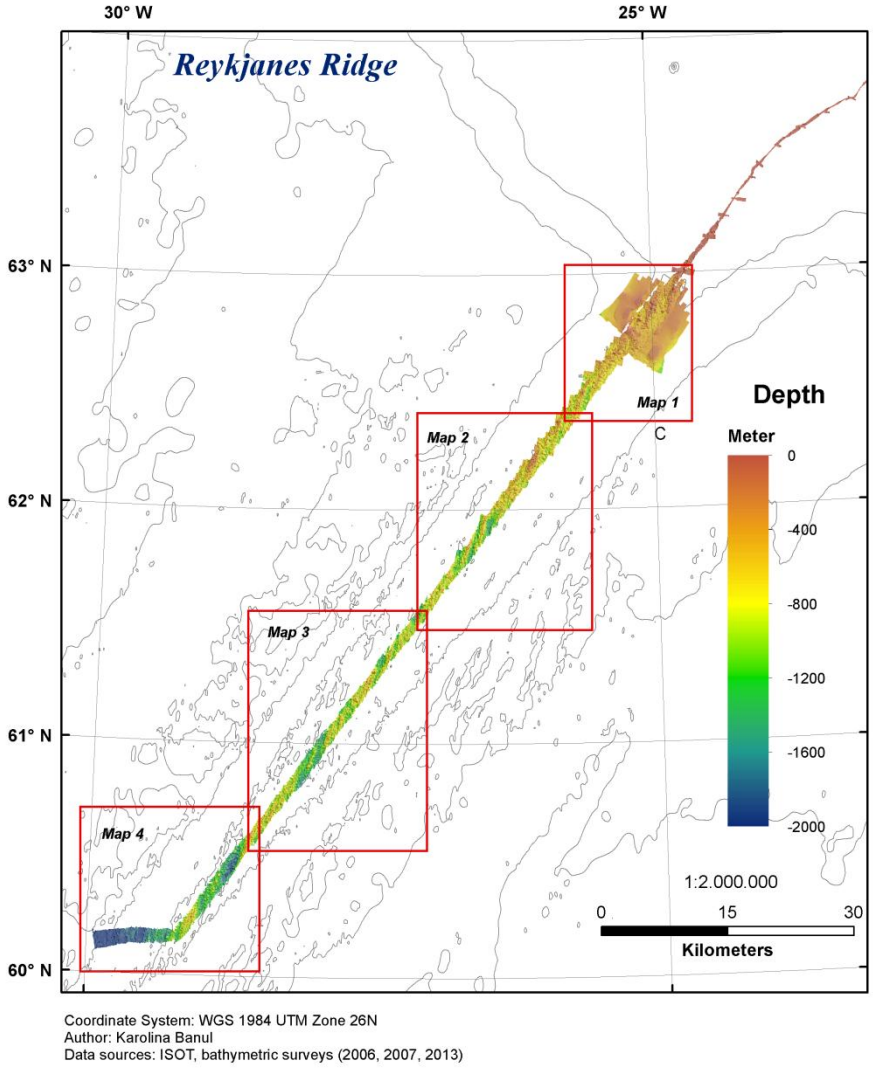

Figure 25 Bathymetry of northern Reykjanes Ridge. Map based on multibeam data from various surveys (2006, 2007, 2013). Red boxes outline regions shown in Figure 26,Figure 27, Figure 28 and Figure 29. The contour lines (500m interval) was generated from bathymetric grid with coarse resolution (0,008 degree).

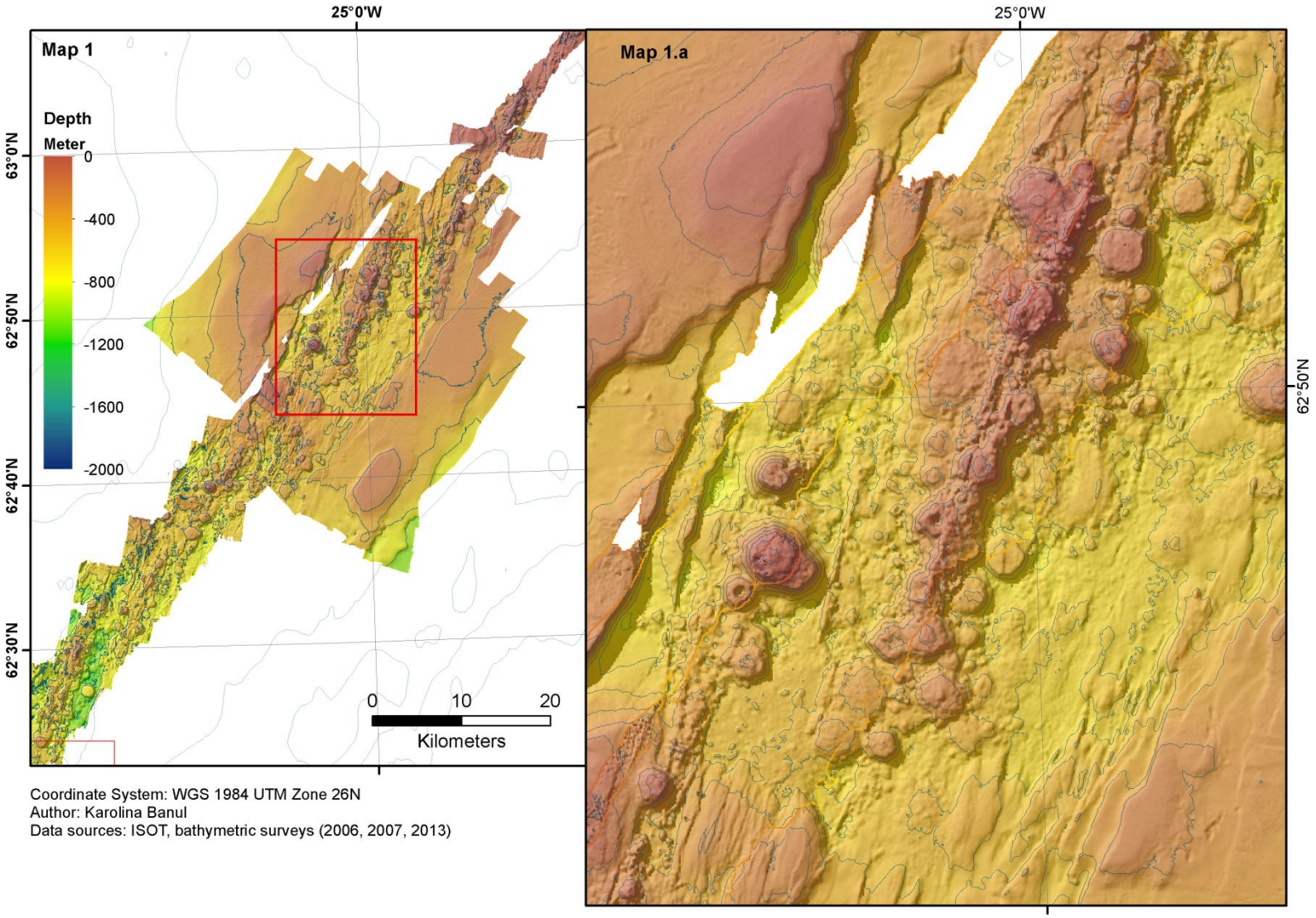

Figure 26 (Map 1) Bathymetry map of Reykjanes Ridge axis from 24°30'W to 25°30'Wbased on the multibeam data from RV Marcus Langseth (2013), RV Knorr (2007), RV Arni Fridriksson (2006) surveys. Location of the area is presented in the Figure 23. The data was gridded with 30m resolution and using TIN as the interpolation method. Surface is contoured at 100 m interval and is illuminated from the northwest. Red boxes outline the region shown in the Map 1.a. (Map 1.a) Detailed bathymetry map of the portion of the Reykjanes Ridge. Map is contoured at 50 m interval and hillshade is illuminated from the northwest.

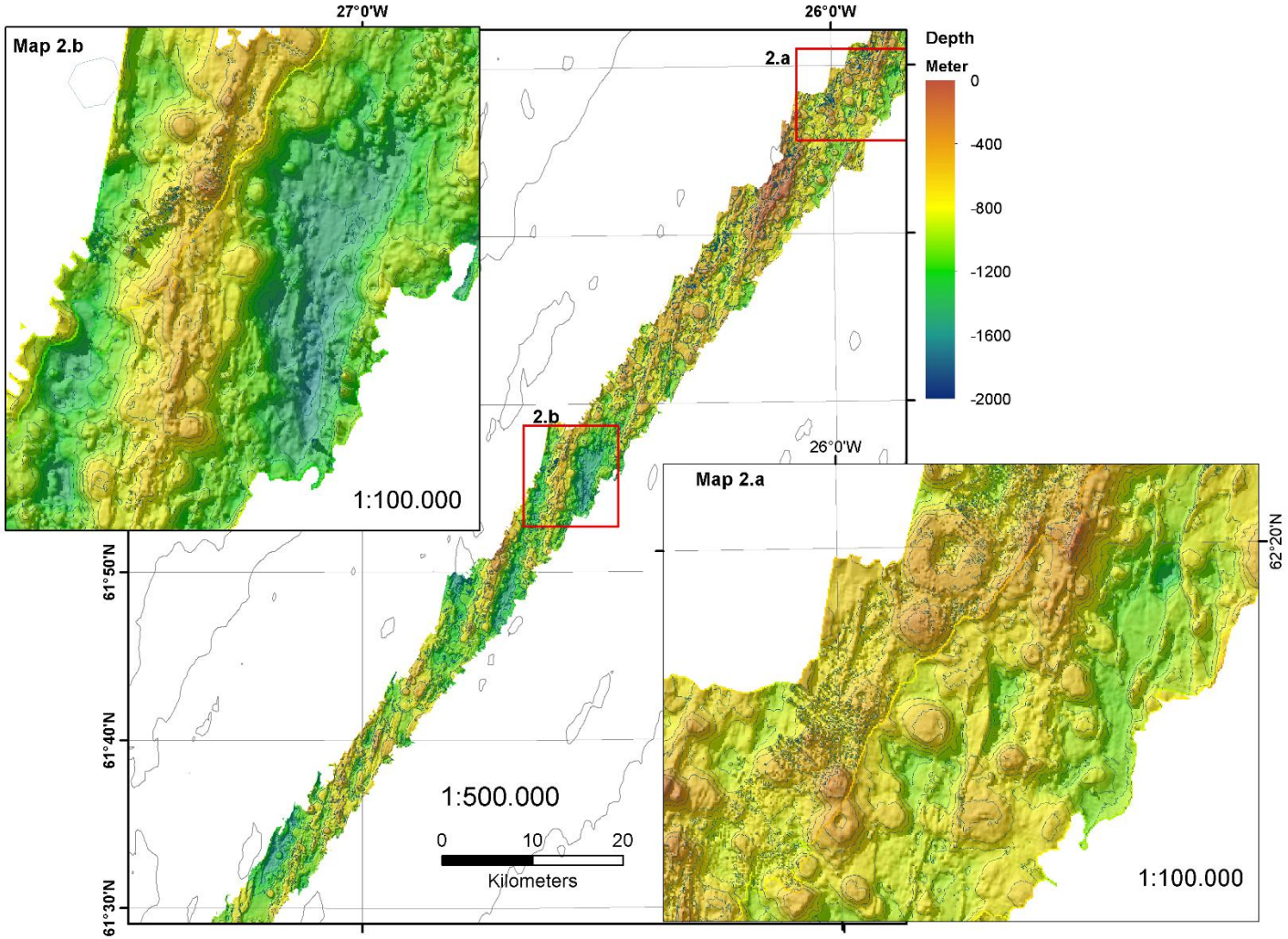

Figure 27 (Map 2) Bathymetry map of Reykjanes ridge axis from 25°30'W to 27°10'W based on the multibeam data from RV Marcus Langseth (2013), RV Knorr (2007) surveys. Location of the area is presented in the Figure 23. The data was gridded with 30m resolution and using TIN as the interpolation method. Surface is contoured at 100 m interval and is illuminated from the northwest. Red boxes outline regions shown in the Map 2.a. and Map 2.b. (Map 2.a) Detailed bathymetry map of the portion of the Reykjanes Ridge. Map is contoured at 50 m interval and hillshade is illuminated from the northwest. The most visible structures on the map 2.a are seamounts, and calderas with characteristic depression inside. (Map 2.b) Bathymetric map is contoured at 50 m interval and hillshade is illuminated from the northwest. The characteristic volcanic ridge that is created from multiple fissures and seamounts.

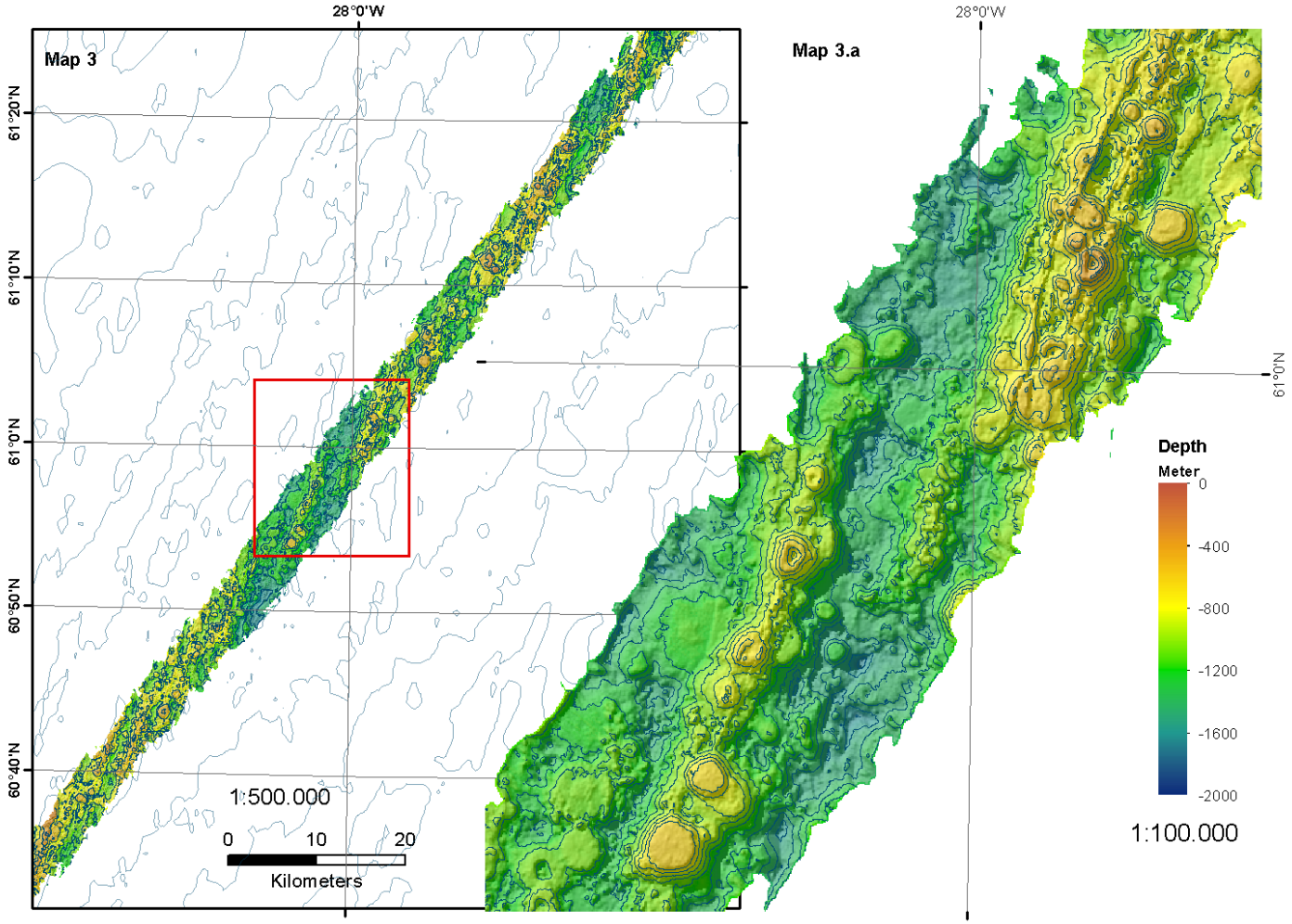

Figure 28 (Map 3) Bathymetry map of Reykjanes Ridge axis from 27°10'W to 38°50'W based on the multibeam data from RV Marcus Langseth (2013) surveys. Location of the area is presented in the Figure 23. The data was gridded with 30m resolution and using TIN as interpolation method. Surface is contoured at 100 m interval and is illuminated from the northwest. Red boxes outline regions shown in the Map 3.a. (Map 3.a) Detailed bathymetry map is contoured at 50 m interval and hillshade is illuminated from northwest. The map 3.a presents axial volcanic ridges and valleys characteristic for the study area.

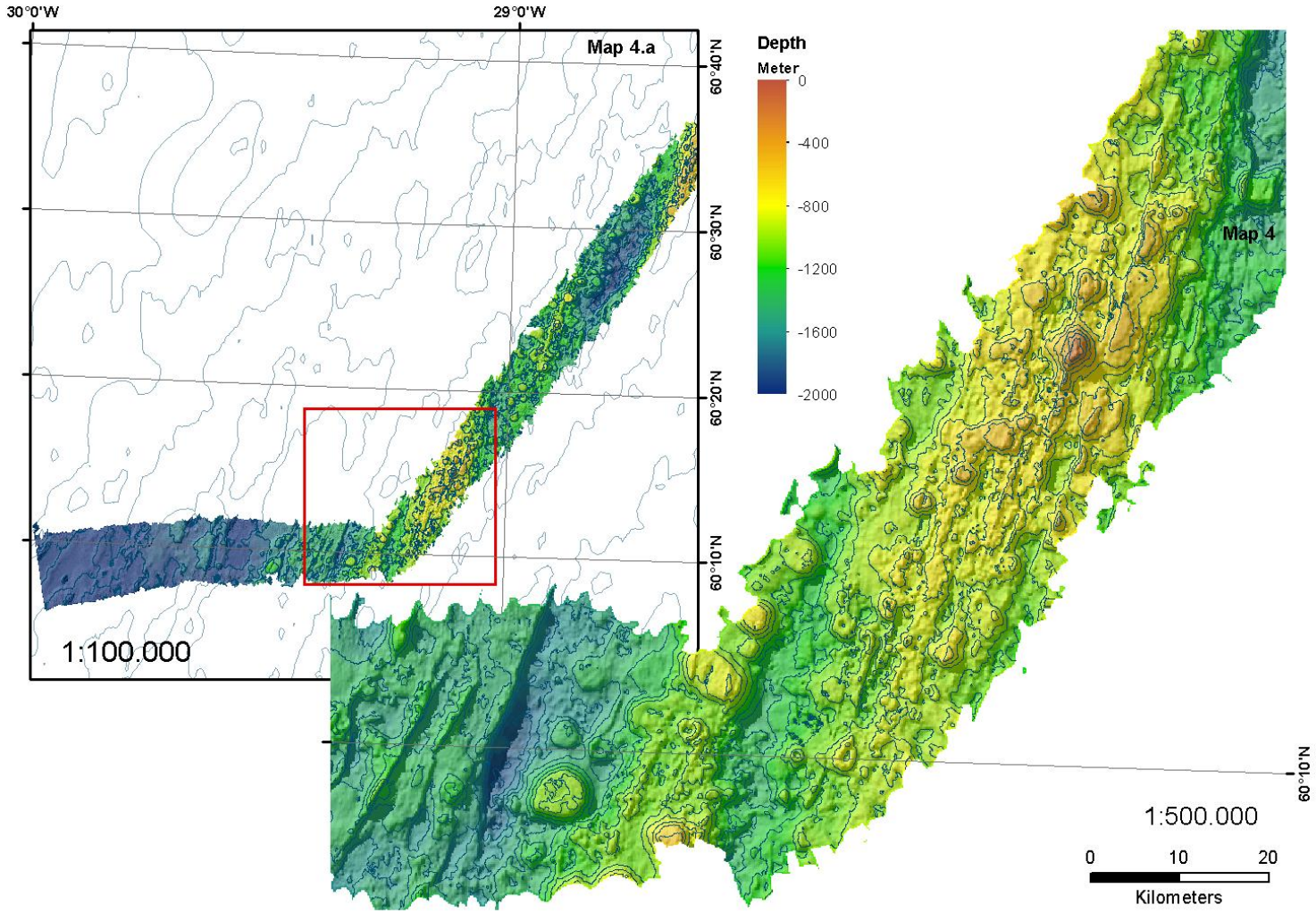

Figure 29 (Map 4) Bathymetry map of Reykjanes Ridge axis from 28°30'W to 30°00'W based on the multibeam data from RV Marcus Langseth (2013) surveys. Location of the area is presented in the Figure 23. The data was gridded with 30m resolution and using TIN as interpolation method. Surface is contoured at 100 m interval and is illuminated from the northwest. Red boxes outline regions shown in the Map 4. (Map 4.a) Detailed bathymetry map is contoured at 50 m interval and hillshade is illuminated from the northwest. The map 4.a presents axial volcanic ridges and valleys characteristic for the study area. In the left bottom corner, the seamount on the bottom of the valley can be recognized.

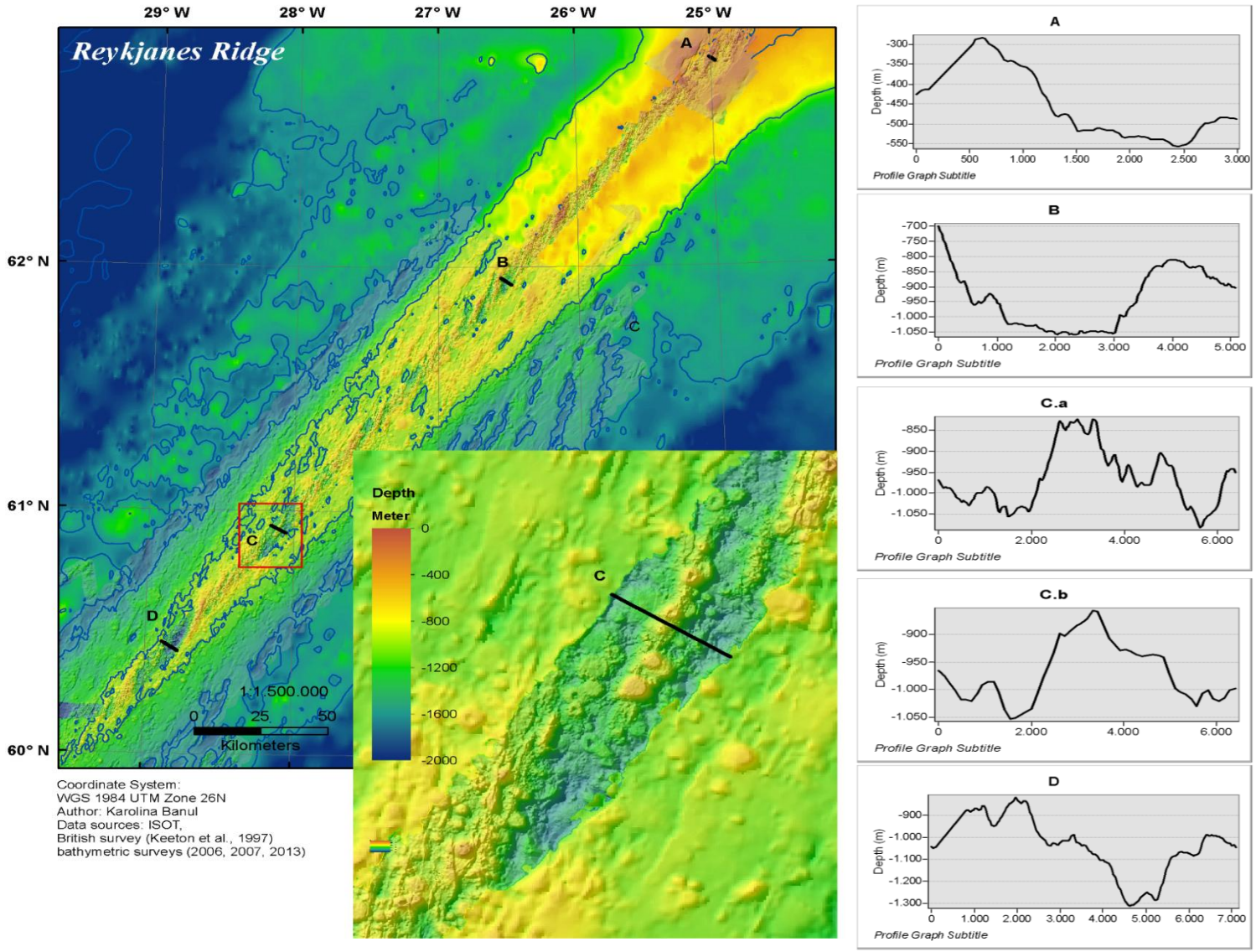

Figure 30 Profiles of the Reykjanes Ridge. They were measured over four locations indicated on the map above (Figure 30). Graphs C.a and C.b show the difference between profiles at the same location but from raster maps of different resolutions – 120 meter (C.b) and 30 meter (C.a).

4.3 Morphology of volcanic structures

The resulting map covers most of the northern part of the Reykjanes Ridge as it extends 535 km from 60°N to 63°40‘N (*cf.* Figure 25, p. 48), where it reach the terrain at the Reykjanes Peninsula. The study area is characterized by transition in axial morphology of MAR from central valley to a central high, as the ridge gets closer to the hot spot (Appelgate & Shore, 1994). The ridge appears narrow in the south, but it gradually expands and elevates while approaching Iceland. This is illustrated on Figure 30 where isobaths contour of -750 and -1000 meter below the sea level delineate characteristic V shaped ridge rising up from the rift on the junction of the two tectonic plates. Also terrain profiles (Figure 30) show that differences amongst elevations become smaller with proximity to Iceland - from 450 meter in the south up to 250 m in the north.

The results clearly show that the spreading centre of the ridge is characterized by axial volcanic ridges (AVR) located perpendicular to the spreading direction and run parallel to the ridge axis. They overlap with each other creating en-echelon formations. AVRs are separated by grabens what is an effect of normal faulting in the area. Faults are easy to distinguish the map below (Figure 31) on the base of the narrow, long linear shape, steep slope and vertical offsets. They are oriented parallel to ridges (off-axis faults) or almost perpendicular to the spreading directions (axial faults). Some of those identified faults are with a height of 200 meters.

Analysis of the volcanic formations is focused on the area between 62-63°N. Morphological structures are recognized mostly on the basis of bathymetry and using supplementary intensity reflection from the backscatter images. The bathymetric and acoustic characteristics of the main morphological structures are described by previous authors (Chadwick et al., 1998; Searle et al., 2010). The identification and classification of the features that appear on the topographic map is based on surface analysis using bathymetric contours, surface slope and curvature, as well as 3D analysis for volume estimation.

The examples of the main **volcanic structures** identified along the whole study area are presented in the maps below (Figure 31 and Figure 32). Volcanic ridges can be distinguished by linear shapes of the crest and steep, deepening flanks on both sides. Identified 23 AVR are 3-20 km long, a 0,5 – 2,6 km wide and 50-320 meters high. The estimated volume range is between 0,1 - 3,4 cubic km (Table 6). For a comparison, AVR identified by Keeton et al. (1997) south of 62°N are between 10-40 km in length, 1.5 – 4.5 km in width, and 200-400 m in height above the sea floor. AVR are separated by garbens (Figure 31) that are characterized by wide area of flat sea floor surrounded by faults. They also consist of smaller and narrower ridges that are created by lines of volcanic hummocks (Appelgate & Shore, 1994).

Seamounts are defined as isolated circular highs that rise above the surrounding sea floor. They are flat-topped and steep-walled with heights larger than 50 meters and diameters between 500-1200m with possible craters. They are also often located over the valley floor of spreading segments. In comparison, hummocky ridges are rounded mounds with heights smaller than 50m, widths less than 500m, and lengths between 1000 and 3500m. Those volcanic cones, circular with 50-500 diameter and moderate slopes, are observed on the top and sides of larger edifices (Smith et al, 1995; Shore & Appelgate, 1994). While it is possible to automatically search bathymetric grid map for enclosed contours (Cochran, 2008), in this study the identification of seamounts is based on the visual analysis of terrain using above described criteria. 42 seamounts are recognized in the area between 62-63°N. They have a diameter from 0,5 to 2 km, and a height of 60-240 m. The average estimated volume range is 0,07-0,1 cu km. Six out of 42 identified seamounts are higher than 100 m and wider than 1 km, with an estimated volume between 0,1-0,31 cu km (Table 7).

All structures of volcanic origin are build up by pillow lava that has a characteristic bumpy and rough shape and can be found along the whole ridge (Figure 33).

Table 6 The morphological characteristics of AVRs between 62-63°N.

AVR	Lower Area [km^2]	Length [km]	Width [km]	Height [m]	L/W ratio	Volume* [km^3]	Volume [km^3]
AVR 1	21,17	14,7	1,7	270	8,9	1,87	2,86
AVR 2	32,80	20,0	2,6	210	7,7	2,63	3,44
AVR 3	6,31	5,3	1,3	250	4,1	0,40	0,79
AVR 4	6,88	6,6	1,4	110	4,9	0,33	0,38
AVR 5	7,55	6,2	1,3	160	4,8	0,67	0,60
AVR 6	15,76	7,7	1,3	120	5,9	0,73	0,95
AVR 7	7,54	5,8	1,6	110	3,6	0,40	0,41
AVR 8	2,09	3,3	0,6	50	5,6	0,06	0,05
AVR 9	3,77	3,5	1,2	160	2,9	0,34	0,30
AVR 10	14,30	9,5	1,4	300	7,0	1,45	2,15
AVR 11	11,41	9,3	1,7	160	5,5	0,88	0,91
AVR 12	14,10	9,0	0,9	280	10,0	1,90	1,97
AVR 13	3,78	4,8	0,5	160	9,6	0,25	0,30
AVR 14	4,12	5,2	1,0	220	5,2	0,64	0,45
AVR 15	3,65	4,7	1,0	260	4,7	0,53	0,47
AVR 16	5,70	4,6	1,5	280	3,1	1,22	0,80
AVR 17	2,29	3,8	0,8	320	5,1	0,53	0,37
AVR 18	9,95	8,3	1,1	240	7,5	1,63	1,19
AVR 19	5,84	4,8	0,6	160	8,0	0,37	0,47
AVR 20	7,96	8,4	1,2	210	7,0	1,05	0,84
AVR 21	6,28	6,5	1,0	170	6,5	0,52	0,53
AVR 22	4,95	5,0	1,0	150	5,0	0,45	0,37
AVR 23	2,00	3,5	0,9	110	3,9	0,08	0,11
MIN	2,0	3,3	0,5	50,0	2,9	0,1	0,1
MAX	32,8	20,0	2,6	320,0	10,0	2,6	3,4
AVARAGE	8,7	7,0	1,2	193,9	5,9	0,8	0,9

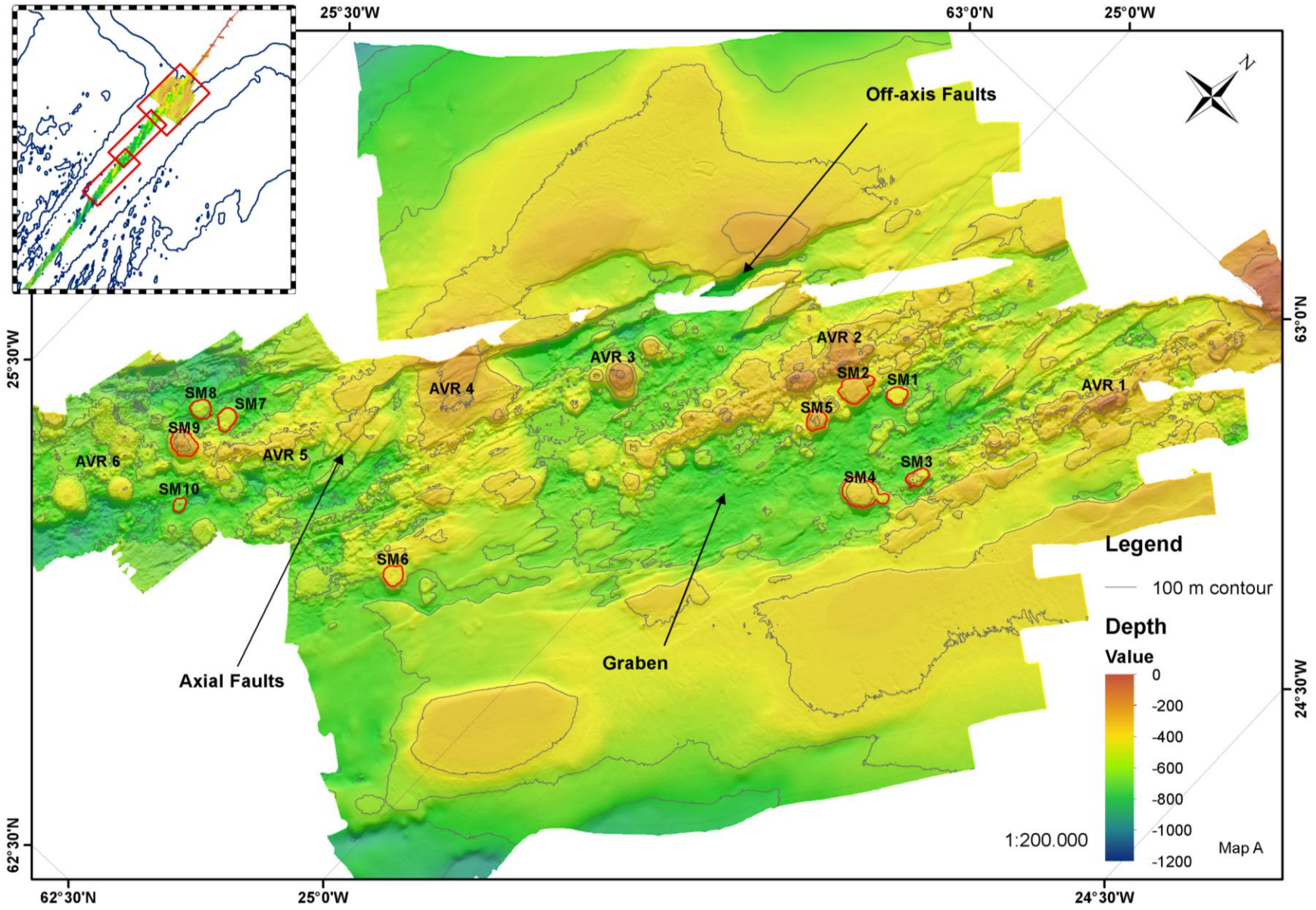
25°30'W
63°0'N
25°0'W
Off-axis Faults
N
AVR 2
AVR 3
AVR 4
AVR 1
AVR 5
AVR 6
SM1
SM2
SM3
SM4
SM5
SM6
SM7
SM8
SM9
SM10
Axial Faults
Graben
Legend
100 m contour
Depth
Value
0
-200
-400
-600
-800
-1000
-1200
1:200.000
Map A
63°0'N
25°30'W
24°30'W
62°30'N
62°30'N
25°0'W
24°30'W

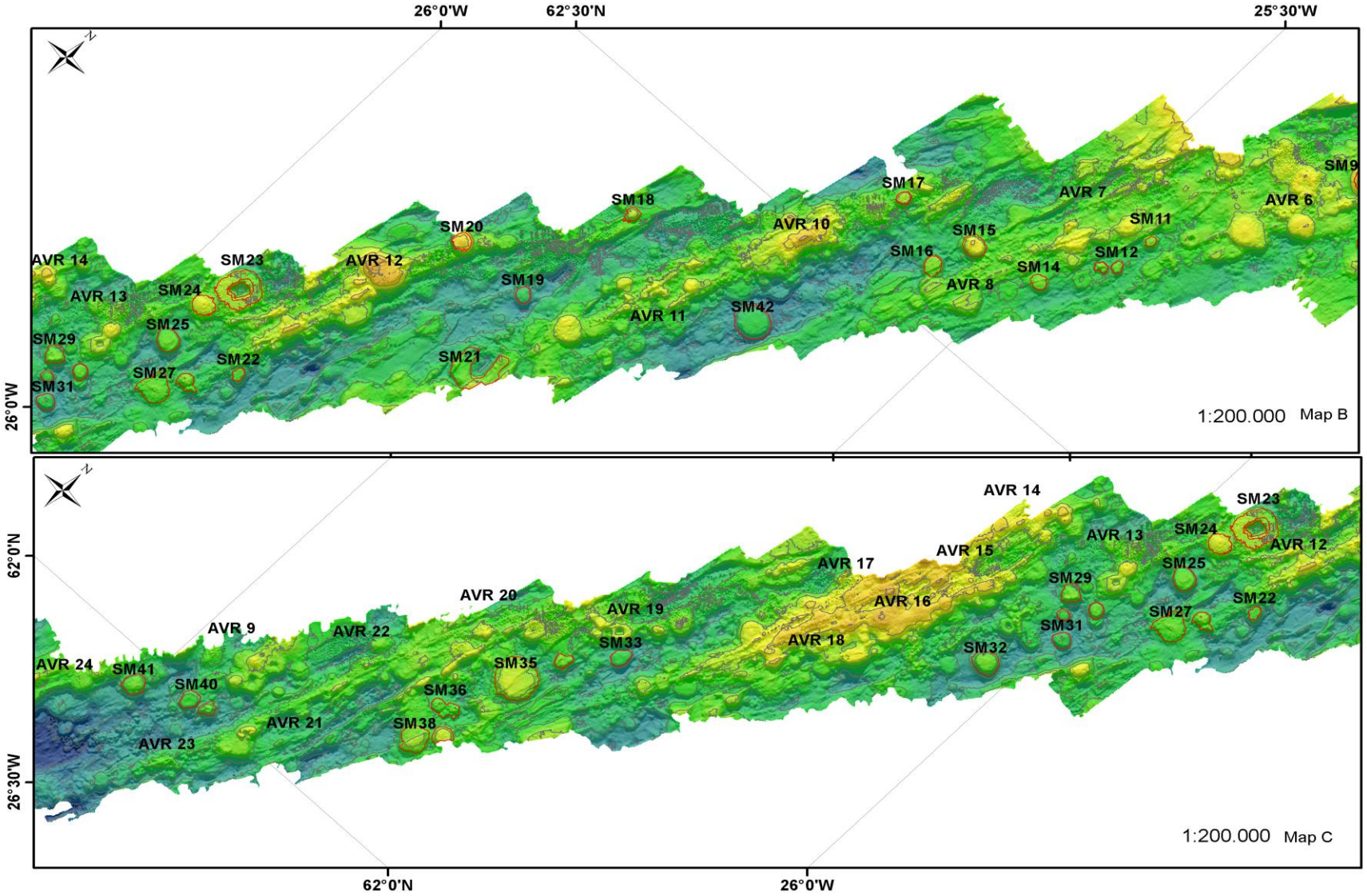

Figure 31 Morphological structures of the Reykjanes Ridge. The maps A, B, and C indicate examples of tectonic and volcanic structures in the study area.

Table 7 The morphological characteristics of Seamounts between 62-63°N.

Seamounts	Lower Area [km^2]	Diameter [m]	Height [m]	Volume* [km^3]	Volume [km^3]
SM1	0,6	800	80	0,04	0,04
SM2	1,4	1100	100	0,11	0,14
SM3	0,6	600	80	0,03	0,04
SM4	1,9	1300	140	0,16	0,26
SM5	0,7	850	120	0,06	0,08
SM6	0,7	900	80	0,06	0,05
SM7	0,6	650	160	0,09	0,10
SM8	0,7	950	120	0,07	0,08
SM9	1,1	950	240	0,20	0,26
SM10	0,3	500	80	0,02	0,02
SM11	0,2	500	80	0,01	0,01
SM12	0,2	500	60	0,01	0,01
SM13	0,2	500	100	0,02	0,02
SM14	0,4	700	100	0,03	0,04
SM15	0,8	900	160	0,08	0,13
SM16	0,5	700	160	0,08	0,09
SM17	0,3	550	100	0,03	0,03
SM18	0,3	580	120	0,03	0,04
SM19	0,4	630	100	0,03	0,04
SM20	0,5	730	160	0,07	0,08
SM21	2,2	2000	140	0,16	0,31
SM22	0,2	500	160	0,02	0,04
SM23	2,3	1800	100	0,15	0,23
SM24	0,7	900	140	0,09	0,10
SM25	0,9	950	100	0,07	0,09
SM26	0,5	700	120	0,04	0,06
SM27	1,4	1200	60	0,05	0,08
SM28	0,4	700	80	0,02	0,03
SM29	0,6	800	100	0,05	0,06
SM30	0,2	500	100	0,02	0,02
SM31	0,5	700	120	0,04	0,06
SM32	1,0	1100	160	0,13	0,16
SM33	0,5	750	100	0,05	0,05
SM34	0,4	550	120	0,03	0,04
SM35	2,9	1800	140	0,31	0,41
SM36	0,7	600	80	0,03	0,06
SM37	0,5	900	120	0,05	0,06
SM38	1,2	1000	120	0,10	0,14
SM39	0,3	550	120	0,02	0,04
SM40	0,6	900	60	0,03	0,03

SM41	0,7	900	160	0,10	0,12
SM42	2,0	1600	140	0,21	0,28
MIN	0,16	500	60	0,01	0,01
MAX	2,94	2000	240	0,31	0,41
AVARAGE	0,78	864	116	0,07	0,10

*Area of the polygon delineated by usually enclosed contour on the bottom of the ridge or seamount.

** Volume was estimated on the basis of terrain surface analysis, which calculates volume for the lower area (polygon) above the reference plane (depth for the lower area).

4.4 Analysis of backscatter images

The intensity reflection supports in identification various geological and morphological structures. The backscatter image (Mosaic of GeoBaRs) is draped over the topography within selected areas of the Reykjanes Ridge (Figure 32). The intensity image generated with Geocoder engine from Langseth data is of very good quality and allows one to recognize major structures on the Ridge such as faults (C) that appear as darker linear reflection, circular reflection of calderas and seamounts (B and C), lava flows – flat lighter in reflection, and sediments – darker in reflections. It is also possible to recognize a small vent that appears as a small, light circular reflection (A). Intensity data interpretation follows the examples presented by Searle et al. (2010). Figure 33 presents 3D images representing volcanic and tectonic structures found in the study area. All backscatter images (mosaic) were exported from Caris as ASCII and then loaded to ArcInfo, as it offers more tools for further image processing and display (Figure 34).

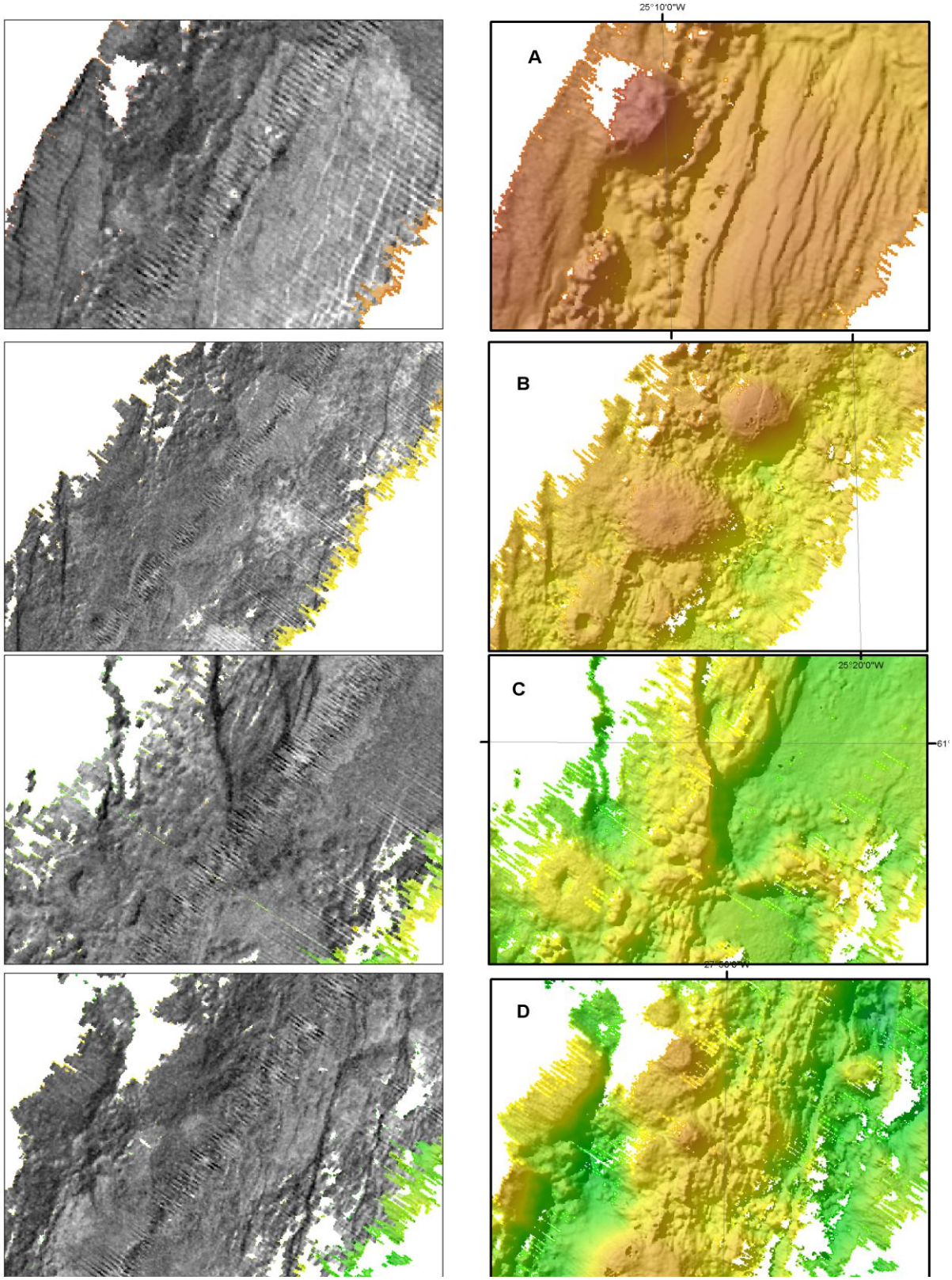

Figure 32 The appearance of main morphological structures on backscatter images in comparison to the topographic maps.

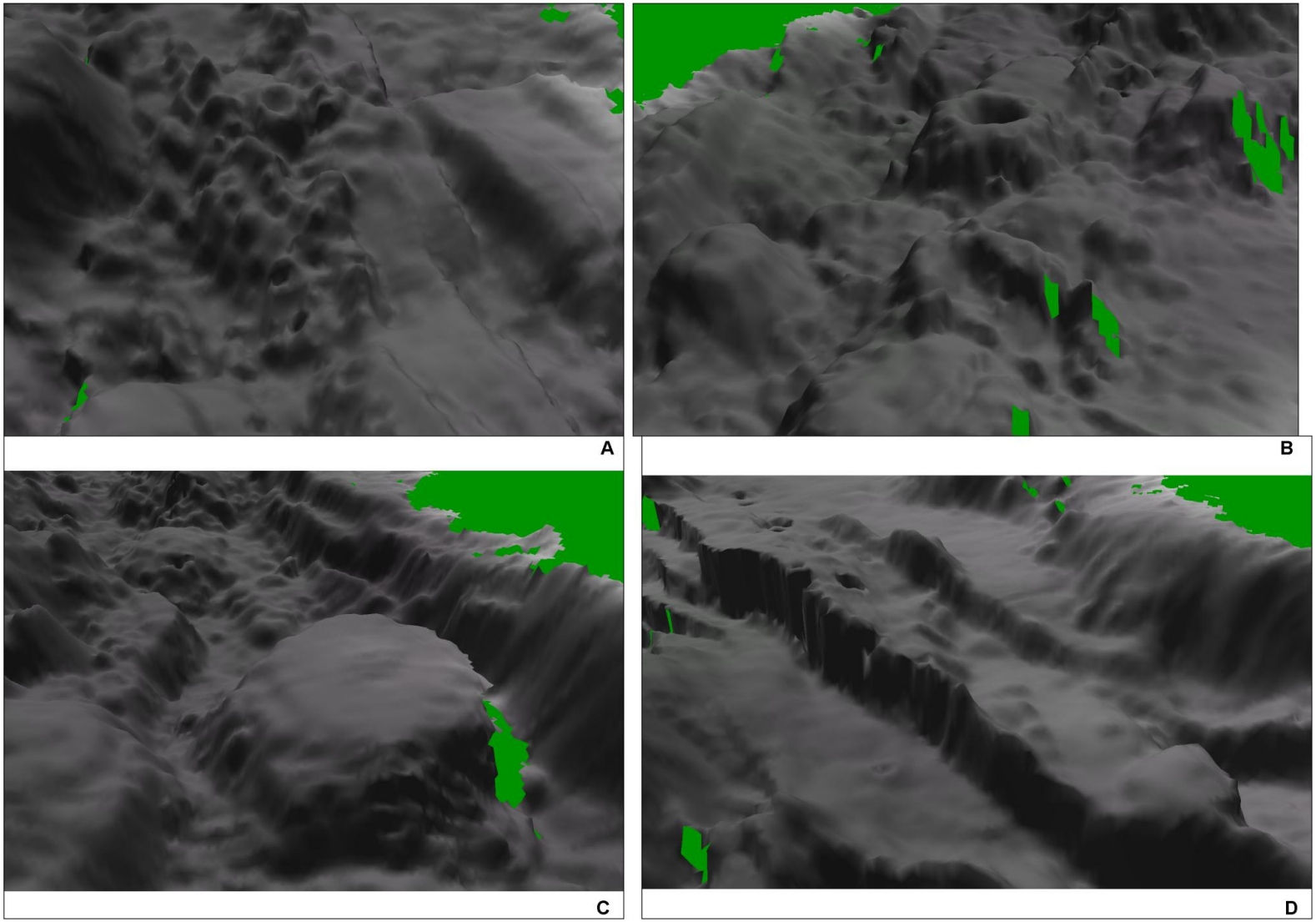

Figure 33 The 3D images of volcanic and tectonic structures. Backscatter image is draped over the elevation.

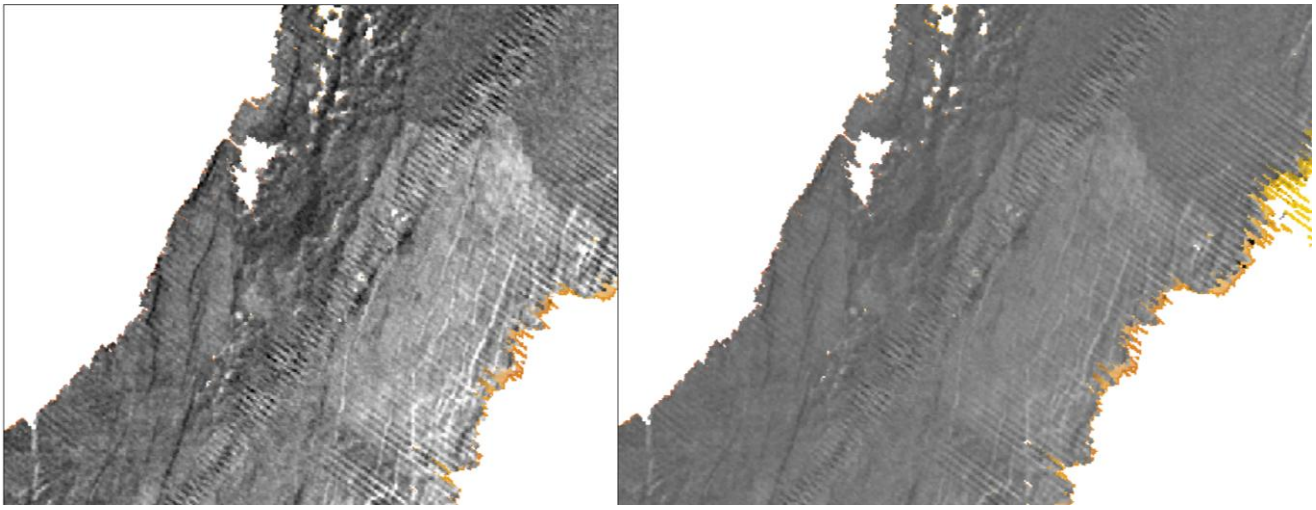

Figure 34 The comparison of backscatter images editing in ArcInfo and Caris. Image on the left side was produced in Arc Info and appears with more contrast, than one produced in Caris (in the right).

4.5 Changes over time

In order to detect potential changes in the morphology of the study area, the overlapping parts of the datasets are compared. This is done on the basis of raster calculations, and three difference rosters are presented in the Appendix C. All difference grids show change in elevation that ranges from 200 m lost to more than 200 m gain in some of the locations. Furthermore, the results of overlay between maps created from two most recent surveys revealed the pattern of the ship tracks (Figure 35). Thus, even after all corrections involved in the processing stage, the significant systematic error remains in the datasets from 2007. However, the comparison of the oldest and the newest datasets after smoothing and setting threshold for significant change indication (2 and 3 standard deviation when classifying the raster for display) uncovers an accumulation of changes on elevation around one of the seamounts located at 26°15'W 62°13'N. There is a gain in elevation on the top of the seamount, while loss of material around it. This change is visible also in the difference map between 1994 -2007, but the extent of change is even wider in the difference grid 1994-2013 (Figure 36).

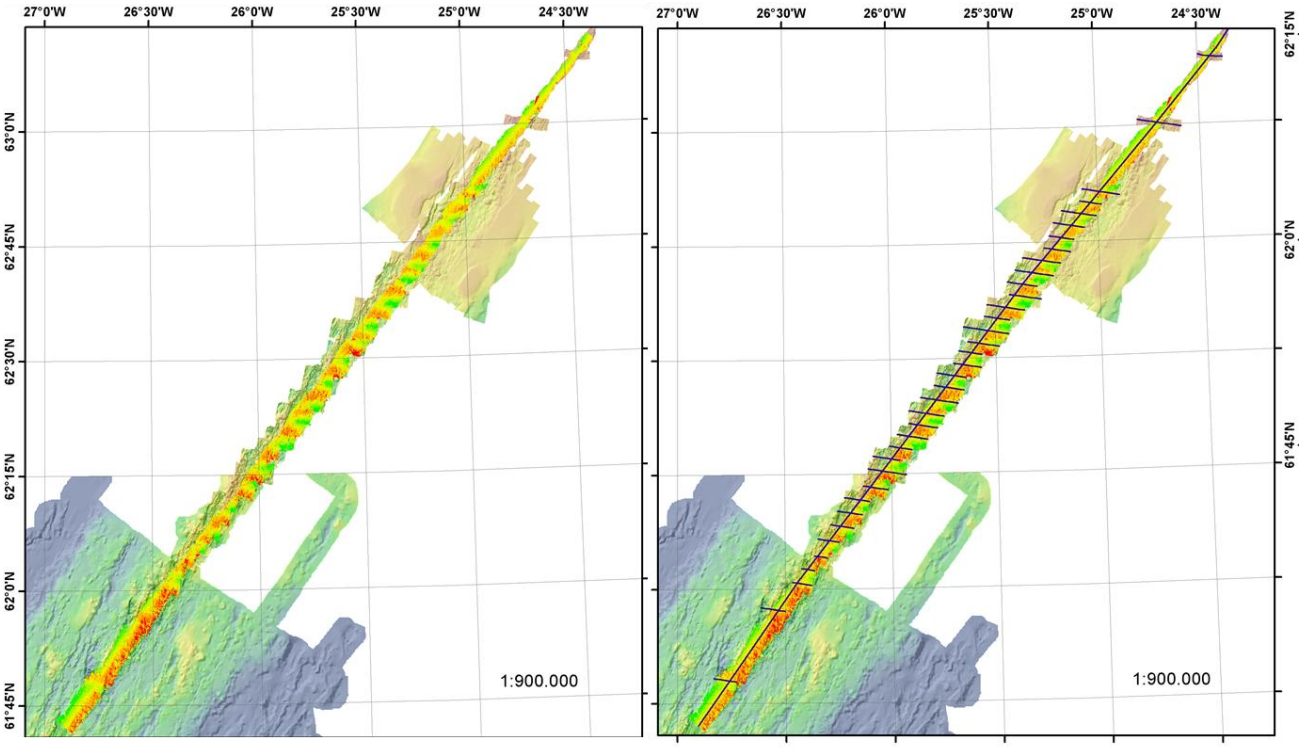

Figure 35 The comparison of "difference" grid from years 2007-2013 and survey ship tracks from 2007.

The results from raster based change analysis are compared with seismic activity data. This shows that between 1994 and 2014, there were 5 earthquakes with magnitude from 4.3-4.4 mb that had epicenter within 7- 9 km from the place of potential change.

Finally, the location was investigated in the 3D display in Caris using both 2007 and 2013 datasets. Unfortunately, the overlap between datasets at this place is too narrow and the image from 2007 appears to have poor quality (Figure 37). Thus only a high-resolution image from 2013 is used for the analysis (Figure 38). The visual analysis of 3D surface model with draped backscatter reflection did not revealed any light intensity reflection. If it did, it would indicate a soft and rough surface from which the signal was reflected, and consequently extrusion of magma in the locations.

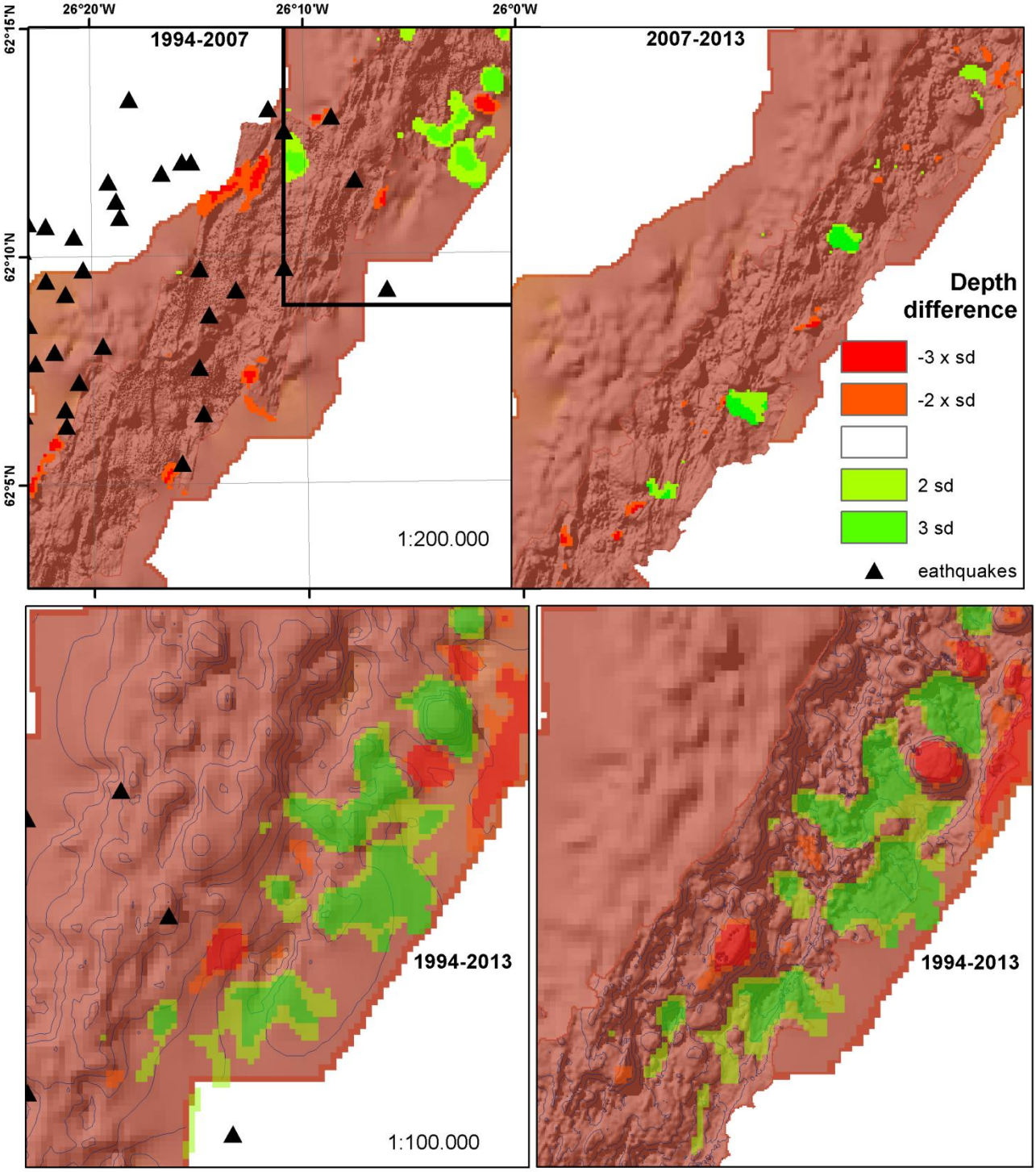

Figure 36 Changes over time based on the raster based difference method. The difference in elevation was calculated using the 120 m resolution raster maps. On the map above the higher resolution - 30 meter raster surfaces from newest bathymetric surveys (2007, 2013) are draped over the lower resolution map produced from older dataset (1994). The difference map was classified according to the histogram – breaks were set at 2 and 3 standard deviations. Black triangles shows the earthquakes events in years 1994-2014 with magnitude between 3.5 -5.7.

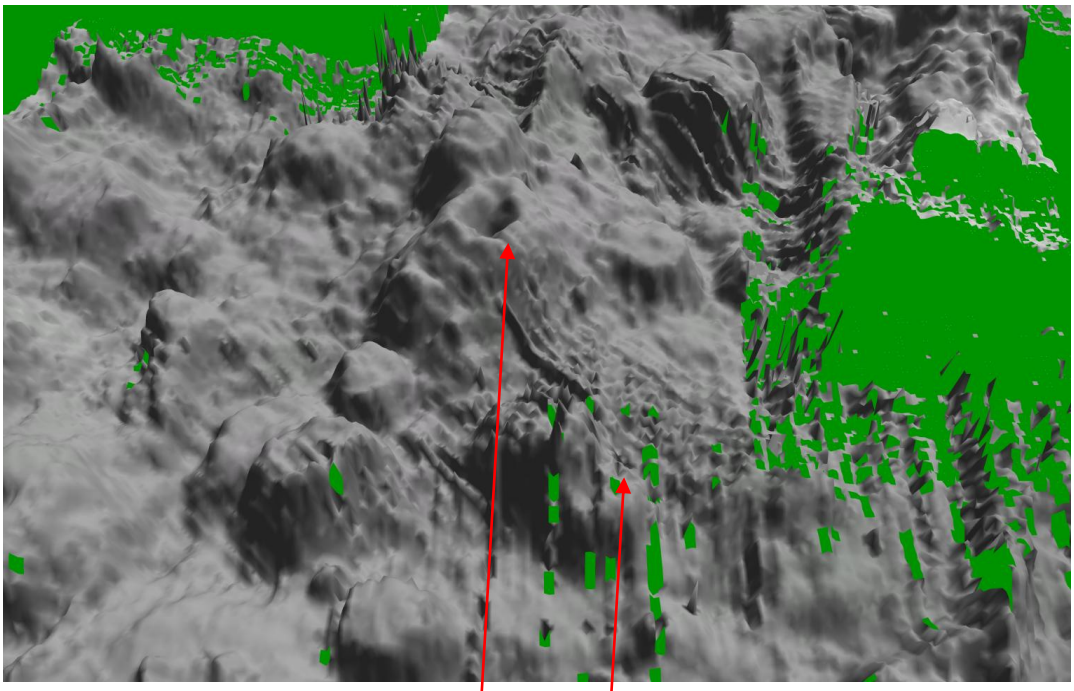

Figure 37 Backscatter image draped over the topography (2007 dataset). View on the location of the potential elevation change.

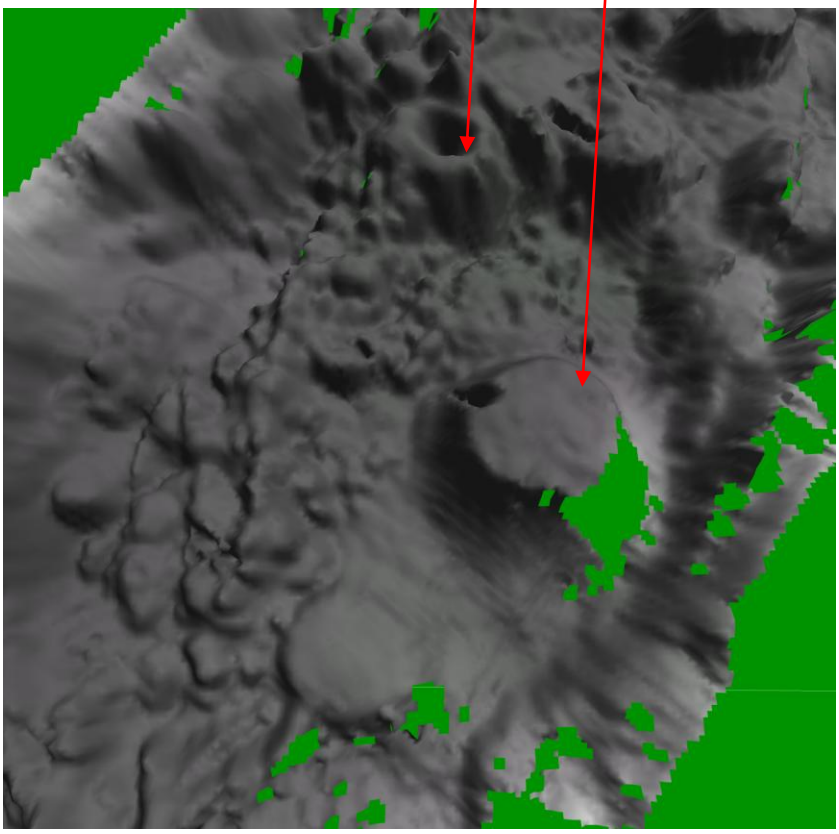

Figure 38 Backscatter image draped over the topography (2013 dataset). Red arrows indicate potentially corresponding structures on the image.

5 Discussion and Conclusions

The results of the comparison analysis do reveal evidence about changes in topography of the Reykjanes Ridge and confirm the hypothesis of this study. Thus, for the first time an area of the ridge has been identified as a potential eruption and/or volcano-tectonic site between 1994 and 2013. However, the error margin is large and interpretation of results from comparison analysis results should take into account the problems with data that were identified during maps modeling and analysis.

Especially the pattern of vessel tracks (survey in 2007) in difference grids indicates the systematic error remaining in the dataset, which puts into question the quality of the processing stage. Also, in many places, data overlap between Knorr and Langseth surveys is too narrow, and the distance between ship tracks is approximately 2.5 km. This result in situations where overlapping parts of the grids consist of data from the swath edges that are usually the most distorted and erroneous.

Furthermore, the problem with Bridge data format (did not allow for direct gridding in ArcInfo) and uneven grid cells (0,002 and 0,001 degree) creates risk for data modification. Data points (ASCII file) were regularly spaced as if they would already be nodes of gridded surface. But after converting those data points to raster, nodes that should be in the centre were moved to the sides and edges of the cells. That could possibly change elevation values and influence the final result of raster calculations.

Even though the comparison analysis encountered problems with data, the aim to create a high-resolution map of the Reykjanes Ridge was achieved. Still, the decision about 30 meter cell size for grids to convert desecrate bathymetric measurements into a continuous raster surface was a compromise between accuracy and visual effect of the map. During the whole process of map creating, the leading goal was to keep as many original values as possible. Therefore, the interpolation was the last choice when testing various techniques to grid bathymetric measurements. As it was discussed before, the differences in spaces between data points depends on the water depth. That makes it challenging to find an appropriate cell size, which keeps enough detail, but at the same time, does not leave empty space on the continuous map surface. Without utilizing any interpolation method, significant down scaling would have to be applied. Therefore, TIN was applied to create a raster surface without data gaps.

Another solution could be creating a multi-resolution raster surface. It means that data points would be divided into subsets depending on separating distances, multiple raster surfaces would be created with different resolutions, and then a few grids would be overlaid to create one map of the study area. However, that kind of raster map would be problematic for terrain analysis and impossible to use for raster calculations and analyses.

Besides, successful modeling of bathymetric maps and intensity images in ArcInfo accomplished the aim of developing method for interoperability of bathymetric data between raw analytical program for multibeam data and a spatial analytical program of geographical data.

Finally, the series of high resolution, bathymetric maps of an unexplored, geologically active oceanic ridge meets the general aim to increase knowledge and understanding of submarine volcanic and tectonic processes. As volcanic edifices can be found on the topographic maps along the Reykjanes Ridge, the specific effusive activity associated with those structures can be recognized. The summary

describing morphological characteristics of volcanic structures is provided in the study. However, further interpretation of the presented results – the map of the Reykjanes Ridge – is beyond the scope of this project.

References

Amante Ch., Eakins B.W. (2009) *ETOPO1: 1 Arc-Minute Global Relief Model: Procedures, Data Sources and Analysis*. Boulder, Colo: U.S. Dept. of Commerce, National Oceanic and Atmospheric Administration, National Environmental Satellite, Data, and Information Service, National Geophysical Data Center, Marine Geology and Geophysics Division. http://www.ngdc.noaa.gov/mgg/global/relief/ETOPO1/docs/ETOPO1.pdf

Amante Ch., Eakins B.W, Taylor L.A (2010). *Spline interpolation of sparse bathymetric data for Digital Elevation Models (DEMs).* Conference poster presentation from 15th September 2010, Retrieved from http://www.gebco.net/about_us/gebco_science_day/documents/gebco_fifth_science_day_amante.pdf

AML Oceanographic (n.d.). *What is a Multibeam System*? Website material. Retrieved on January 29th, 2014 from http://www.amloceanographic.com/CTD-Sound-Velocity-Environmental-Instrumentation-Home/Multibeam-Overvew.

Appelgate B., Shor A.N. (1994). The northern Mid-Atlantic and Reykjanes Ridges: Spreading center morphology between 55°50'N and 63°00'N. *Journal of Geophysical Research*, 99 No. B9, pp. 17695–18203.

Artilheiro, F. M. F. (1998). *Analysis and Procedures of Multibeam Data Cleaning for Bathymetric Charting.* Department of Geodesy and Geomatics Engineering. Technical Report No. 192, University of New Brunswick, Fredericton: New Brunswick.

Atkins D. (2013). *Exploration Techniques for Locating Offshore Geothermal Resources*. Master thesis: Reykjavik University, School of Science and Engineering, Reykjavik. Retrieved from Skemman.is.

Bacon Ch. R., Gardner J. V., Mayer L. A., Buktenica M. W., Dartnell P., Ramsey D. W. and Robinson J. E., (2002). Morphology, volcanism, and mass wasting in Crater Lake, Oregon. *Geological Society of America Bulletin*, 114, no. 6, pp. 675-692.

Benson H. (1996). *University Physics*. Wiley & Sons, Inc.: New York, NY, pp. 347-358.

Bjorke J.T., Nilsen S. (2009). Fast trend extraction and identification of spikes in bathymetric data. *Computers & Geosciences 35*, pp. 1061–1071. Available Online at: http://www.sciencedirect.com/science/article/pii/S009830040800280X#.

Caress D.W., Clague D.A., Paduan J.B., Martin J.F., Dreyer B.M., Chadwick Jr W.W., Denny A., Kelley D.S. (2012). Repeat bathymetric surveys at 1-metre resolution of lava flows erupted at Axial Seamount in April 2011. *Nature Geoscience*, 5, Online at: www.nature.com/naturegeoscience.

Caris (2011). *Caris HIPS and SIPS User's Guide*. Heeswijk, The Netherlands.

Caris (2012). *Caris: Training manual. HIPS and SIPS 7.1.* Heeswijk, The Netherlands.

Chadwick W.W Jr, Embley R.W, Fox Ch.G. (1995). SeaBeam depth changes associated with recent lava flows, CoAxial Segment, Juan De Fuca Ridge: Evidence for multiple eruptions between 1981-1993. *Geophysical Research Letters*, 22, no.2, pp. 167-170.

Chadwick W.W. Jr, Embley R. W., Shank T. M. (1998).The 1996 Gorda Ridge eruption: Geologic, mapping, sidescan sonar, and SeaBeam comparison results. *Deep-Sea Research II* 45, pp. 2547-2569.

Christophersson R.W. (2012). *Geosystems: Introduction to physical geography*. Prentice-Hall: Boston, MA.

Cochran J. R. (2008). Seamount volcanism along the Gakkel Ridge, Arctic Ocean. *Geophysical Journal International*, 174, pp. 1153–1173.

Costa B.M., Battista T.A., Pittman S.J. (2009). Comparative evaluation of airborne LiDAR and ship-based multibeam Sonar bathymetry and intensity for mapping coral reef ecosystems. *Remote Sensing of Environment*, 113, pp. 1082–1100.

DeMers M.N. (2009). *Fundamentals of Geographic Information System* (4th ed.). John Willey & Sons, Inc.: New York, NY, pp. 247-268.

Dunn R. A., Scheirer D.S., Forsyth D. W. (2001). A detailed comparison of repeated bathymetric surveys along a 300-km-long section of the southern East Pacific Rise. *Journal of Geophysical Research*, 106, No. B1, pp. 463-471.

Earthquake Hazard Programme. (2013). Page Last Modified: November 07, 2013. Retrieved March March 15, 2014, from http://earthquake.usgs.gov/earthquakes/?source=sitenav.

Eysteinsson H., Danielsen P.E. (2003). *Multibeam bathymetry at Aegir Ridge*. Project report no. OS-2003/027. Orkustofnun: Reykjavik.

Embley R.W, Chadwick W.W., Clague D.A, Stakes D. (1999). 1998 Eruption of Axial Volcano: Multibeam anomalies and seafloor observations. *Geophysical Research Letters*, 26, no.23, pp. 3425-3428.

Fonseca L., Calder B. (2005). *Geocoder: an efficient backscatter map constructor*. Proceedings of the U.S. Hydrographic Conference 2005, San Diego, C.A. Online at: http://www.thsoa.org/hy05/08_3.pdf.

Fox C.G., Chadwick W.W. Jr, Embley, R.W. (1992). Detection of changes in ridge-crest morphology using repeated multibeam surveys. *Journal of Geophysical Research*, 97, no B7, pp. 11149-11162.

Frye Ch. (2007). Choosing an appropriate cell size when interpolating raster data. ArcGIS Resources, ESRI. Online article, retrieved on April, 25th, 2014 from: http://blogs.esri.com/esri/arcgis/ 2007/07/03/choosing-an-appropriate-cell-size-when-interpolating-raster-data/.

Gafeira, J. (2010). *A geomorphological interpretation of multibeam data from the nearshore area between Belfast Lough and Cushendun, Northern Ireland*. British Geological Survey Commissioned Report, CR/10/075.

GEBCO (2013). *Ocean Mapping Phases. Data processing*. Online article published on Nippon fundation/Gebco Training Programme in 2013, retrieved on March 27th 2014 from http://ccom.unh.edu/gebco2013/data_processing.html.

Goslin J., Lourenço N., Dziak R.P., Bohnenstiehl D.R., Haxel J.,Luis J. (2005). Long-term seismicity of the Reykjanes Ridge (North Atlantic) recorded by a regional hydrophone array. *Geophysical Journal International*, 162, no. 2, pp. 516-524.

GVP (1992). Young lava flow identified from submersible. *Bulletin of the Global Volcanism Network* 17:08. Available online at: http://volcano.si.edu/world/vol_extra.cfm?name=Northern_Reykjanes _Ridge#bgvn_1708.

Heywood I., Cornelius S., Carver S. (2006). *An introduction to Geographical Information System (3rd edition)*. Pearson: Harlow, pp. 71-107.

Höskuldsson Á., Hey R., Kjartansson E., Guðmundsson G. B. (2007). The Reykjanes Ridge between 63◦10'N and Iceland. *Journal of Geodynamics*, 43, 73–86. Available online at: http://dx.doi.org/10.1016/j.jog.2006.09.003.

Höskuldsson Á. (2014). *Interview*. Personal communication, March 31st 2014.

Hughes Clarke J.E. (2012). *Swath-Sonar Related Sites*. Website of Ocean Mapping Group, University of New Brunswick, http://www.omg.unb.ca/omg/SwathSites.html.

IHO (2011). The Need for International Hydrographic Service. IHO Publication M-2.Version 3.0.1 – October 2011. http://www.iho.int/iho_pubs/misc/M-2_3.0.2_E_JAN2014.pdf.

IHO (2013). *Bathymetry and Ocean Mapping*. Online article published on March 21st, 2013. Retrieved on March 1st, 2014 from: http://www.iho.int/srv1/index.php?option=com_content&view= article&id=300&Itemid=744.

Jensen, J. R. (2000). *Remote sensing of the environment: an earth resources perspective*. New York, NY: Prentice-Hall, Inc , pp. 379-406.

Jones E.J.W (1999). *Marine Geophysics*. Chichester: John Wiley, pp. 1-61.

Kearns T.A., Breman J. (2010). Bathymetry – the art and science of seafloor modeling foe modern applications. In Breman J. (ed.), *Ocean Globe*. ESRI Press, pp. 1-36. Available online at: http://downloads2.esri.com/ESRIpress/images/169/OGLOBE_ch01.pdf.

Keeton J. A., Searle R. C., Parsons B., White R. S., Murton B. J., Parson L. M., Peirce C., Sinha M. C. (1997). Bathymetry of the Reykjanes Ridge. *Marine Geophysical Researches* 19, 55-64. Available online at: http://link.springer.com/article/10.1023%2FA%3A1004266721393.

Kongsberg Maritime AS (2013) *Kongsberg EM®122. Data sheet*. Retrieved from: http://www.km.kongsberg.com/ks/web/nokbg0397.nsf/AllWeb/E016DF00EBFC2964C12571B1003F9 DDA/$file/306105_em122_product_specification.pdf?OpenElement.

Krom M.D. (2005) Plate tectonics. In Holden J. (ed.). *An introduction to Physical Geography and Environment*. London: Pearson Education Limited, pp. 97-117.

L-3 Communications SeaBeam Instruments (2000). *Multibeam sonar. Theory of operation*.

L-3 Elac Nautik (n.d.) *SeaBeam 3012. Full Ocean Depth Multibeam System*. Brochure. Retrieved on January 27th, 2014 from: http://www.elac-nautik.de/_uploads/images/pdf/L3_ELAC_Nautik_SeaBeam3012.pdf.

Lamont-Doherty Earth Observatory (n.d.). *R/V Marcus G. Langseth. Scientific Instrumentation*. Retrieved on January 27th, 2014 from: https://www.ldeo.columbia.edu/research/office-of-marine-operations/langseth/scientific-instrumentation.

Lirakis C.B., Bongiovanni K.P. (2000). Automated Multibeam Data Cleaning and Target Detection. *Oceans 2000, IEEE Conference Proceedings*, pp.719-723. Available Online at: http://ieeexplore.ieee.org/xpl/articleDetails.jsp?tp=&arnumber=881336&searchWithin%3Dp_Authors%3A.QT.Lirakis%2C+C.B..QT.%26searchWithin%3Dp_Author_Ids%3A38015119100.

Liu J.G., Mason P.L. (2009). Essential Image Processing and GIS for remote sensing. John Wiley & Sons, Inc.: Hoboken, NY.

Macdonald A.J., Collins C. (2008). Taking Geocoder to work. Making Geocoder part of your Daily Routine. *Shallow survey*. Available online at: http://www.Caris.com/downloads/brochures/CARIS%20SIPS%20and%20Geocoder.pdf.

Magde L.S., Smith D.K. (1995). Seamount volcanism at the Reykjanes Ridge: Relationship to the Iceland hot spot. *Journal of Geophysical Research*, 100, no. B5, pp. 8449-8468.

Mochizuki M., Brandsdóttir B., Shiobara H., Gudmundsson G., Stefánsson R., Shimamura H. (2000). Detailed distribution of micro-earthquakes along the northern Reykjanes Ridge, off SW-Iceland. *Geophysical Research Letters*, 27, no 13, pp. 1945–1948. Available online at: http://onlinelibrary.wiley.com/doi/10.1029/1999GL011264/abstract.

MRI – Hafrannsóknastofnun (n.d.). *Research vessels. Árni Friðriksson RE 200 / 2350*. Website material. Retrieved on January 30th, 2014 from http://www.hafro.isundir_eng.php?REFID=53&ID=55&REF=1.

Murton B.J., Taylor R., Thirlwall M.F. (2002). Plume ridge interaction: Geochemical perspective on Reykjanes ridge. *Journal of Petrology* 43, 1987-2012.

NOAA (n.d.). *Uses of Hydrographic Survey Data*. Retrieved on January 27th, 2014 from: http://www.ngdc.noaa.gov/mgg/bathymetry/noshdb/nosuses.HTML.

Pumer Ch. C., MacGeary D., Carlson D.H. (2005). *Physical Geology* (10th ed.). McGraw Hill Companies, Inc.: New York, NY, pp. 443-467.

Rogala J.T. (1999). *Bathymetry*. Upper Mississippi River System Navigation Feasibility Study. Upper Midwest Environmental Sciences Center: USGS, Retrieved on March 20th, 2014 from: http://www.umesc.usgs.gov/aquatic/bathymetry/methods.html).

Sabins F.F. (1996). *Remote Sensing. Principals and interpretation (3rd ed.).* New York, NY: W.H.Freman and Company, pp. 314-322.

Schmitt T., Mitchell N.C., Tony A., Ramsay S. (2008).Characterizing uncertainties for quantifying bathymetry change between time-separated multibeam echo-sounder surveys. *Continental Shelf Research* 28, pp. 1166– 1176.

Searle R.C., Keeton J., Owens R.B., White R.S., Mecklenburgh R., Parsons B., Lee S.M. (1998). The Reykjanes Ridge: structure and tectonics of a hot-spot-influenced, slow-spreading ridge, from multibeam bathymetry, gravity and magnetic investigations. *Earth and Planetary Science Letters* 160, pp. 463-478. Available online at http://dx.doi.org/10.1016/S0012-821X(98)00104-6.

Searle R.C., Field P.R., Owens R.B. (1994). Segmentation and a nontransform ridge offset on the Reykjanes Ridge near 58ºN. *Journal of Geophysical Research*, 99, no. B12, pp.24159–24172.

Searle R.C., Murton B.J. , Achenbach K., LeBas T., Tivey M., Yeo I., Cormier M.H., Carlut J., Ferreira P. , Mallows C., Morris K., Schroth N., van Calsteren P., Waters C. (2010). Structure and development of an axial volcanic ridge: Mid-Atlantic Ridge, 45°N. Earth and Planetary Science Letters 299, pp. 228–241.

Seibold E., Berger W.H. (1993). *An introduction to Marine Geology* (2nd Ed.) Berlin: Springer Verlag, pp. 21-25.

Smith D. K., Humphris S. E., Bryan W. B. (1995). A comparison of volcanic edifices at the Reykjanes Ridge and the Mid-Atlantic Ridge at 24° - 30°N. *Journal of geophysical research*, 100 No. B11, pp. 22485-22498.

Sturkell E., Einarsson P., Sigmundsson F., Geirsson H.,Ólafsson H., Pedersen R., de Zeeuw-van Dalfsen E., Linde A.T., Sacks S. I., Stefánsson R. (2006). Volcano geodesy and magma dynamics in Iceland. *Journal of Volcanology and Geothermal Research*, 150, pp. 14–34.

Sterling D. L., (2003), *A Comparison of Spatial Interpolation Techniques For Determining Shoaling Rates of The Atlantic Ocean Channel.* Master Thesis. Retrieved from: http://scholar.lib.vt.edu/ theses/available/etd-09162004 094346/unrestricted/Full_Thesis_Doc_9_28_04.pdf;

Tarbuck E.J., Lutgens F.K., Tasa D. (2011). *Earth. An introduction to Physical Geology. 10th Edition.* Pearson Education, Inc.: New Jersey. Chapter 13 – Divergent Boundaries: Origin and Evolution of the Sea floor, pp. 335-380.

Thordarson T., Larsen G. (2007). Volcanism in Iceland in historical time. Volcano types, eruption styles and eruptive history. *Journal of Geodynamics*, 43, pp. 118–152.

University of Rhode Island (2013). How fast does sound travel? Discovery of Sound in the Sea. Website material. Retrieved on January 29th, 2014 from http://www.dosits.org/science/ soundmovement/speedofsound/#.

Vésteinsson Á.T. (2014). Personal interview, on 9.05.2014, Reykjavik. Icelandic Coast Guard Office.

Voght P. (1986). Morphology, topography, sediments and paleoenvironments. In Hurdle, B. (ed.), *Nordic Seas*. New York, NY:Springer-Verlag, pp. 237-279.

Voght P. (1986b). Historic Volcanism. Geophysical and geochemical signatures and plate tectonics. In Hurdle, B. (ed.), *Nordic Seas*. New York, NY:Springer-Verlag, pp. 448-455.

Voght P. (1986c). Geophysical and geochemical signatures and plate tectonics. In Hurdle, B. (ed.), *Nordic Seas*. New York, NY:Springer-Verlag, pp. 571-592.

WHOIa, (n.d.). *R/V Knorr Specifications*. Retrieved on January 19th, 2014 from: http://www.whoi.edu/main/ships/knorr/specifications.

WHOIb, (n.d.). *R/V Knorr SEABEAM*. Retrieved on January 19th, 2014 from: http://www.whoi.edu/page.do?pid=8576.

WHOIb, (n.d.). R/V Knorr Navigation Equipment. Retrieved on January 19th, 2014 from: http://www.whoi.edu/page.do?pid=8575.

Wright I.C., Chadwick Jr. W.W., de Ronde C. E. J., Reymond D., Hyvernaud O., Gennerich H.H., Stoffers P., Mackay K., Dunkin M. A., and Bannister3 S. C. (2008). Collapse and reconstruction of Monowai submarine volcano, Kermadec arc, 1998–2004. *Journal Of Geophysical Research*, 113, B08s03. Available Online at: http://onlinelibrary.wiley.com/doi/10.1029/2007JB005138/abstract.

Young H. D., Freedman R. A., Ford A. L. (2012). Sound and Hearing. In: *University Physics with Modern Physics*. 13th Edition. Addison-Wesley: San Francisco, CA, pp.509-550. Available Online at: http://repo.woogers.net/University%20Physics%20with%20Modern%20Physics%20-%2013th%20Edition.pdf

Yang F, Li J., Chu F., Wu Z. (2007). Automatic Detecting Outliers in Multibeam Sonar Based on Density of Points. *OCEANS 2007 - Europe*, pp. 1 – 4. Available Online at: http://ieeexplore.ieee.org/stamp/stamp.jsp?tp=&arnumber=4302202&tag=1.

Appendix A Summary information about data and software used in the project

Dataset	British Survey 1994	ArniFred_2006	Knorr_2007	Langseth_2013
Original data format	Grid map (.grd)	Swath data (partly processed)	Swath data (raw data)	Swath data (raw data)
Processing software	GMT, text editor, ArcGIS	Caris, text editor, ArcGIS	Caris, text editor, ArcGIS	Caris, text editor, ArcGIS
Bathymetry Files	RRfinalbathN.txt RRfinalbathS.txt	RR_ArniFred2006.txt	RRKnorr2007.txt	RRLangseth2013.txt
Backscatter images			Beam pattern_20070713005623_Knorr2007.bp SIPS engine, side scan Corrections: 5% Despeckle Resolution 15m	Beam pattern: line 0609 GeoCoder engine, Time series Corrections 1-weak despeckle Resolution: 15 m
Raster maps:	Resolution: 120 meter Extent: Statistics: min - , max, mean -	Resolution: 30 meter Extent: Statistics: min - , max, mean -	Resolution: 30 & 120 meter Extent: Statistics: min - , max, mean -	Resolution: 30 & 120 meter Extent: Statistics: min - , max, mean -
Coordinate System	WGS1984	UTM-WGS84, zone 26N	UTM-WGS84, zone 26N	UTM-WGS84, zone 26N

Appendix B Notes from the interview with Vésteinsson the Icelandic Coast Guard

Interview with Árni Vésteinsson, on 9.05.2014 in Hydrographic Office of Icelandic Coast Guard, Reykjavik.

Hydrographic procedure applied by Icelandic Coast Grad to map surrounding territorial waters is focused on charting nautical contour maps rather than producing the continuous raster terrain models of the sea floor.

The procedure applied by the ICG to produce contour and raster maps from raw multibeam soundings is following:

1. XYZ data (projected, meters, depths values) from HIPS and SIPS.

2. Plotting the points (Export events to points) to check their spacing. According to the point density, dividing the dataset into sectors with similar points spacing /depth (range).

3. Creating DTM (TIN) from point data and its edges delineation according to the length for the longest edge of generated triangles. (10xspaceing/ resolution). This will limit the extent of the model.

4. From TIN surface the contours are generated. The interval (irregular) are defined with regard to nautical standards that takes into account ship´s draft.

Appendix C Bathymetric maps (1:100.000)

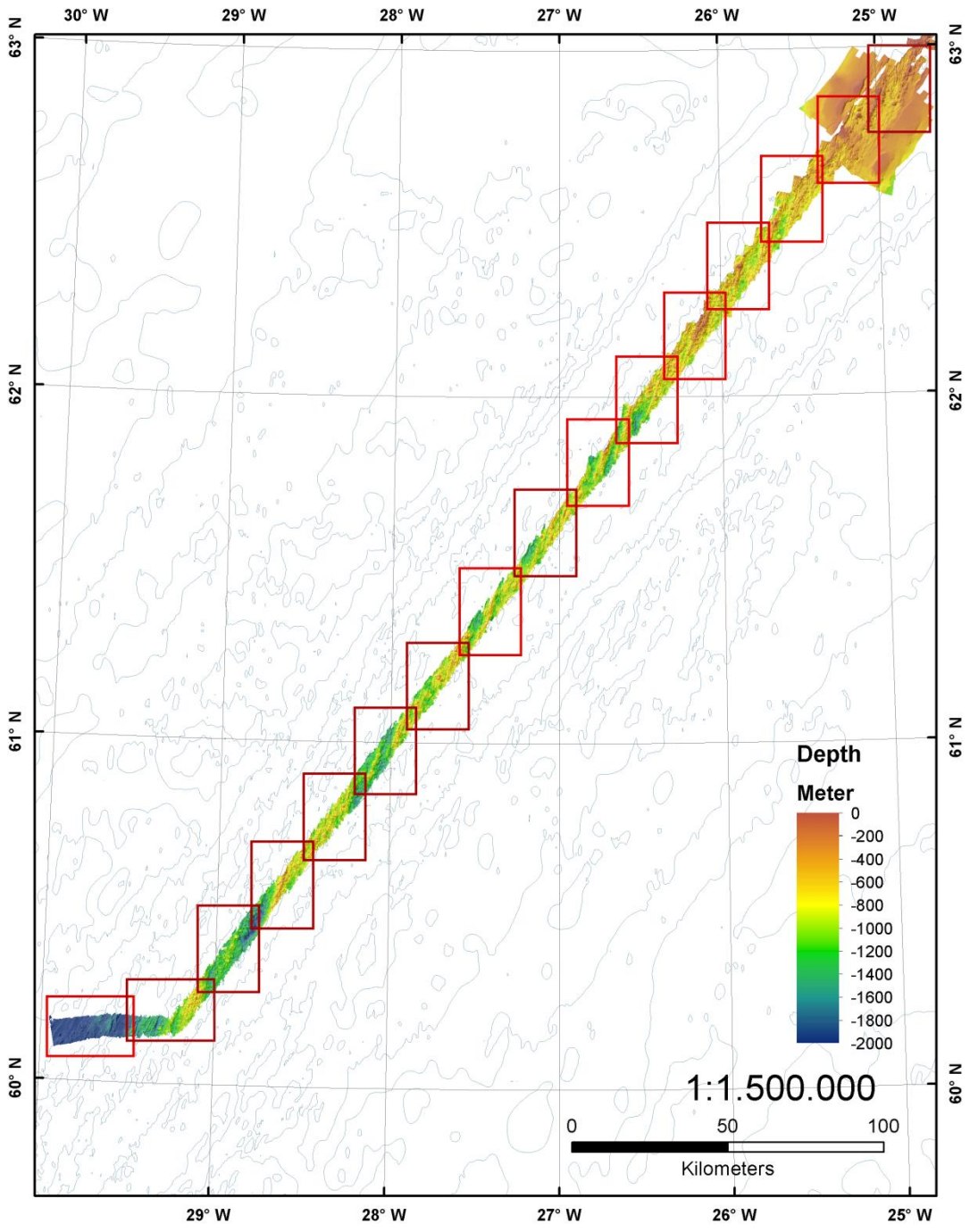

Coordinate System: WGS 1984 UTM Zone 26N
Author: Karolina Banul
Data sources: ISOT, bathymetric surveys (2006, 2007, 2013)

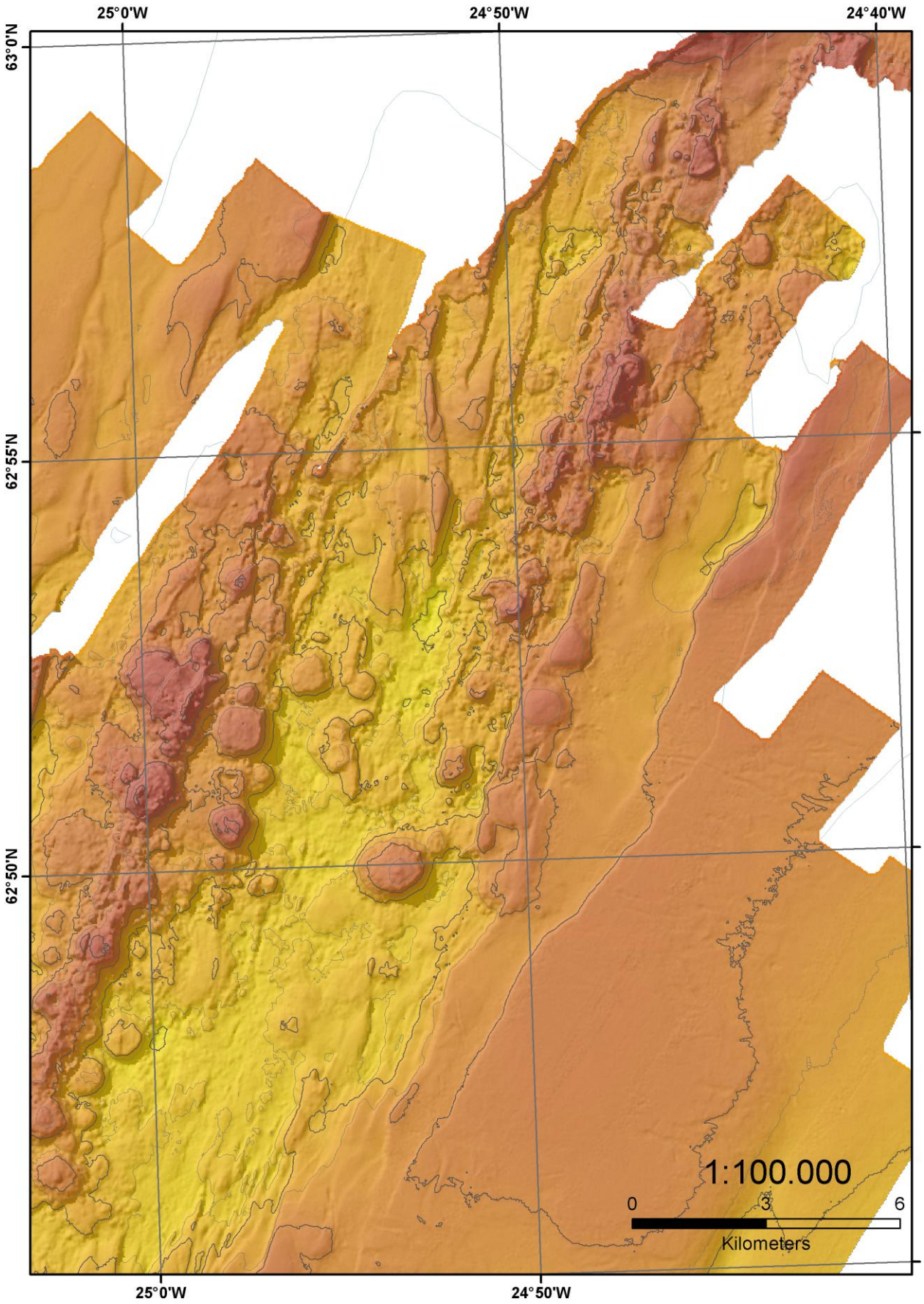
25°0'W
24°50'W
24°40'W
63°0'N
62°55'N
62°50'N
25°0'W
24°50'W
1:100.000
0
3
6
Kilometers

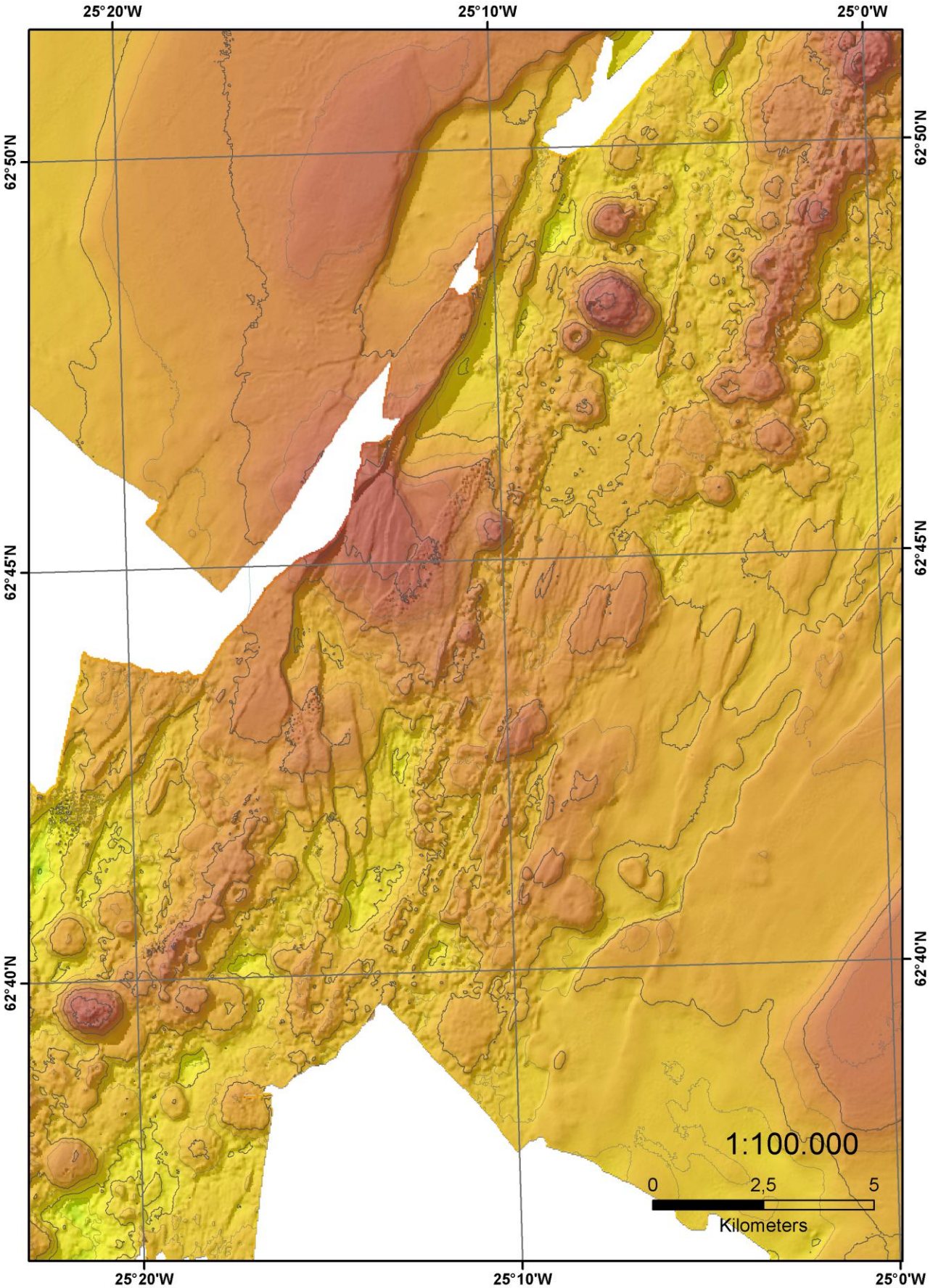
25°20'W
25°10'W
25°0'W
62°50'N
62°45'N
62°40'N
1:100.000
0
2,5
5
Kilometers

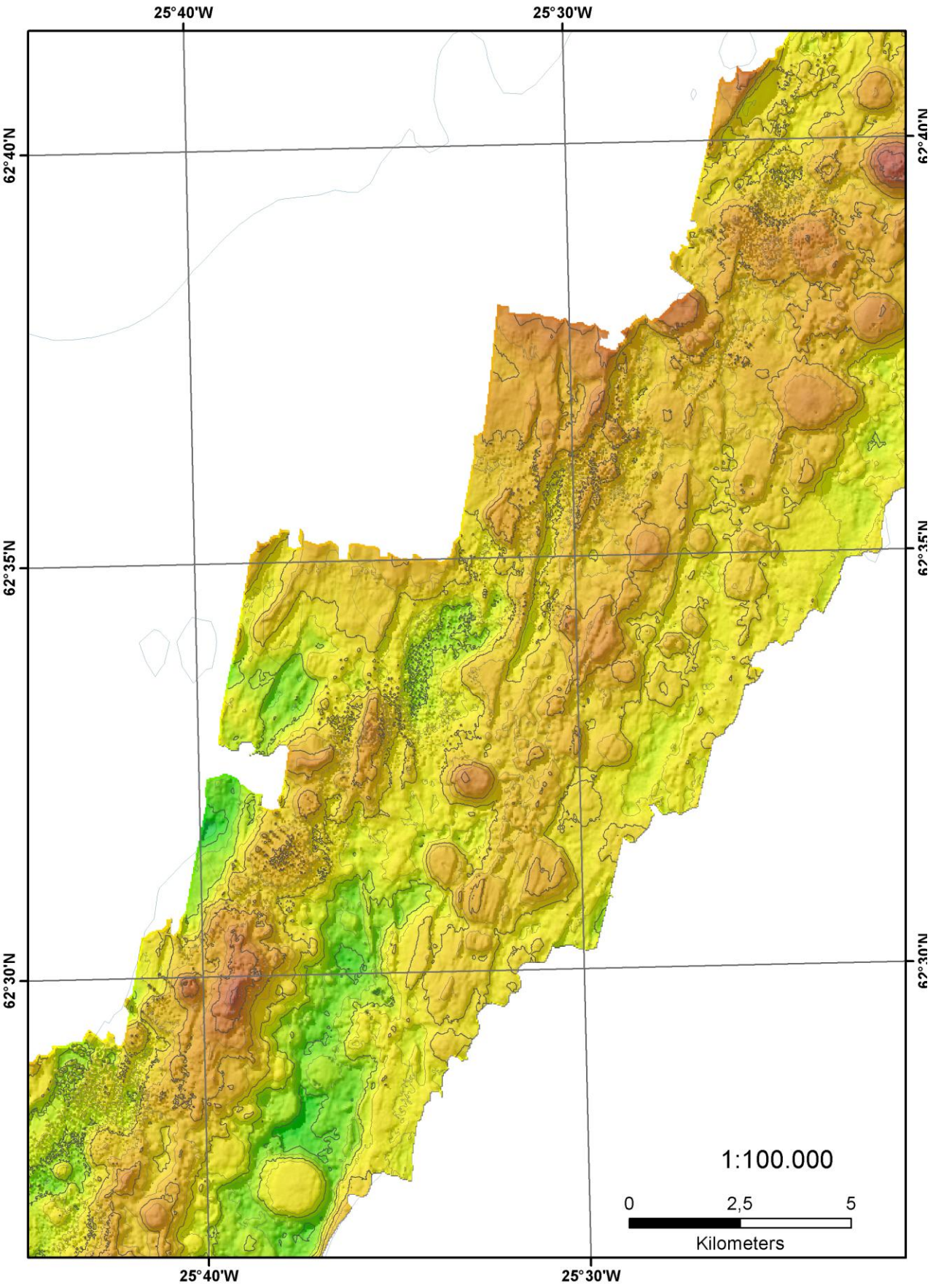
25°40'W
25°30'W
62°40'N
62°35'N
62°30'N
1:100.000
0
2,5
5
Kilometers

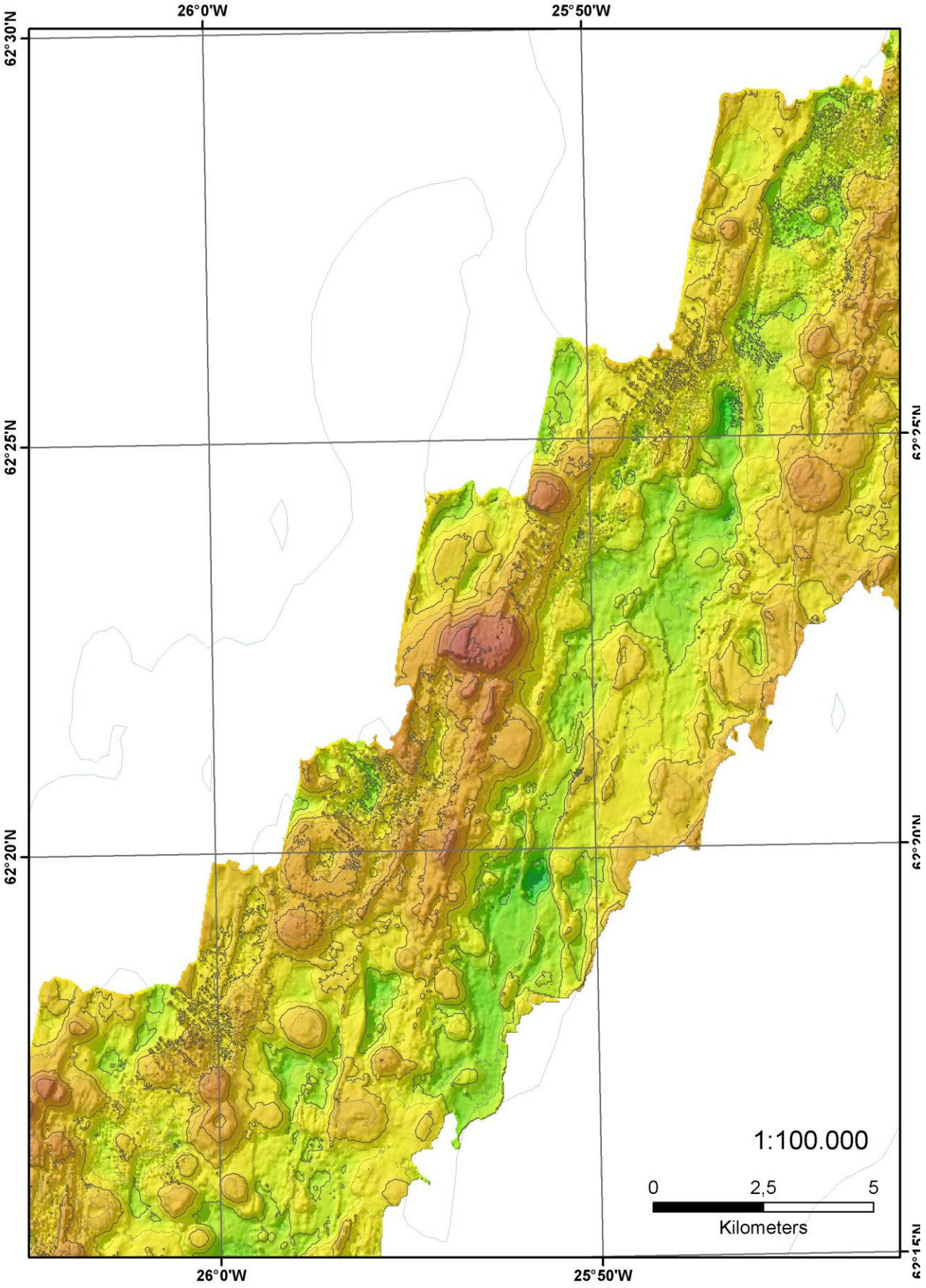
26°0'W
25°50'W
62°30'N
62°25'N
62°20'N
62°15'N
1:100.000
0
2,5
5
Kilometers

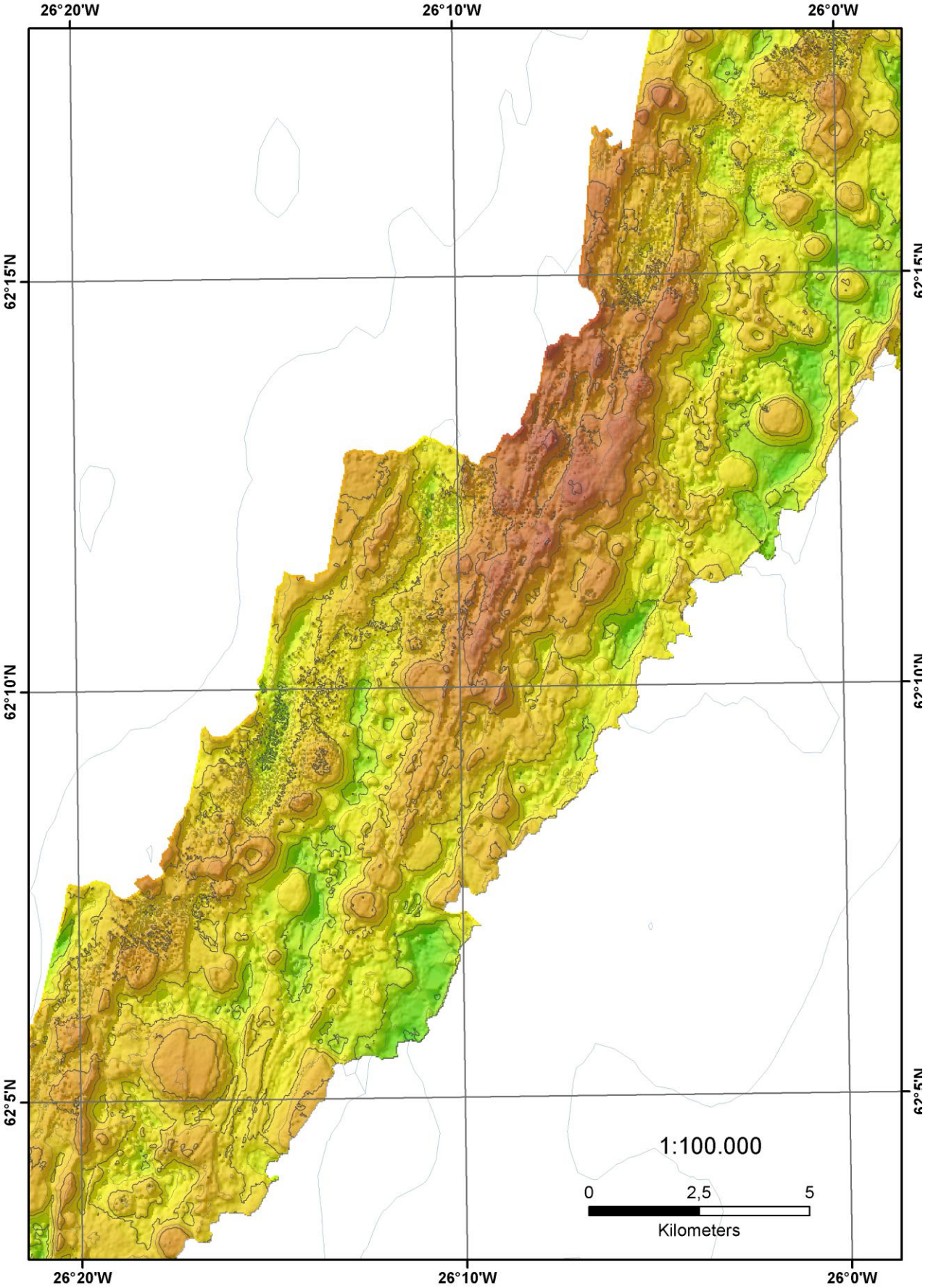
26°20'W
26°10'W
26°0'W
62°15'N
62°10'N
62°5'N
1:100.000
0
2,5
5
Kilometers

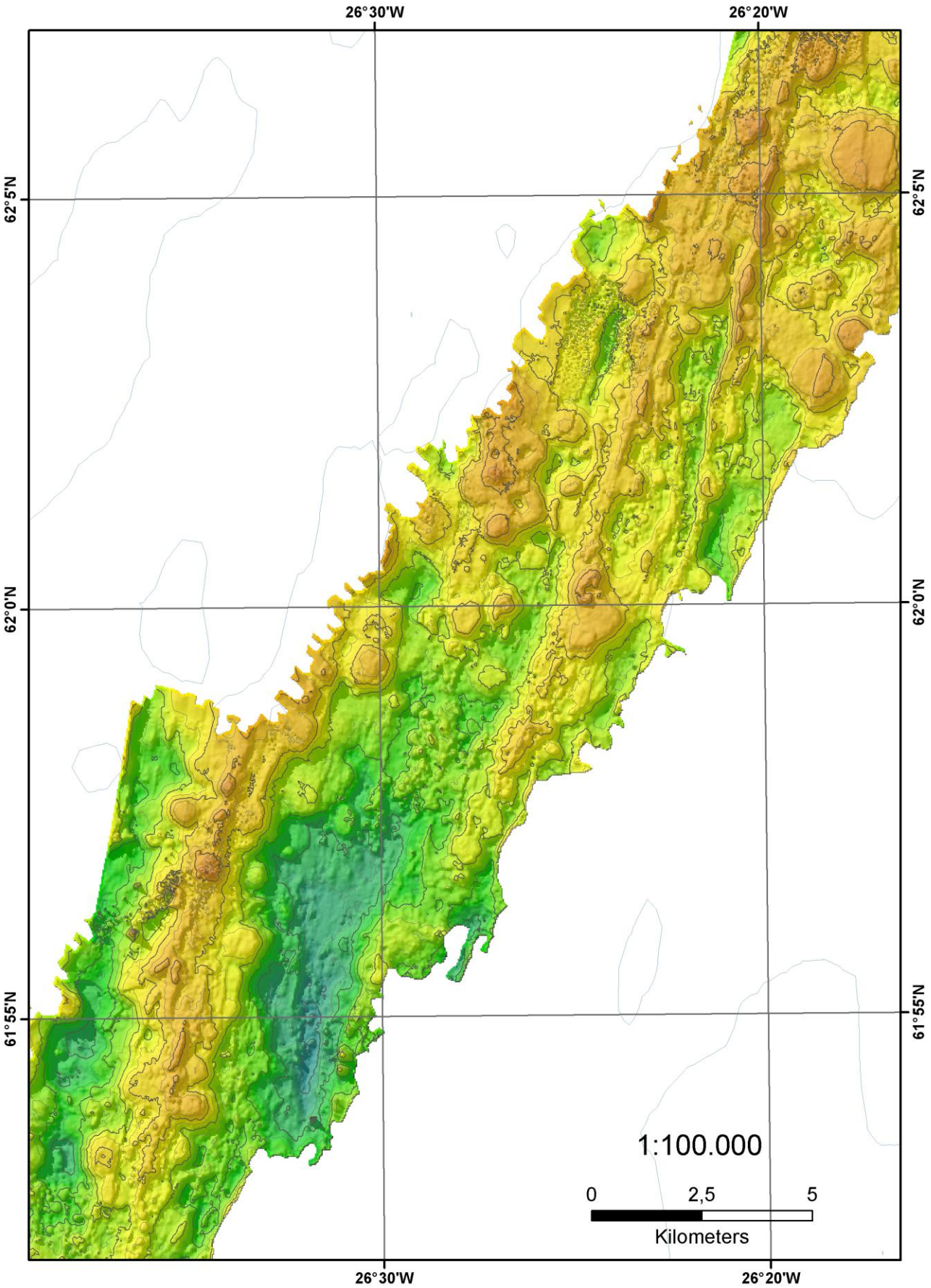
26°30'W
26°20'W
62°5'N
62°0'N
61°55'N
1:100.000
0
2,5
5
Kilometers

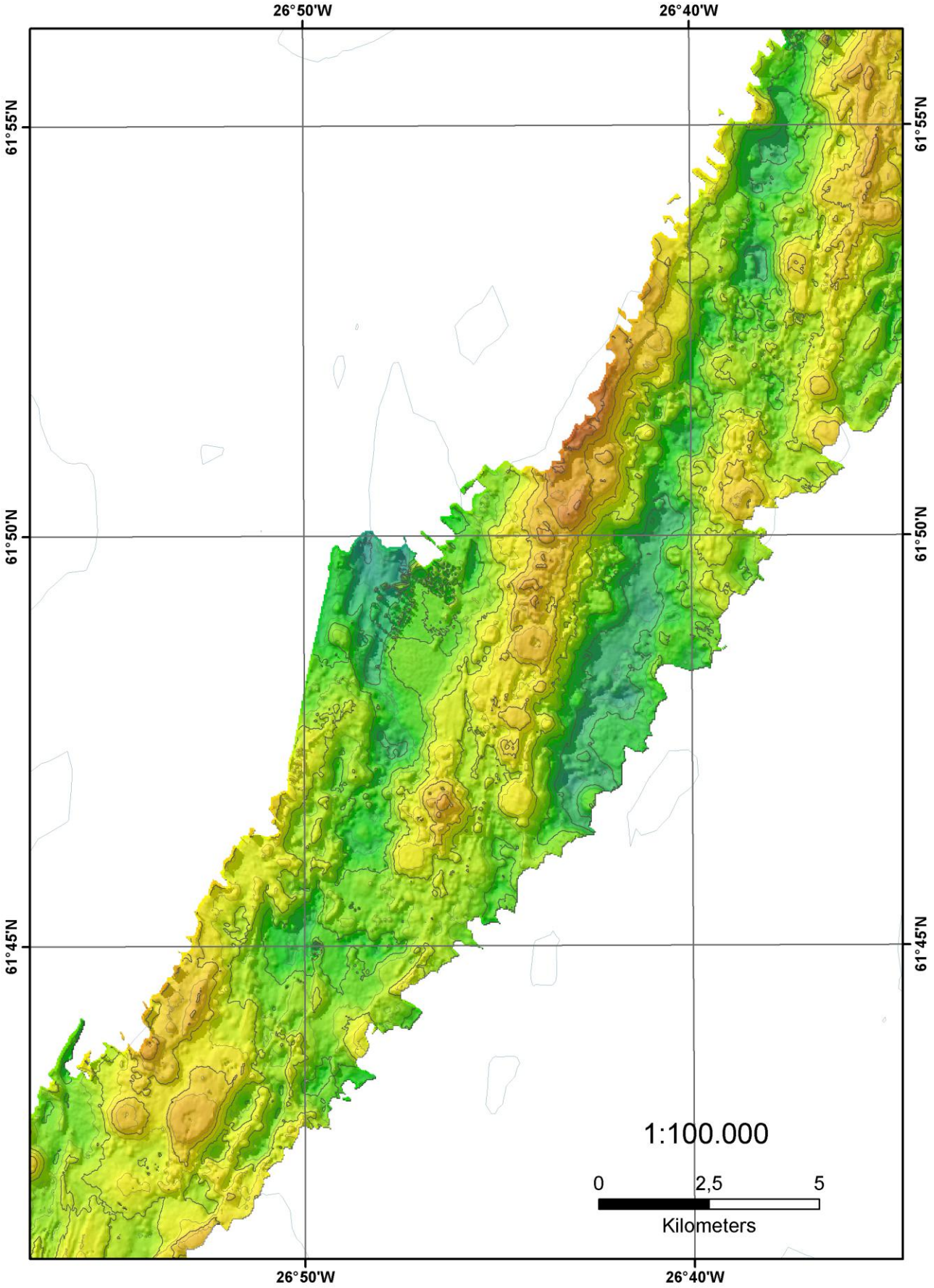
26°50'W
26°40'W
61°55'N
61°50'N
61°45'N
1:100.000
0
2,5
5
Kilometers

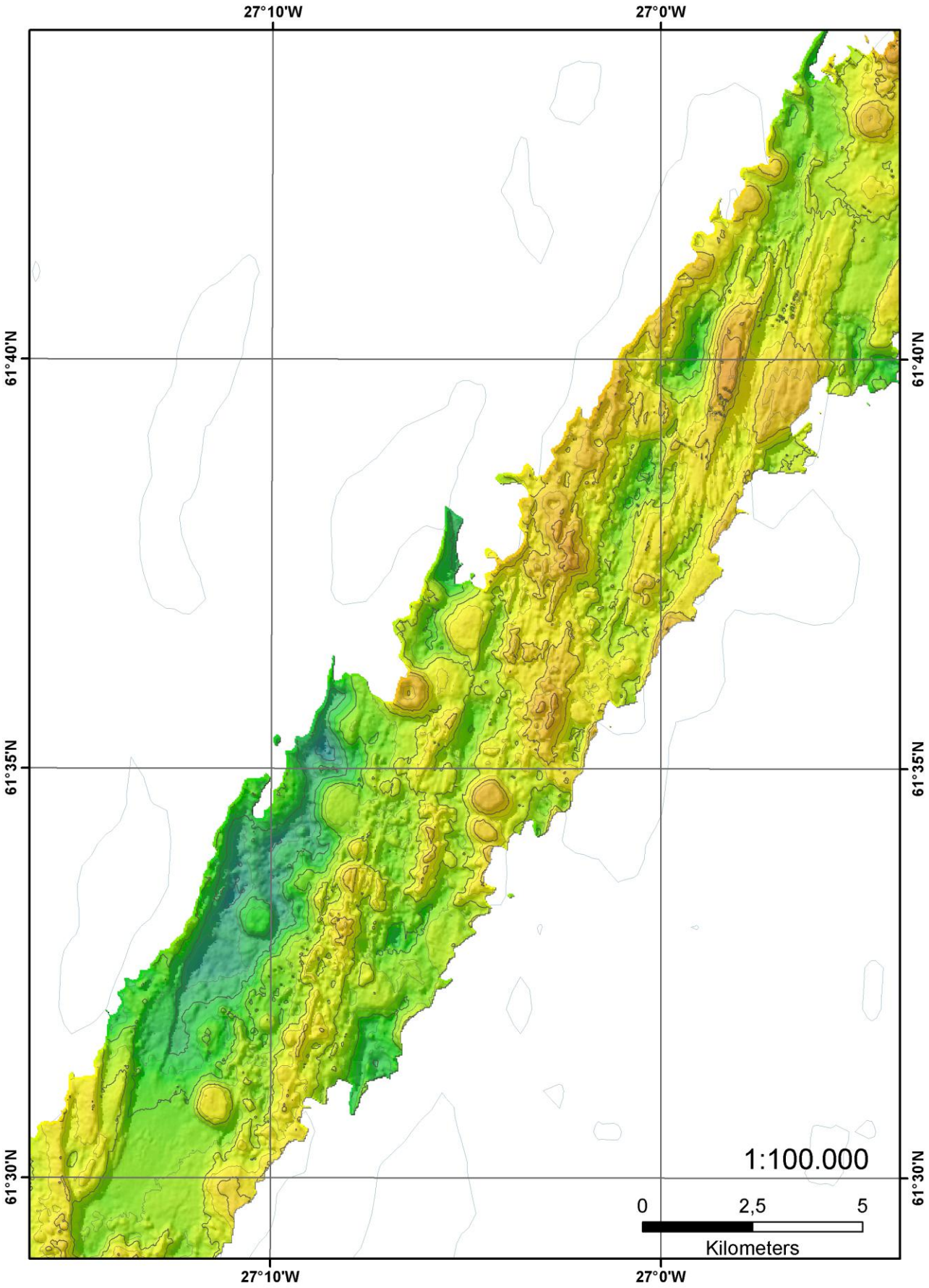
27°10'W
27°0'W
61°40'N
61°35'N
61°30'N
1:100.000
0
2,5
5
Kilometers

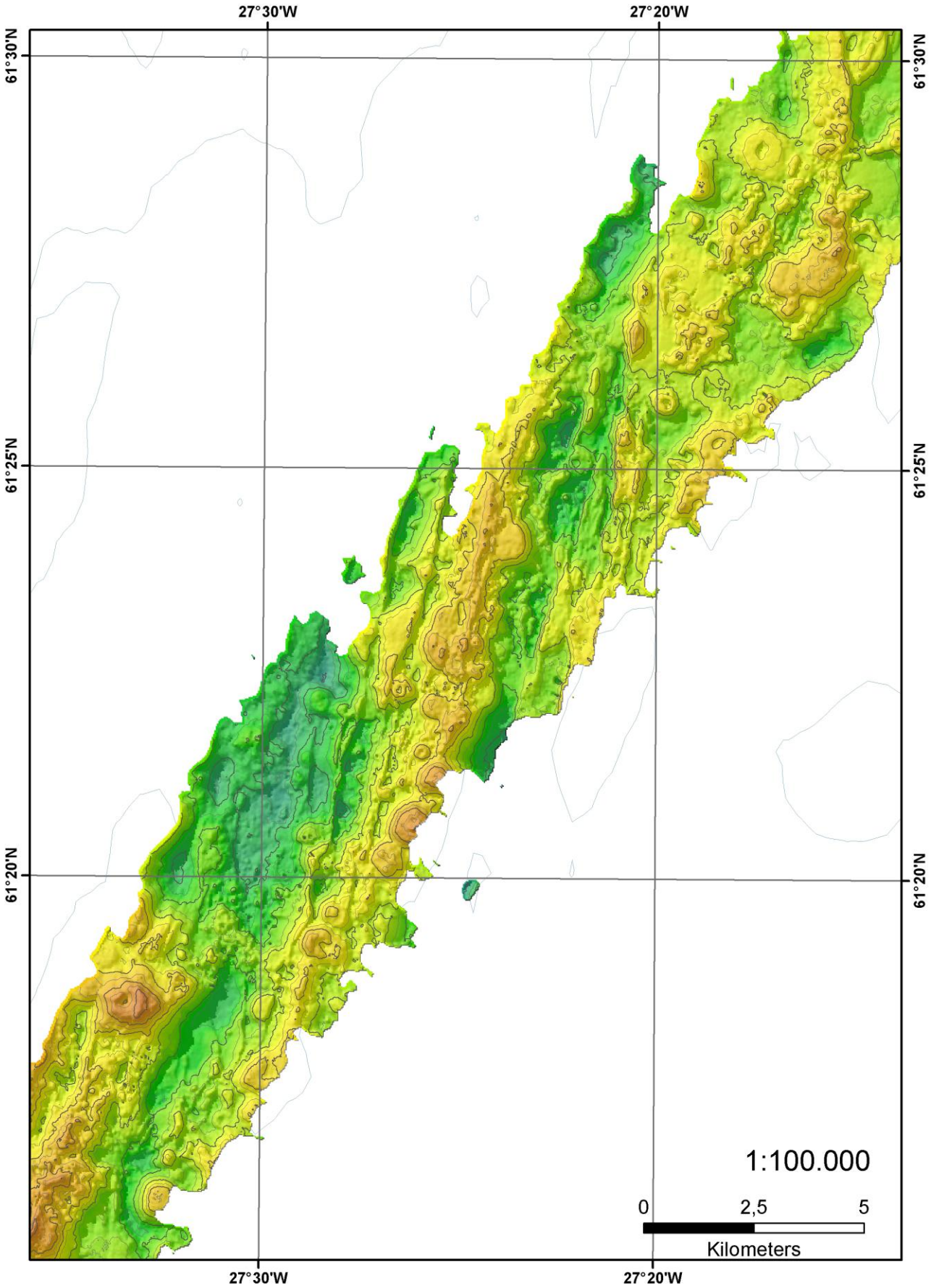
27°30'W
27°20'W
61°30'N
61°25'N
61°20'N
1:100.000
0
2,5
5
Kilometers

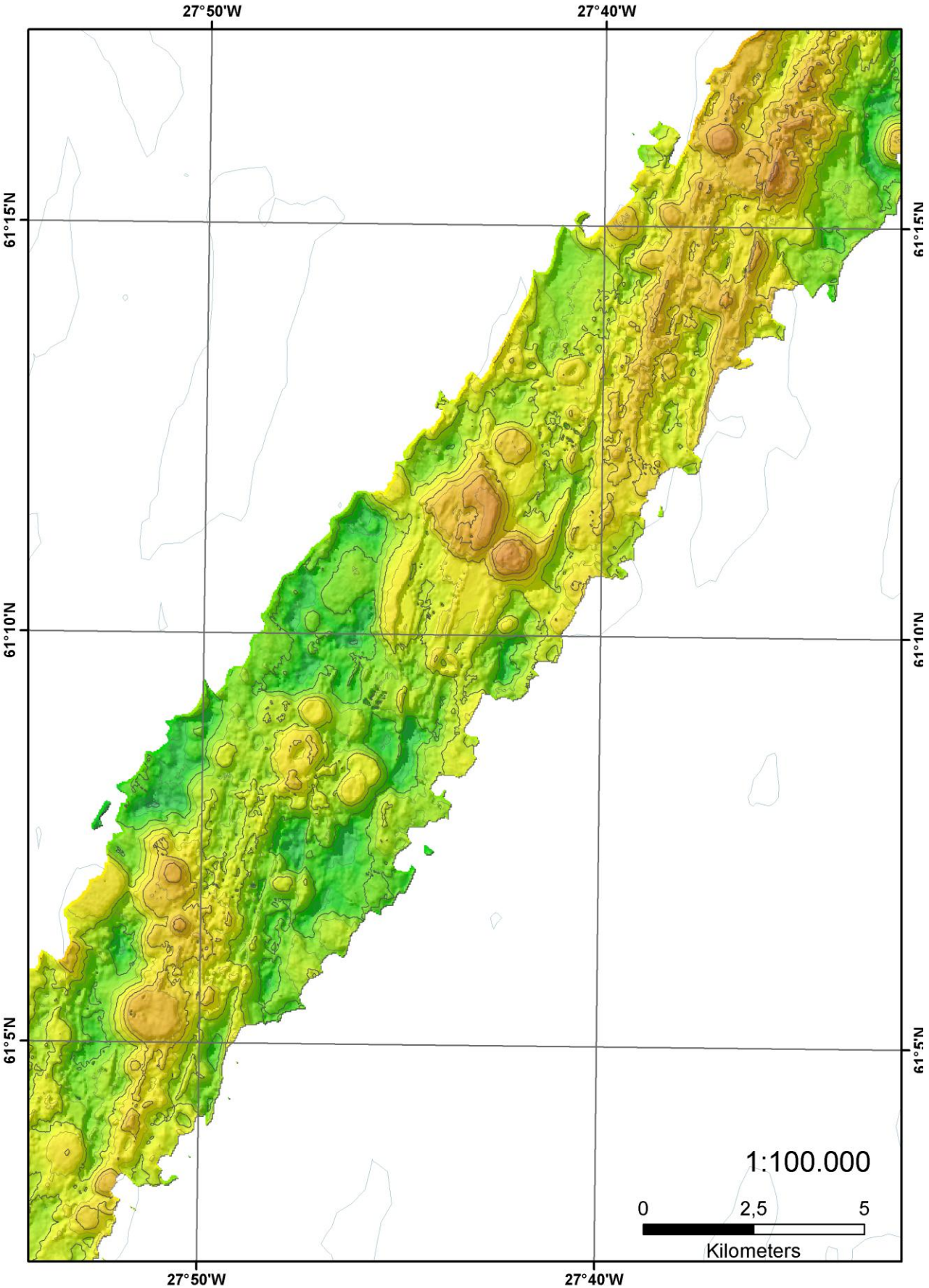
27°50'W
27°40'W
61°15'N
61°10'N
61°5'N
1:100.000
0
2,5
5
Kilometers

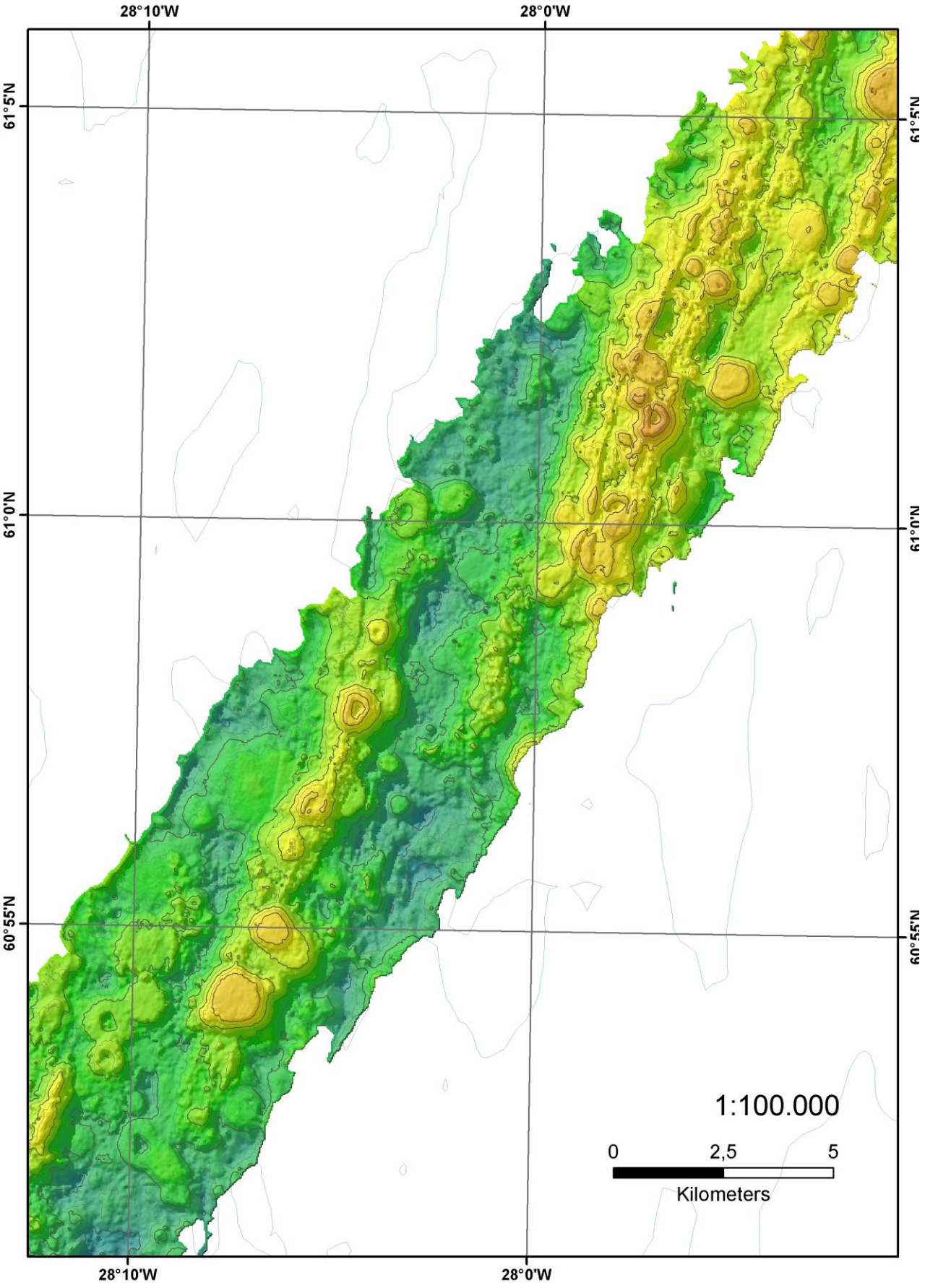
28°10'W
28°0'W
61°5'N
61°0'N
60°55'N
1:100.000
0
2,5
5
Kilometers

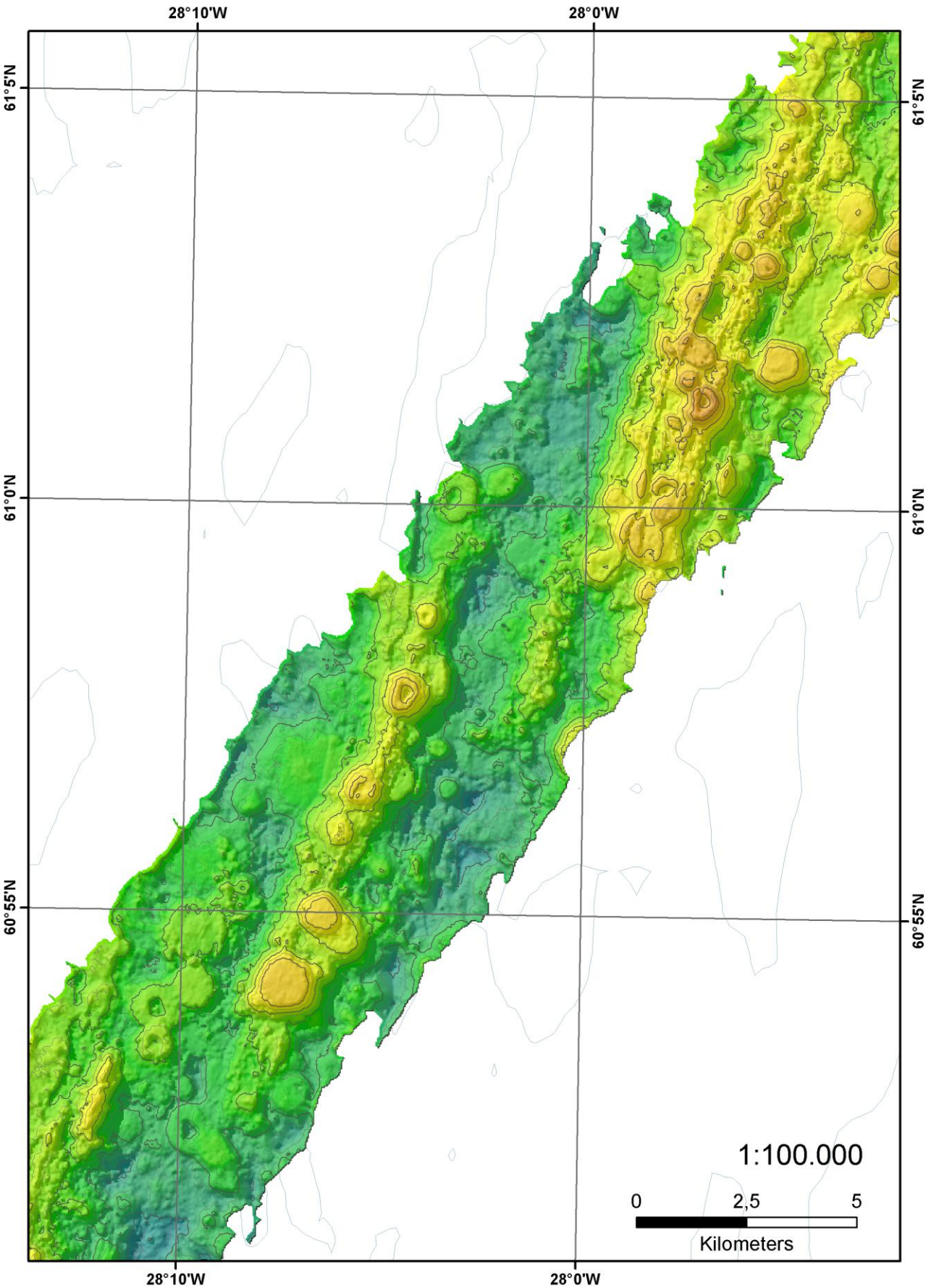
28°10'W
28°0'W
61°5'N
61°0'N
60°55'N
1:100.000
0
2,5
5
Kilometers

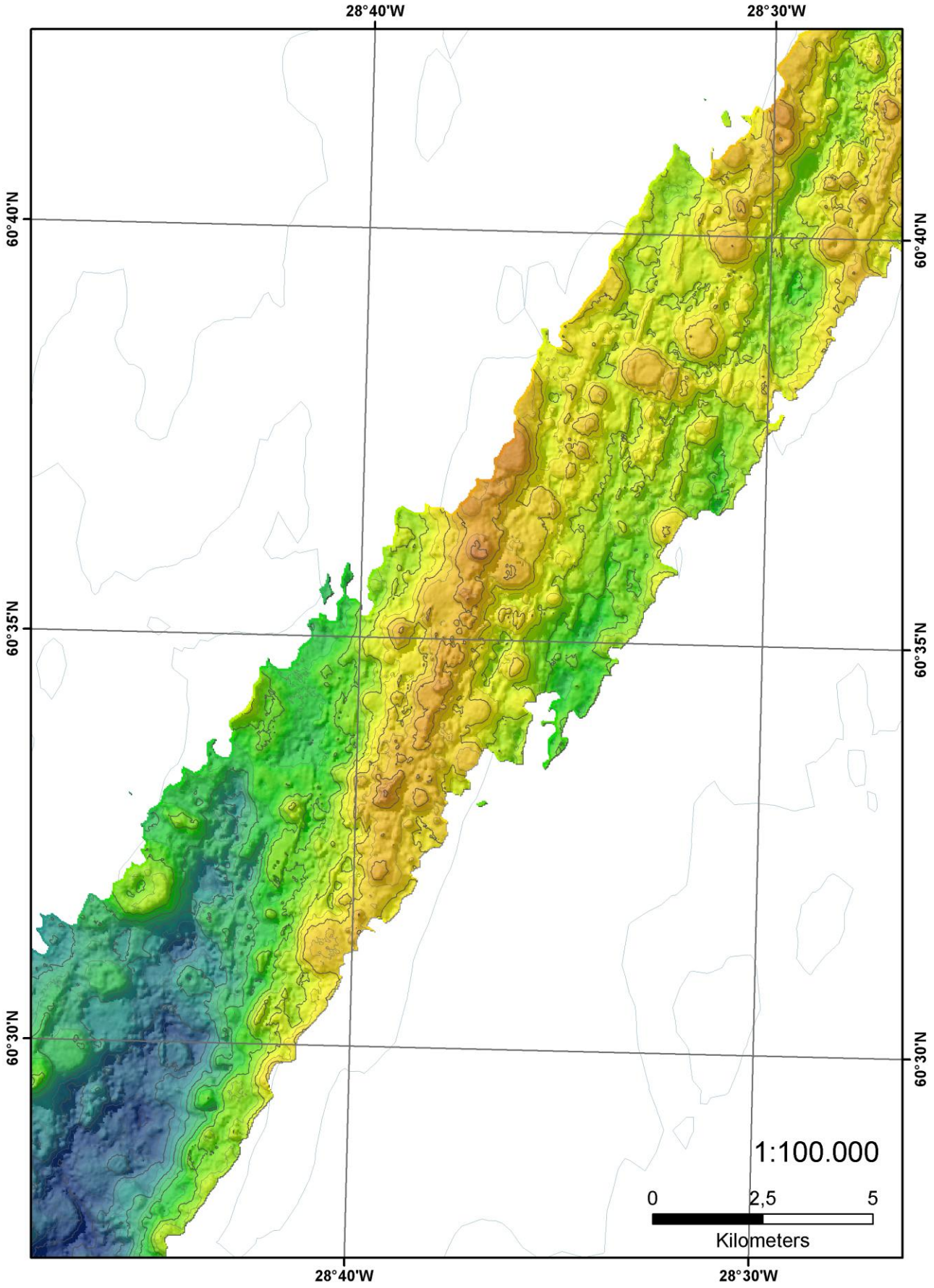
28°40'W
28°30'W
60°40'N
60°35'N
60°30'N
1:100.000
0
2,5
5
Kilometers

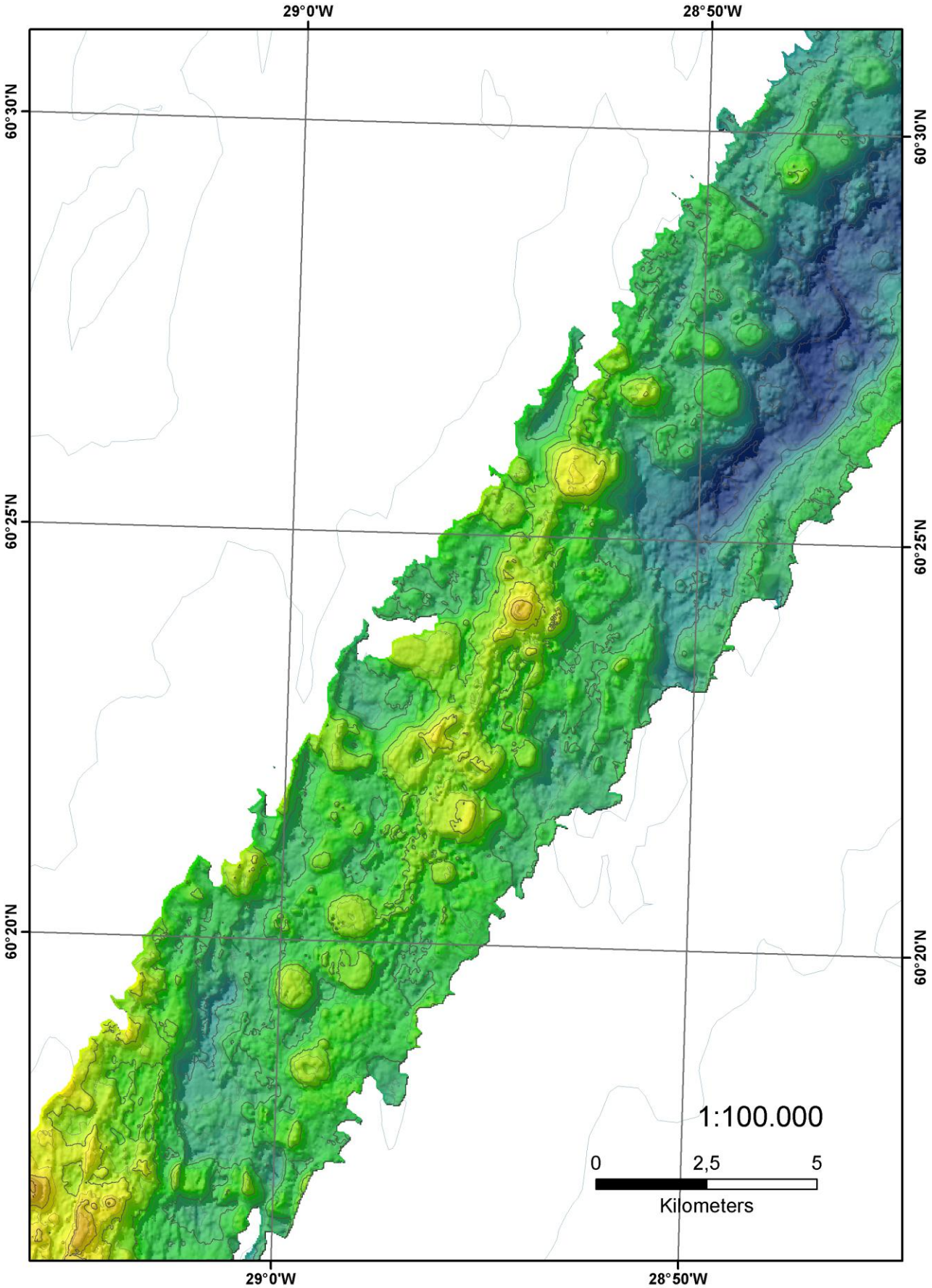
29°0'W
28°50'W
60°30'N
60°25'N
60°20'N
1:100.000
0
2,5
5
Kilometers

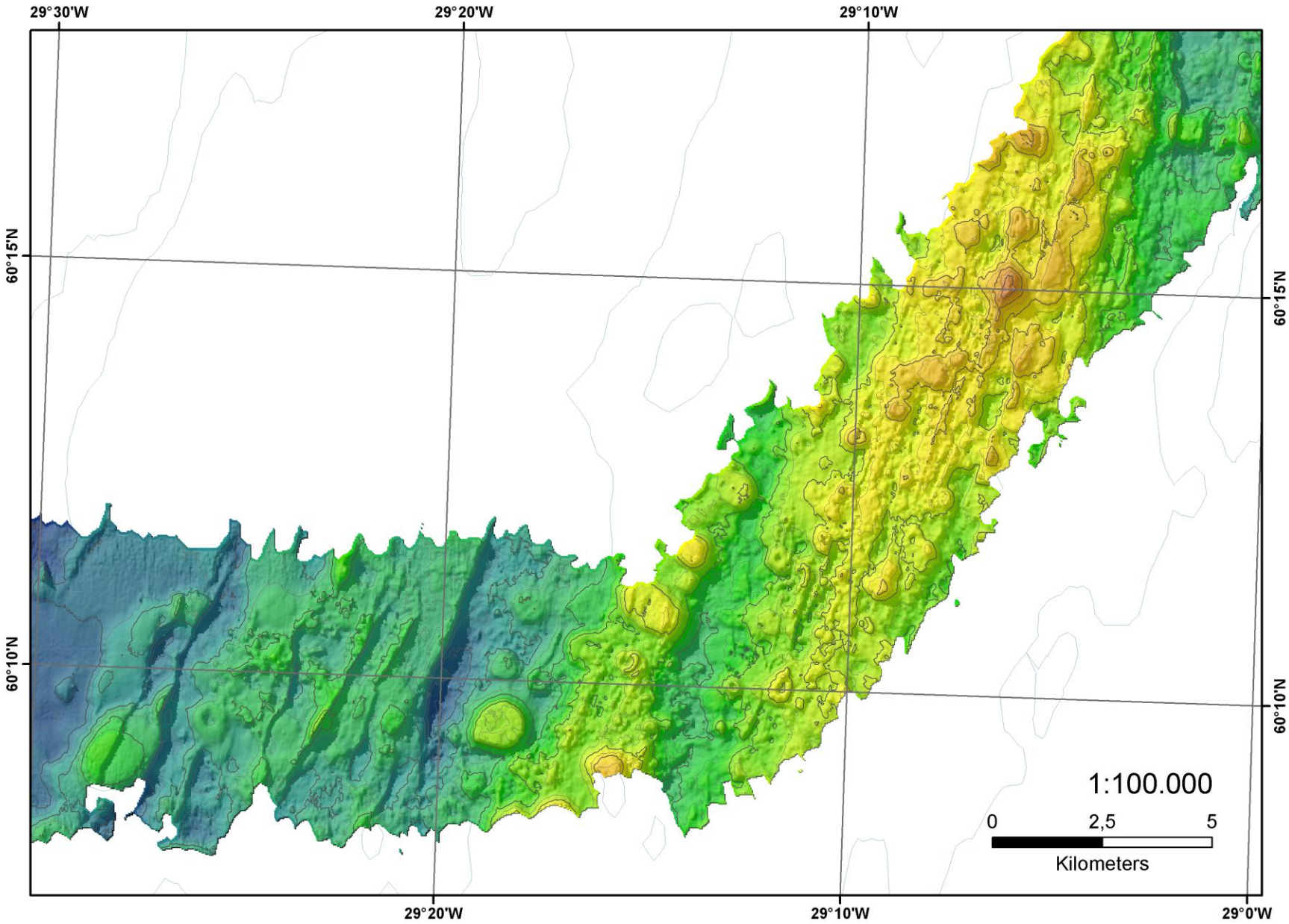
29°30'W
29°20'W
29°10'W
60°15'N
60°10'N
29°20'W
29°10'W
29°0'W
1:100.000
0
2,5
5
Kilometers

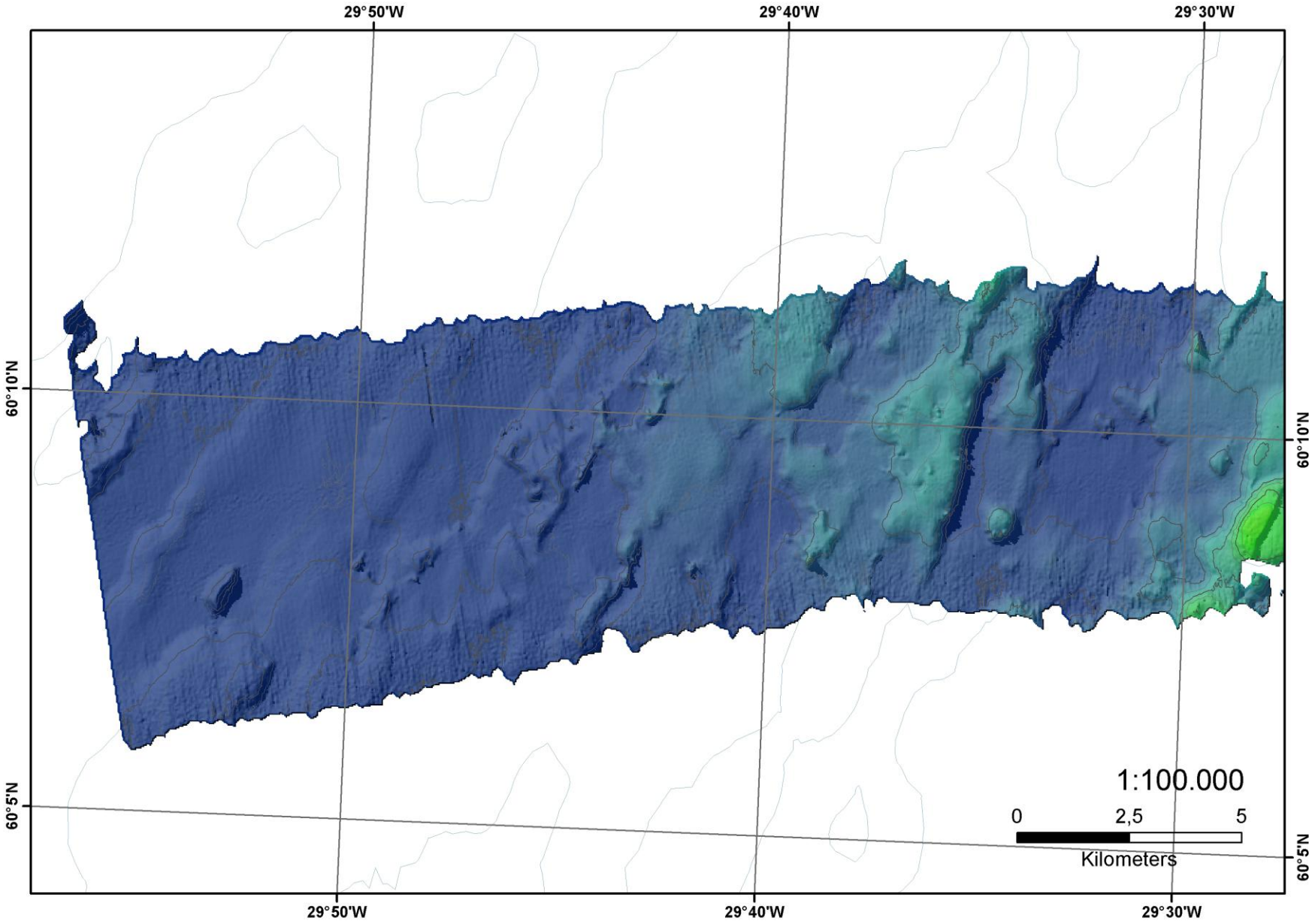
29°50'W
29°40'W
29°30'W
60°10'N
60°5'N
1:100.000
0
2,5
5
Kilometers

Appendix D Results of the grid differencing analysis

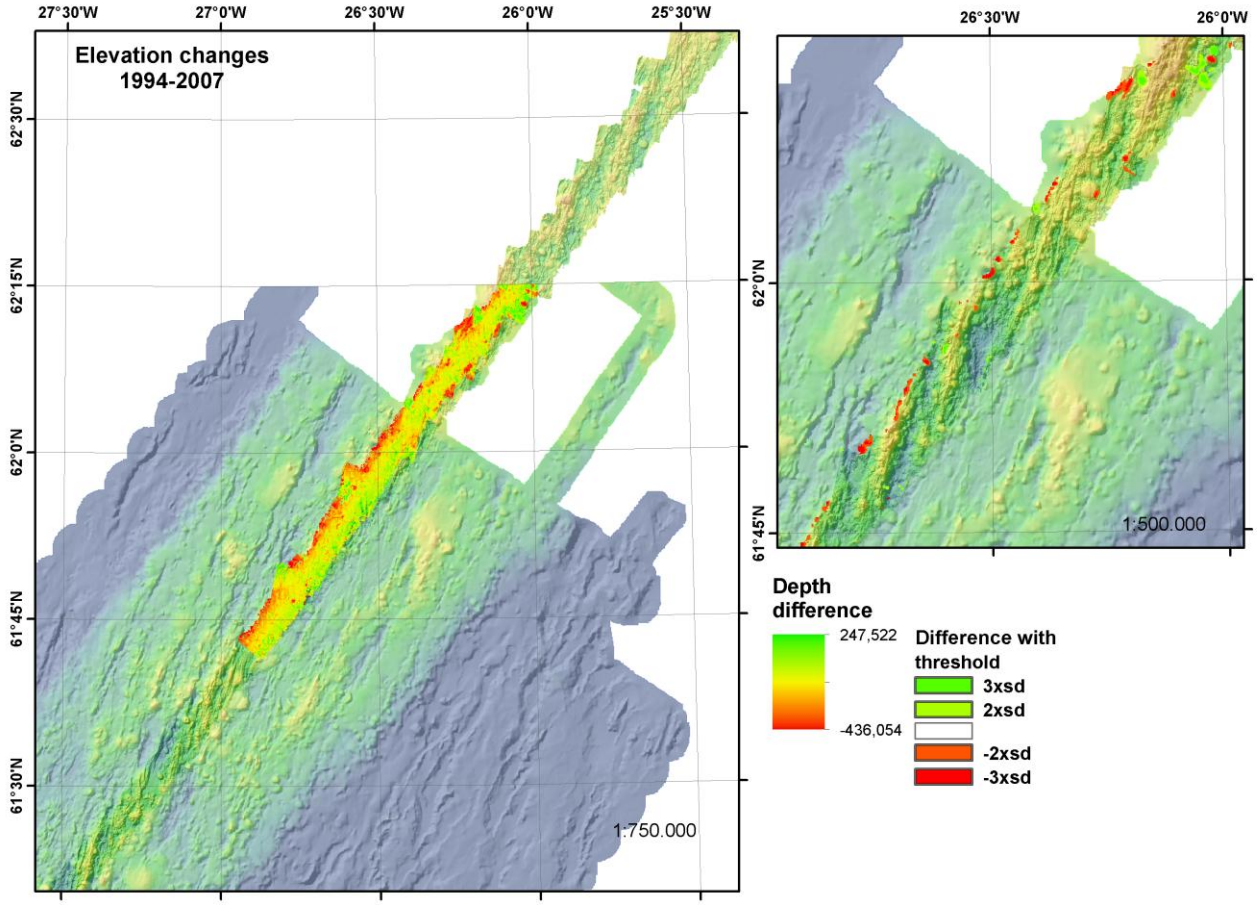

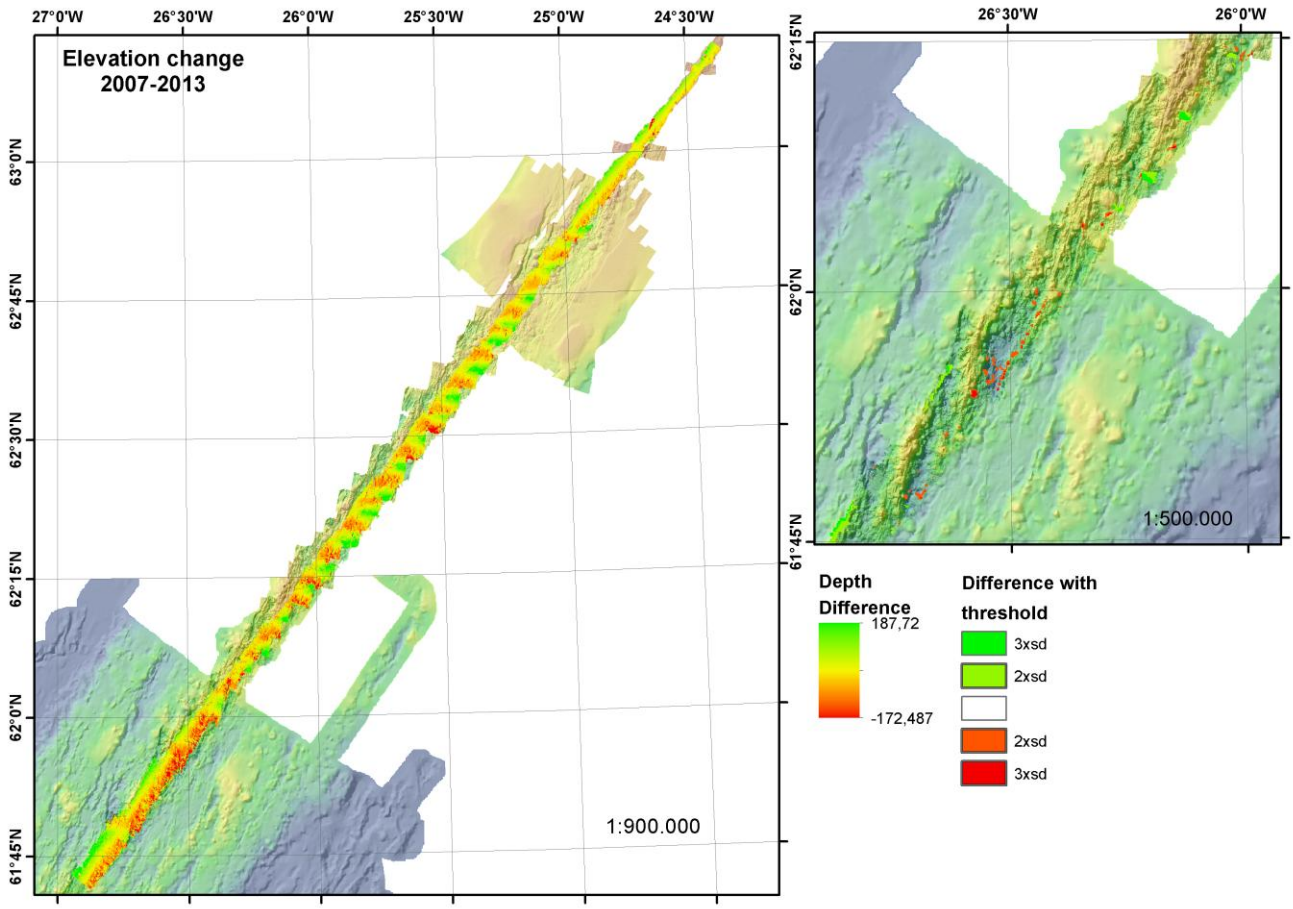
Elevation change
2007-2013
27°0'W
26°30'W
26°0'W
25°30'W
25°0'W
24°30'W
63°0'N
62°45'N
62°30'N
62°15'N
62°0'N
61°45'N
1:900.000
26°30'W
26°0'W
62°15'N
62°0'N
61°45'N
1:500.000
Depth Difference
187,72
-172,487
Difference with threshold
3xsd
2xsd
2xsd
3xsd

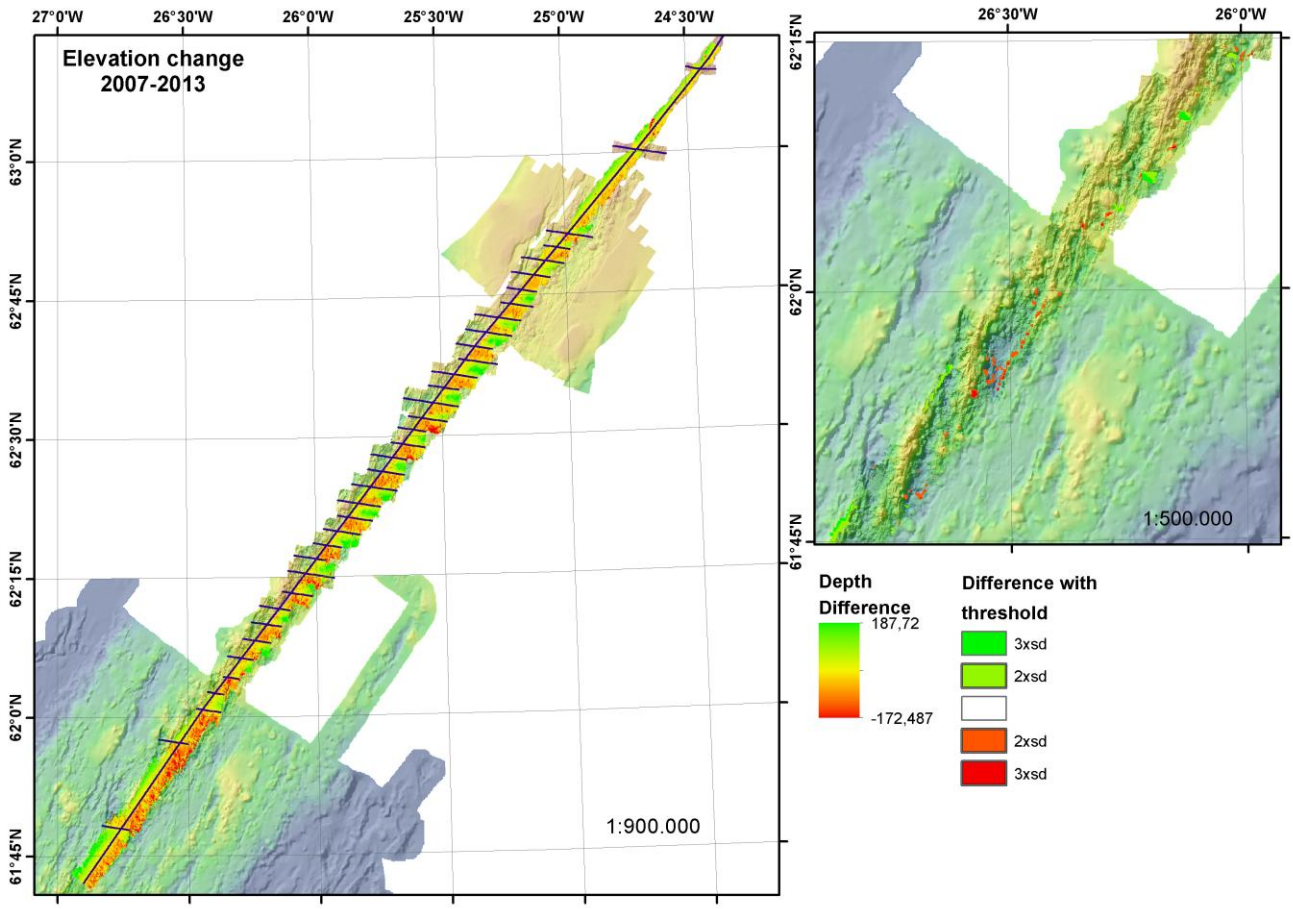
Elevation change
2007-2013
27°0'W
26°30'W
26°0'W
25°30'W
25°0'W
24°30'W
63°0'N
62°45'N
62°30'N
62°15'N
62°0'N
61°45'N
1:900.000
26°30'W
26°0'W
62°15'N
62°0'N
61°45'N
1:500.000
Depth Difference
187,72
-172,487
Difference with threshold
3xsd
2xsd
2xsd
3xsd

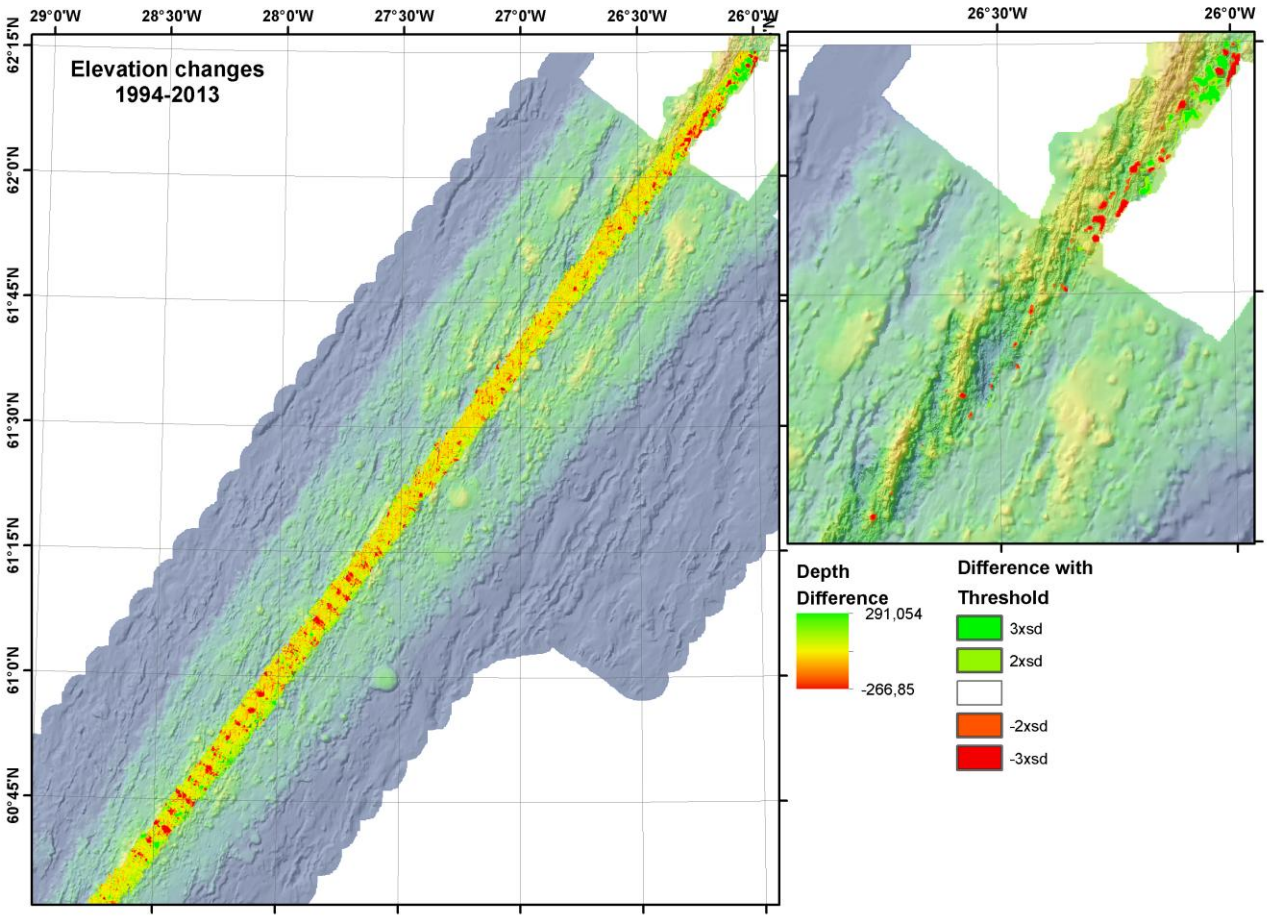
Elevation changes
1994-2013
29°0'W
28°30'W
28°0'W
27°30'W
27°0'W
26°30'W
26°0'W
62°15'N
62°0'N
61°45'N
61°30'N
61°15'N
61°0'N
60°45'N
Depth
Difference
291,054
-266,85
Difference with
Threshold
3xsd
2xsd
-2xsd
-3xsd